UNIVERSITÀ DI PISA

Facoltà di Scienze Matematiche Fisiche e Naturali
Corso di Laurea in Scienze fisiche

Tesi di Laurea Specialistica

Scintillation in the Inter Galactic Medium

Relatore:
Andrea Ferrara

Candidato:
Andrea Pallottini

Luglio 2011

Contents

Introduction

The scintillation phenomenon consists in a light wave, coming from a compact enough source, that, passing through a ionized inhomogeneous medium, is subject to a random variation of the refraction index, and thus suffers multiple phase changes which lead to fluctuations in all the wave related quantities; the aim of this Thesis is to exploit the effects of this process when the light comes from a distant quasar and the random medium is given by the InterGalactic Medium, namely the baryon mass fraction of the universe laying between galaxies that is not locked up in stellar objects.

The motivation that drives us toward this purpose is that either until now in this specific context a full investigation has not been developed in the literature, and either the IGM scintillation can, as we eventually show, be relevant in explaining some of the current discrepancies between theory and observations; furthermore this can prove to be a useful investigation tool, complementary to the ones available.

To achieve the result proposed we have decided to employ the standard cosmological model, which gives the proper tools to analyze the environment we want to deal with, which is described in Chapter 1, and to numerically simulate the IGM, with the tools provided and depicted in Chapter 2.
Next, in Chapter 3, we review the scintillation physical basis and its application to the InterStellar Medium, and then we naturally extend the ISM results to the IGM case.
In Chapter 4 we expose and discuss the results of the simulation and finally, in Chapter 5, we apply our model to the simulation and analyze the behaviour of the IGM scintillation, confronting it with the observations.
To conclude, in Chapter 6 we summarize the results obtained and the possible future developments.

Chapter 1

Cosmological background

... The universe itself keeps on expanding and expanding
In all of the directions it can whizz
As fast as it can go, at the speed of light, you know,
Twelve million miles a minute, and that's the fastest speed there is.

So remember, when you're feeling very small and insecure,
How amazingly unlikely is your birth,
And pray that there's intelligent life somewhere up in space,
'Cause there's bugger all down here on Earth.

1983, Galaxy Song, Monty Python

1.1 Smooth universe

Before even starting to talk about scintillation it is mandatory to understand the system in which we want to observe its action and its effects, and, in order to properly describe the universe and its structure, it is necessary to begin this work with a Section introducing the base cosmological notions.

1.1.1 Brief relativity overview

Let's begin to fix the notation: latin index ranges from 1 to 3 while greek ones spans from 0 to 4, in addition we are going to employ Einstein convention such that the world line element is indicated by

$$\mathrm{d}s^2 = g_{\mu\nu}\mathrm{d}x^\mu \mathrm{d}x^\nu \tag{1.1}$$

and we choose the flat metric signature to be $(+, -, -, -)$.

The covariant derivate operate as a partial derivate for a scalar field f

$$\nabla_\mu f = \partial_\mu f \tag{1.2a}$$

and its action on the generic vector field X^ν is indicated as

$$\nabla_\mu X^\nu = \partial_\mu X^\nu + \Gamma^\nu_{\mu\rho} X^\rho \tag{1.2b}$$

while applied to the cotangent field X_ν it act as

$$\nabla_\mu X_\nu = \partial_\mu X_\nu - \Gamma^\rho_{\mu\nu} X_\rho \tag{1.2c}$$

and this can easily be generalized to a n_1 times covariant and n_2 time countervariant generic tensor field $X^{\nu_1\ldots\nu_{n_1}}_{\mu_1\ldots\mu_{n_2}}$; here the $\Gamma^\rho_{\mu\nu}$ are called the Christoffel symbol, and they describe how the derivate change the coordinate base; they are uniquely determined upon assuming that the metric is torsion-less and compatible:

$$\Gamma^\rho_{\mu\nu} = \frac{1}{2} g^{\rho\lambda} \left(\partial_\mu g_{\nu\lambda} + \partial_\nu g_{\mu\lambda} - \partial_\lambda g_{\nu\mu} \right) \tag{1.3}$$

To be able to handle gravity we must know the curvature, which can be viewed as the tensor that determines the difference in following a tangent vector along the two direction of a loop path; thus is given by the commutator of two successive covariant derivate

$$\left[\nabla_\mu, \nabla_\rho\right] X^\nu = R^\nu_{\mu\rho\lambda} X^\lambda \tag{1.4}$$

and the curvature can be calculated straightforward from the definition using equation (1.3)

$$R^\nu_{\mu\rho\lambda} = \nabla_\rho \Gamma^\nu_{\mu\lambda} - \nabla_\lambda \Gamma^\nu_{\mu\rho} + \Gamma^\beta_{\mu\lambda} \Gamma^\nu_{\beta\rho} - \Gamma^\beta_{\mu\rho} \Gamma^\nu_{\beta\lambda} \tag{1.5a}$$

From this operator the Ricci tensor (1.5b) and the Ricci scalar (1.5c) can be formed by contraction as follows

$$R_{\mu\nu} = R^\rho_{\mu\rho\nu} \tag{1.5b}$$

$$R = R^\mu_\mu \tag{1.5c}$$

and one can define the Einstein tensor as

$$G_{\mu\nu} = R_{\mu\nu} - \frac{1}{2} g_{\mu\nu} R \tag{1.5d}$$

The equation of motion can be derived from the action principle: the invariant volume element is $\mathrm{d}x^4\sqrt{-g}$ and our need is to find a Lagrangian density; following the Einstein-Hilbert treatment we chose a gravitational Lagrangian of the form

$$\mathcal{L}_g \propto R \tag{1.6a}$$

where the proportionality constant can only be fixed retrospectively, as it is ruled by matching the relativistic description with Newtonian gravity

$$\mathcal{L}_g = -\frac{1}{16\pi G}R \tag{1.6b}$$

Then adding a source term $\mathcal{L}_s$ the complete action S we are to employ is

$$S = \int \mathrm{d}x^4\sqrt{-g}\left(\mathcal{L}_s - \frac{1}{16\pi G}R\right) \tag{1.7}$$

It is fruitful to view this source as associated with its stress-energy tensor

$$T_{\mu\nu} = \frac{2}{\sqrt{-g}}\left(\frac{\partial}{\partial g^{\mu\nu}} - \partial_\lambda\frac{\partial}{\partial\left(\partial_\lambda g^{\mu\nu}\right)}\right)\sqrt{-g}\mathcal{L}_b \tag{1.8}$$

since, in term of this, the fixed extremes variation calculation of the action yields

$$G_{\mu\nu} = 8\pi G T_{\mu\nu} \tag{1.9}$$

which is known as the Einstein equation.

1.1.2 Friedman equations

As a start we want to find the founding equations of the smooth universe: forcing homogeneity and isotropy at every time instant is equivalent to require a maximal three dimensional symmetric space, and there are only three kind of space of this sort, which are characterized by the sign of their spatial curvature k

$$\mathrm{d}x^i\mathrm{d}x_i = \frac{\mathrm{d}r^2}{1-kr^2} + r^2\mathrm{d}\Omega^2 \tag{1.10}$$

thus, up to coordinate transformation, the Robertson-Walker metric is given by

$$\mathrm{d}s^2 = c^2\mathrm{d}t^2 - a^2(t)\left(\frac{\mathrm{d}r^2}{1-kr^2} + r^2\mathrm{d}\Omega^2\right) \tag{1.11}$$

and these coordinates are called the comoving ones; from now on we consider the $k = 0$ case only.
In order to write down Einstein equation, we have to choose at least the form of the stress energy tensor: for our purpose $T_{\mu\nu}$ represent a perfect fluid with energy density ρ, pressure p, and velocity U^μ, thus its general form is given by

$$T^{\mu\nu} = (\rho + p)U^\mu U^\nu - g^{\mu\nu}p \tag{1.12}$$

Since by symmetry the fluid has to be in rest with the comoving frame the velocity U^μ must be (1,0,0,0) and either ρ and p have to be constant in space.

Moreover one can note that as $G_{\mu\nu}$ is symmetric[1] equation (1.9) translates into a ten equations system, but, due to isotropy there must be no off-diagonal term and, thanks to homogeneity, the equations are further reduced from four to two, as the spatial part must be redundant: in the end we are left with the two Friedman equations

$$\frac{\ddot{a}}{a} = -\frac{4\pi G}{3}\left(\rho + \frac{3}{c^2}p\right) \tag{1.13a}$$

$$\left(\frac{\dot{a}}{a}\right)^2 = \frac{8\pi G}{3}\rho \tag{1.13b}$$

It is useful for later to recognize now the Hubble parameter functional dependence

$$H(a) = \frac{\dot{a}}{a} = H_0 E(a) \tag{1.14}$$

and parametrize the Hubble constant with h

$$H_0 = \left.\frac{\dot{a}}{a}\right|_{t_0} = 100h \text{ Kms}^{-1}\text{Mpc}^{-1} \tag{1.15}$$

But if one has to solve the Friedman equations the stress energy tensor must be further specialized.

1.1.3 Perfect fluid approximation

The stress-energy tensor must take into account all the components the universe is made up of: luminous matter, dark matter, photon radiation, neutrino radiation, and so on, and, since these objects interact with one another accordingly to their nature, the picture can become very complicated, but for now, we are dealing with the Robertson-Walker metric, which assumptions rule that the various fluids do not interact at all.
Hence, leaving out the cosmological constant issue, the main distinction is the one between matter and radiation, which, in the perfect fluid limit, is exploited simply using their equation of state

$$\begin{cases} p_r = \dfrac{1}{3}c^2\rho_r & \text{radiation} \\ p_m = 0 & \text{matter} \end{cases}$$

[1] Of course also $T_{\mu\nu}$ is symmetric.

Since the universe is regarded as a closed system and, as said, these fluids do not interact, the conservation of energy must hold separately; from either the definition (1.8) of the stress energy tensor or from the application of the metric compatibility to the Einstein equation (1.9) it is easy to see that

$$\nabla^\mu T_{\mu\nu} = 0 \tag{1.16}$$

This fact joint with the equation of state allows one to solve the scale factor dependence of the densities

$$\rho_m \propto a^{-3} \tag{1.17a}$$
$$\rho_r \propto a^{-4} \tag{1.17b}$$

and, as one might suspect, it is often useful to rewrite the equations in terms of the density to the critical density ratio

$$\Omega_x = \frac{\rho_x}{\rho_c} = \rho_x \frac{8\pi G}{3H_0^2} \tag{1.18}$$

where x could stand either for the matter or the radiation.

Now it is time to take into account the consmological constant, and this can be done either adding a term to the gravitational Lagrangian $\mathcal{L}_g$ or allowing the existence of a fluid which energy tensor is of the form

$$T_{\mu\nu} = \Lambda g_{\mu\nu} \tag{1.19}$$

Even if it may seem mathematical juggling, the two ways have a profound and different meaning, as the former implies Λ is connaturated with the essence of gravitation itself, while the latter states that this is due to some kind of fluid with an akward equation of state, namely

$$p_\Lambda = -\frac{1}{3} c^2 \rho_\Lambda \tag{1.20}$$

but this is not the place to meddle in this discussion, as we don't want to explore the implication of this choice; for our purpose we can rather take it as granted and assign a scaled energy density to Λ with the identification

$$\Omega_\Lambda = \frac{\Lambda c^2}{3H_0^2} \tag{1.21}$$

and note that, using equation (1.16) is immediate to see that in this limit Ω_Λ does not evolve with time.

1.2 Linear perturbation theory

With what we have seen through here one is ready to solve the Friedman equations (1.13a) and (1.13b), but in this context we are more interested in structure formation, which isn't allowed in a pure Friedman Robertson Walker universe.
Thus to purse further our aim, and to have less boring universe, we need to introduce a little inhomogeneity and anisotropy, that together with the gravitational instability will lead to the objects we want to study.

Here we want to brifly present the method which is usally used either for analytical treatment and as a start for numerical simulation, remembering that it is outside the aim of the Thesis to show it in its full details, as we want mainly to catch a glimpse of the techniques used.

1.2.1 Perturbing the metric

The first step is to select the type of perturbation that affects the metric; various theories allow different perturbations, which can be characterized by their transformation properties and thus they can be distinguish between scalar, vector and tensor perturbations, as their evolution is uncorrelated thanks to the decomposition theorem (i.a. [6]).

In this context we chose to employ scalar perturbation, as they are directly linked to the density perturbation we want to analyze; thus we need two functions, let these be Ψ and Φ, of both t and $\overrightarrow{x}$, which action on the metric is described as

$$g_{00} = c^2 \left(1 + 2\frac{\Psi}{c^2}\right) \tag{1.22a}$$

$$g_{ij} = -a^2 \delta_{ij}(1 + 2\Phi) \tag{1.22b}$$

Obviously, if these perturbing functions are null we are left with the Robertson-Walker metric, but it is more interesting to note that if the expansion factor is identically equal to one, the metric would describe gravity in the weak field limit, and thus, in the general case, Ψ can be interpreted as a Newtonian potential and Φ a perturbation affecting the spatial curvature.
Once the perturbed stress energy of the universe is computed its evolution can be calculated through the Einstein equation (1.9).

1.2.2 Boltzmann equation

Upon perturbing the smooth universe the perfect fluid limit no longer holds and things gets messy: luminous matter must be distinguish between relativistic and

cold, namely[2] protons and electrons, and they are coupled in different ways with photons and all of them, along with neutrinos and dark matter are affected and affect the metric, hence creating an autoconsistent system once the initial perturbation is known.

The tool usually chosen to take into account all this contributions is the Boltzmann equation, which is an equation for the distribution function in the extended phase space:

$$\frac{\mathrm{d}}{\mathrm{d}t} f(t, \overrightarrow{x}, \overrightarrow{p}) = C(f) \tag{1.23}$$

and there is one equation for each of the various species roughly described above; even if it may look simple it retains the entire complexity needed to describe the complete picture: the left hand side takes into account the interaction through gravity and the peculiar characteristic of the chosen component, while the right hand side is the collision term, which depict the eventual couplings with the other distribution functions.

Note that, besides the physical situation, even the calculation could become a little messy, hence, for the rest of the Section, we are to use god-given unit[3].

Cold dark matter case

As an example of this method, and since it is important as a solid base for later on, let's apply the Boltzmann equation to the dark matter distribution f_{dm} .

By definition, dark matter perturbation is linked only to the metric, thus we don't need to bother with the collision term; in addition, as we want to deal with cold dark matter, it must be treated as a massive particle, and this gives a constraint on the momentum:

$$P^\mu = \frac{\mathrm{d}}{\mathrm{d}\lambda} x^\mu \tag{1.24a}$$

$$P^2 = g_{\mu\nu} P^\mu P^\nu = m_{dm}^2 \tag{1.24b}$$

and with these the spatial impulse and the energy are naturally defined as

$$\begin{cases} p^2 = g_{ij} P^j P^i \\ E = \sqrt{p^2 + m_{dm}^2} \end{cases}$$

[2] This is strictly true only from a certain epoch.

[3] Mainly $G = c = 1$.

Now we can express the impulse of the matter using the modulus of the spatial impulse p and its direction $\hat{p}^i$ and, letting the energy swallowing up the unpleasant mass dependence, we get

$$P^\mu = \left(E(1-\Psi), p\hat{p}^i \frac{1-\Phi}{a} \right) \tag{1.25}$$

hence now we can see the functional dependence of the dark matter distribution as $f_{dm} = f_{dm}(t,x^i,E,\hat{p}^i)$: inserting this in the collisonless Boltzmann equation yields

$$\partial_t f_{dm} + \frac{p\hat{p}^i}{aE}\partial_{\hat{p}^i} f_{dm} - \left(\frac{p^2}{E}\partial_t \log a + \frac{p^2}{E}\partial_t \Phi + \frac{p\hat{p}^i}{a}\partial_{x^i}\Psi \right) \partial_E f_{dm} = 0 \tag{1.26}$$

Since the j-th moment is given integrating last equation by $\left(\frac{p\hat{p}^i}{E}\right)^j \frac{\mathrm{d}^3 p}{(2\pi)^3}$, one can, in a way similar to non-relativistic hydrodynamics, define the numerical density n_{dm} and the velocity v^i_{dm} as

$$\begin{cases} n_{dm} = \displaystyle\int \frac{\mathrm{d}^3 p}{(2\pi)^3} f_{dm} \\ v^i_{dm} = \dfrac{1}{n_{dm}} \displaystyle\int \frac{\mathrm{d}^3 p}{(2\pi)^3} \frac{p\hat{p}^i}{E} f_{dm} \end{cases}$$

and, by using these quantities and by suppressing surface terms as usual, we can take the firsts moments of equation (1.26):

$$\partial_t n_{dm} + \frac{1}{a}\partial_{x^i} n_{dm} v^i_{dm} + 3\left(\partial_t \log a + \partial_t \Phi\right) n_{dm} = 0 \tag{1.27a}$$

$$\partial_t n_{dm} v^i_{dm} + 4\left(\partial_t \log a\right) n_{dm} v^i_{dm} + \frac{n_{dm}}{a}\partial_{x^i}\Psi = 0 \tag{1.27b}$$

Linearization

It is time to drop high order term: checking the zero moment equation (1.27a) it easy to see that, for an unperturbed universe, it would read

$$\partial_t n^0_{dm} + 3\left(\partial_t \log a\right) n^0_{dm} = 0 \tag{1.28}$$

This, which one could call the zero order equation, is equivalent to the conservation of energy for matter in (1.17a), namely $n^0_{dm} \propto a^{-3}$; thus it seems natural to choose a numerical density of the form

$$n_{dm} = n^0_{dm}(t)(1 + \delta_{dm}(t, \overrightarrow{x})) \tag{1.29}$$

where δ_{dm} is a first order quantity and it is often called the density contrast. Its equation comes from the first order of (1.27a)

$$\partial_t \delta_{dm} + \frac{1}{a}\partial_{x^i} v^i_{dm} + 3\partial_t \Phi = 0 \tag{1.30}$$

but, as this includes a velocity term, which start to be not identically zero from the first order on, we must turn our attention to the first moment equation (1.27b): neglecting second order terms and using n^0_{dm} time dependence yields

$$\partial_t v^i_{dm} + (\partial_t \log a)\, v^i_{dm} + \frac{1}{a}\partial_{x^i}\Psi = 0 \tag{1.31}$$

Note that we have no first order pressure as, again, the matter is supposed to be cold, and thus these equations can be solved simultaneously once the metric perturbation is known.
We are to talk again about the implication of this evolution in Sections 2.3 and 4.2.1, but for now let's focus on structure formation.

1.3 Beyond linear theory: the growth of perturbations

Up to now the description done fits perfectly the role of following the evolution in the early times, but once the perturbation is settled, sooner or later, in some spots, the matter can contract faster than the expansion, and thus, due to the intrinsic nature of gravity, the density contrast is bound to rise and eventually leave the linear regime; when this happens second order effect are not negligible anymore, the matter struggle to become pressure supported and the evolution is determined by the Jeans instability.

1.3.1 Gravitational instability

Since the situation is progressively dominated by local effect, it is better to analyze this scenario in the Newtonian limit and a suitable method is to slightly modifying the metric we have been using: we state that the energy-energy perturbation Ψ is mainly due to cosmological background plus a perturbation given by the dark matter component itself; in addition we can set the matter-matter Φ component to zero since it is an higher order in c respect to Ψ, so that the equations (1.22a) and (1.22a) retain the same form but are constrained by

$$\Psi = -\frac{1}{2}\frac{\partial_{t^2} a}{a}|x|^2 + \delta\Psi \tag{1.32a}$$

$$\Phi = 0 \tag{1.32b}$$

and the self-consistency is guaranteed by a Poisson equation for $\delta\Psi$.
Note that, as Φ is identically null, in this limit the zero order velocity is given by the Hubble flow, so we have no reason to neglect anymore the pressure term: it can be showned that the spatial Fourier transformed equation for the overdensity $\delta(k)$ become

$$\partial_{t^2}\delta + 2\frac{\partial_t a}{a}\partial_t\delta + \frac{k^2v^2}{a^2}\delta \simeq 4\pi G\rho^0_{dm}\delta \tag{1.33}$$

where the $\simeq$ symbol is to stress the fact that, in the real world, $\delta\Psi$ is also due to the other components of the universe, but, for the discussion to come, this is irrelevant as it would only mean that one has to substitute the unperturbed matter density ρ^0_{dm} with something like the total unperturbed energy density.

One can note that this equation resambles the Jean's one for describing the instability of a fluid due to self gravity, thus we can describe the evolution in term of Jeans length compared to the length of the structures, only remembering that, since the damping term $\partial_t\delta$ is present, the former evolve accordingly to the expansion of the universe, which act against the self gravitation of the objects considered.

The main drawback of equation (1.33) is that can be used only in the Newtonian limit, which in terms of Fourier wavenumber translates into the impossibility to use this equation if the perturbation length is larger than the causal horizon.

1.3.2 Spherical collapse

Even if equation (1.33) can be seen as the approximation of an approximation, it is complicated enough to forbid an easy analytical solution , but, as we want to have only a qualitative picture of the Jeans instability, we can limit our analysis to a particular case by adding some assumptions.
Let the initial overdensity of the region to be spherically symmetric about a point and let us use it as the origin of the spatial coordinate: the evolution of a infinitesimal shell located at $r = a\,|\overrightarrow{x}|$ is determined by the potential Ψ, that can be expressed in terms of the mass of the shell and the mean mass of the region inside the shell itself:

$$\frac{\mathrm{d}^2}{\mathrm{d}t^2}r = -\frac{GM}{r^2} \tag{1.34}$$

where $M\,(\overrightarrow{x},t) = M_b\,(\overrightarrow{x}) + \delta M\,(\overrightarrow{x},t)$ with

$$M_b = \frac{4\pi}{3}\rho^0_{dm}r^3 = \mathrm{cost} \tag{1.35a}$$

$$\delta M = 4\pi\rho^0_{dm}\int_0^r \delta r'^2\mathrm{d}r' \tag{1.35b}$$

Now we further assume that the spherical shells do not cross each other during their evolution: this guarantee that we can label each layer with increasing radii and that the order is maintained; thus this makes δM constant in time once r_i is chosen and in turn equation (1.34) can be integrated to yield

$$\frac{1}{2}\left(\frac{\mathrm{d}}{\mathrm{d}t}r\right)^2 - \frac{GM}{r} = E \tag{1.36}$$

where E is the constant which sign determines if the region final destiny is to collapse or to expand; since E is a constant of integration we can evaluate it at the time t_i chosen such that the peculiar velocities are negligible and thus, using the subscript i for the quantity at t_i we have

$$\left.\frac{1}{2}\left(\frac{\mathrm{d}}{\mathrm{d}t}r\right)^2\right|_{t_i} = \frac{1}{2}\left(H_i r_i\right) + o(v_i) \tag{1.37a}$$

$$\left.\frac{GM}{r}\right|_{t_i} = \frac{1}{2}\left(H_i r_i\right)\Omega_i(1 + \langle\delta_i\rangle) \tag{1.37b}$$

where $\langle\delta_i\rangle$ is the mean overdensity inside r_i at the time t_i; now the condition of collapse can be written as

$$\langle\delta_i\rangle > (\Omega_i^{-1} - 1) > 0 \tag{1.38}$$

where the last inequality holds since we are working in a flat universe. Still we have no clue how the region actual collapse happens, to do that we have to solve equation (1.36), and this can be done using a parametric form

$$r \propto (1 - \cos\theta) \tag{1.39a}$$

$$t \propto (\theta - \sin\theta) \tag{1.39b}$$

The picture is clearer: the shell initially expand along with the background, slows down and then turn around and collapse.
Thus in this case the constants of proportionality can be calculated using the bound seen at time t_i and imposing that the maximum expansion is achieved at r_m: the problem would be completely determined and the discussion could be carried further, working out the collapse time, the virial radius and the other parameters of the shell, but instead we want to see another approach to the nonlinear theory.

1.3.3 Zeldovich approximation

The Zeldovich approximation is suitable from scales below the causal horizon and its starting point is to express the linear theory for particles mixing the Euler and the Lagrangian description, but its application goes beyond that, as we are to discuss.

Let's take a smooth universe in which particles are depicted by their position $\overrightarrow{r} = a\overrightarrow{q}$; within the linear theory the perturbation is ought to be due to two function b and $\overrightarrow{p}$ such that

$$\overrightarrow{r}(t) = a(t)\,(\overrightarrow{q} + b(t)\overrightarrow{p}\,(\overrightarrow{q})) \tag{1.40}$$

Taking this as a definition the linear theory implies that the density contrast must satisfy

$$\delta = -b\overrightarrow{\nabla}\overrightarrow{q} \tag{1.41}$$

If one expands the initial density perturbation in its Fourier modes $A_{\overrightarrow{k}}$ the match between the linear and the Zeldovich description is achieved when

$$\overrightarrow{p}\,(\overrightarrow{q}) = \sum_{\overrightarrow{k}} \frac{i}{k^2}\,\overrightarrow{k}\,A_{\overrightarrow{k}} \exp\left(i\,\overrightarrow{k}\,\overrightarrow{q}\right) \tag{1.42}$$

and, defining the potential Φ_0

$$\Phi_0 = \sum_{\overrightarrow{k}} \frac{A_{\overrightarrow{k}}}{k^2} \exp\left(i\,\overrightarrow{k}\,\overrightarrow{q}\right) \tag{1.43a}$$

equation (1.42) become

$$\overrightarrow{p}\,(\overrightarrow{q}) = \overrightarrow{\nabla}\Phi_0\,(\overrightarrow{q}) \tag{1.43b}$$

The relation between the Newtonian potential Φ and the Zeldovich Φ_0 is obtained upon appealing to equation (1.13a)

$$\Phi = 3ab\Phi_0\partial_{t^2}a \tag{1.44}$$

Its meaning is that Φ_0 is directly linked to the gravitational potential and $\overrightarrow{p}$ is proportional to the velocity field; being the latter a gradient of the scalar function its associated matrix is diagonalizable: calling λ_i its eigenvalues the perturbed density contrast can be written as

$$\delta = \left[\sum_{i=1}^{3}(1 - b(t)\lambda_i(\overrightarrow{q}))\right]^{-1} - 1 \tag{1.45}$$

It is trivial to see that the overdense regions are the one in which one of the term approach unity, but, unlike the spherical collapse, it is sufficient for a principal axis to diverge to get to the nonlinear regime and since, by simple probability, this is case is more likely to happen than a triaxial collapse, the first nonlinear structure must be pancake like.
Moreover this approximation is important as it is usually employed to construct initial conditions in N-body simulations.

Chapter 2

Cosmological numerical simulations

Strike the first rune upon the engine's casing employing the chosen wrench. Its tip should be anointed with the oil of engineering using the proper incantation when the auspices are correct. Strike the second rune upon the engine's casing employing the arc-tip of the power-driver. If the second rune is not good, a third rune may be struck in like manner to the first. This is done according to the true ritual laid down by Scotti the Enginseer. A libation should be offered.

If this sequence is properly observed the engines may be brought to full activation by depressing the large panel marked "ON".

Runic Spaceflight - An Introduction

1989, Warhammer 40K Rogue trader

Overview

As anticipated in the introduction, we want a direct method of following the evolution of the universe, in order to have a context in which we can be able to test freely the scintillation process.
Performing a numerical cosmological simulation allows us to have such a background, hence, here, we want to understand the various aspect involved in attaining this goal: as we know the large scale evolution is to be driven by gravity, but baryons also interact through radiative transfer, and, moreover, we need proper initial conditions to start at all; since a brute force approach is not an advisable option, we must analyze the argument via the programs we have decided to use to solve the issue.

2.1 RAMSES

Numerically solving a cosmological system require either an high mass resolution, which is typically an hardware issue, and an high spatial resolution, which, instead, is heavily dependent on the methods used to simulate the physics; for this reason a lot of efforts have been driven into the improvement of numerical techniques to assure the reliability of the results, in order to have what we can call a realistic experiment.
This has spawned a number of programs, each fitting better an aspect or another, each a evolution of its predecessors: for our cosmological simulation we have decided to employ RAMSES (i.e. [30]), which is a code with a "Fully Threaded Tree" data structure where the hydrodynamical Adaptive Mesh Refinement scheme is coupled with improved particle mesh N-body solver, which solves the Poisson equation on a series of nested grids.

2.1.1 Code Implementation

Data structure

RAMSES data structure is defined as FTT, which implies that its basic element are group of cells called octs: these octs, which are made up by 2^{dim} cells[1], are labelled by the index l, that takes into account the level of refinement of the grid they belong to, being $l = 0$ the cartesian one. Each oct is either double linked to the other octs of the same level l and either to their parents and children at, respectively, the level $l - 1$ and $l + 1$; if a cell has children it is called a split cell, otherwise a leaf cell.

To ensure a smooth transition between maps at various levels, for every oct to be refined its neighbours are also marked for refination, and thus every children end up having $3^{dim} - 1$ parents.
Each particle that is inside the boundary of an oct belong to that oct and is linked to the other particles satisfying the same condition; the creation of this list is done initially storing the particles in the coarse grid level $l = 0$ and then recursively splitting them among the children octs up to the maximum chosen level of refinement $l = l_{max}$.

Now on, for the rest of this Chapter, we are to use a rather self explanatory notation, the main non-standard feature being the use of the upperscript p to label particles and, when needed, the subscript l to denote the mesh level the variable belong to.

[1] Where *dim* is the integer indicating the number of spatial dimensions.

Time evolution

The implementation of AMR evolution is done recursively starting from $l = 0$ to $l = l_{max}$. The first step is to generate the new refinement level $l + 1$, and this is done by interpolate conservatively level l variables: the particles are moved testing the boundary of their parents, in this way avoiding to build the whole three from the base level at every time step.

Then the time step Δt_l is calculated applying the standard stability conditions, namely it is chosen to be the minimum among the relevant scale: the free fall time, the crossing cell time and the Hubble time, which is used only in the early stages; additionally the Courant Friedrich Levy stability condition is applied, so that the actual calculation is

$$\Delta t_l = \min \begin{cases} C_1 \min_l t_{ff}, & C_2 \Delta x_l \left(\max_l |\overrightarrow{v}_p| \right)^{-1}, \\ C_3 \dfrac{a}{\dot{a}}, & C_4 \Delta x_l \left(\max_{l,j} v_j + c_s \right)^{-1} \end{cases} \tag{2.1}$$

where the C_i are less then unity constants, c_s is the medium sound speed and the further constraint $\Delta t_l \leq \Delta t_{l-1}$ is imposed.

At this point level $l + 1$ is advanced in time and Δt_l is synchronized with Δt_{l+1} accordingly to the chosen user defined case, which can be either single or adaptive.

After that the boundary conditions for l are generated: while at the base level these are user supplied, the ones needed by the others are given by the solution of level $l - 1$, which is assumed to be constant during the mesh evolution; the proper reconstruction is done using an interpolation which is a generalization of the Min-Mod limiter and is stored in a temporary buffer.
Then the hydrodinamics is computed, the new refinement map is constructed and the cycle is repeted.

2.1.2 Solving methods

In this Section we want to explain the techniques used to solve the equations being responsable for the baryons and the dark matter evolution.
Note that, as RAMSES is thought as a multi-purpose program, the equations are not written directly for the cosmological enviroment: this setting is achieved using the so called super moving coordinate, a set of variable that has the property of transforming all but the Poisson equation in their relativistic counterpart without

changing their form:

$$\mathrm{d}\tilde{t} = \frac{H_0}{a^2}\mathrm{d}t \tag{2.2a}$$

$$\tilde{x}_i = \frac{1}{aL}x_i \tag{2.2b}$$

where L is the size of the computational box. Let's review the method used in solving the evolution.

The gravitational field

The density field is calculated with a Cloud In Cell interpolation scheme: formerly the particle of the level l are checked against the boundary of the mesh, then particles of the parent octs at level $l-1$ are included if they intersect the volume considered; in this way the density inferred is equal to the one obtained from a Cartesian mesh.

Having the density the Poisson equation can be solved

$$\Delta\tilde{\phi} = \frac{3}{2}a\Omega_m\left(\tilde{\rho} - 1\right) \tag{2.3}$$

where $\tilde{\rho}$ is the density evaluated in the super moving reference

$$\tilde{\rho} = \frac{a^3}{\Omega_m\rho_c}\rho \tag{2.4}$$

The Laplacian is approximated by a $2dim + 1$ points finite difference and different approach are used depending on the mesh l.
The base level is solved with the fast Fourier transform, using as Green function the Fourier transform of the "Laplacian", while for finer levels the Gauss Seidel relaxation method is employed: first the potential is calculated solving the Dirichlet problem, then it is corrected using the over relaxation parameter, and the cycle is repeted until the norm of the residual has been reduced by a chosen factor; the initial guess is the potential lineary reconstructed from the level $l-1$, and, since the computational volume is not completely covered by the mesh, a rule of thumb is used to calculate the optimal over relaxation parameter, in order to have the algorithm converging rapidly enough.

N-body

After solving the gravitational potential the following phase is to evolve the particles, and this is done via the standard equations

$$\frac{\mathrm{d}}{\mathrm{d}t}x_i^p(t) = v_i^p(t) \tag{2.5a}$$

$$\frac{\mathrm{d}}{\mathrm{d}t}v_i^p(t) = -\nabla_i\phi(t) \tag{2.5b}$$

Firstly we are interested in the acceleration: this is computed approximating the gradient with the standard 5-points finite difference and then interpolating back with an inverse CIC scheme on the particles currently considered, which are the ones whose cloud is within the level boundary; the cloud may be partially outside the volume of the mesh, for those particles the acceleration is interpolated from their coarser level.

When the acceleration at time n is known, using the finite difference equivalent of equations (2.5), we are ready to evolve the particles, and this is achieved in two step:

$$\left|\begin{array}{l} v_i^p\left(n+\frac{1}{2}\right) = v_i^p(n) - \nabla_i\phi(n)\frac{\Delta t}{2} \\ x_i^p(n+1) = x_i^p(n) + v_i^p\left(n+\frac{1}{2}\right)\Delta t \end{array}\right. \qquad \text{prediction}$$

$$v_i^p(n+1) = v_i^p\left(n+\frac{1}{2}\right) - \nabla_i\phi(n+1)\frac{\Delta t}{2} \qquad \text{correction}$$

Note that the second step can only be completed later when the new acceleration is computed; this is done to avoid an additional call of the Poisson solver, but, in the case of adaptive time step, a correct evolution implies that the state of the particle must be known, requiring an additional integer in the particle data structure.

Hydrodinamics

The final equations to solve are the ones belonging to the fluid component

$$\partial_t\rho + \nabla_i\rho v_i = 0 \tag{2.6a}$$

$$\partial_t\rho v_i + \nabla_i\rho v_j v_i + \nabla_i P = -\rho\nabla_i\phi \tag{2.6b}$$

$$\partial_t\rho e + \nabla_i\rho v_i\left(e+\frac{P}{\rho}\right) = -\rho v_i\nabla_i\phi \tag{2.6c}$$

where e is the internal energy per unit mass, and the system closure is given by the equation of state

$$P = (\Gamma-1)\left(e-\frac{1}{2}v^2\right)\rho \tag{2.6d}$$

and Γ is taken to be a constant.
Note that the hydrodinamical quantities are additionally modified by the supermoving coordinate as follows

$$\tilde{p} = \frac{a^5}{\Omega_m\rho_c H_0^2 L^2} \tag{2.7a}$$

$$\tilde{v}_i = \frac{a}{H_0 L}v_i \tag{2.7b}$$

and again here L is the box length.
The advantage given by the use of the conservative form is that all but the state equation can be viewed as continuity equations for a variable Q and its associated flux F, with the addition of a source S when needed, so that the discretization at the point j and time n of can be done as follows

$$\frac{Q\left(j,n+1\right)-Q\left(j,n\right)}{\Delta t}+\frac{F\left(j+\frac{1}{2},n+\frac{1}{2}\right)-F\left(j-\frac{1}{2},n+\frac{1}{2}\right)}{\Delta x}=S\left(j,n+\frac{1}{2}\right)$$

As pointed early, the hydrodynamic is calculated at the end of the evolution loop: this mean that a single grid Godunov solver is employed to calculate the fluxes, each one is computed using a iterative Riemann solver to give the required precision at the contact discontinuity, averaged with near finer grid ones if necessary and used to update the variables of cell that have no children, while the other cells in the mesh change their variables value accordingly with the averaged fluxes of the finer level.

2.2 ATON

RAMSES alone is not suited to solve the scintillation problem that, as we eventually see in Chapter 3, is explicitly related to the electrons density, which must be properly calculated to have a suitable simulation aimed toward this issue, and thus one is compelled to take into account the radiative transfer.
Thankfully RAMSES distribution come with the built in option to activate a coupled radiative solver, namely ATON (i.e. [1]), which does not solves simultaneously the transfer equation, but rather act post processing the hydrodynamical output every time step, and this solution is what we need considering that, on the scale of interest, the dynamic is mainly driven by the dark matter component.

In the next Sections we are going to analyze the needed radiative process and the techniques used to solve them using ATON.

2.2.1 Radiative transfer with the moment equations

ATON handles the radiative transfer equation solving its moments, but, as it usually happens in this kind of approach, the system is not self-consistent, thus some sort of closure must be introduced and, as an additional feature of this problem, one must ensure that the consistency with the hydrodynamic is preserved.

To illustrate the method used firstly it can be noted that, in terms of the specific intensity per unit of frequency $I^{\nu}=I^{\nu}\left(\overrightarrow{x},\hat{n},t\right)$, the basic equation written in the

supermoving coordinate used by RAMSES reads as in a non relativistic enviroment

$$(\partial_t + l_i \nabla_i)\, I^\nu = -\kappa^\nu I^\nu + \frac{\mu^\nu}{\kappa^\nu} \tag{2.8}$$

where the $\hat{l}$ is the line of sight versor, κ^ν the absorption coefficient and μ^ν the emission coefficient per unit of density.
To solve this equation ATON relays on the first two moments along the line of sight, which can be calculated in terms of the energy density E^ν, the flux, the K-moment and the integrated source.
In this context the source is meant to be isotropic, as it is due to to the diffuse radiation coming from stars and quasar and the recombination photons (i.a. [12]), so that the only useful term it gives is its mean

$$\int \mathrm{d}l \frac{\mu^\nu}{\kappa^\nu} = h\nu S^\nu = h\nu(\dot{N}_* + \dot{N}_{rec}) \tag{2.9}$$

By observing this equation, one can see that it is much more feasible to write the system in term of the photon number density $N^\nu = E^\nu (h\nu)^{-1}$, thus we can slightly change the usual definition of the intensity moments to have

$$\hat{l}^0 \quad \mapsto \quad \partial_t N^\nu + \nabla_i F_i^\nu = -\kappa c N^\nu + S^\nu \tag{2.10a}$$

$$\hat{l}^1 \quad \mapsto \quad \partial_t F_j^\nu + \nabla_i K_{ij}^\nu = -\kappa c F_j^\nu \tag{2.10b}$$

Hydrogen example

As we want only to expose the method employed we can restrict the analysis to the case of a mono hydrogenic composition, remembering that it can be easily generalized to more of complicated mixtures.

Calling n^{H_I} the neutral hydrogen number density and σ^ν the photoionizzation cross section we can write the total absorption as

$$\kappa^\nu = n^{H_I} \sigma^\nu \tag{2.11}$$

and one is tempted to solve the equations in term of the ionizing photons, namely the ones with a frequency greater than the threshold ν_{H_I}

$$N^\gamma = \int_{\nu_{H_I}}^{\infty} \mathrm{d}\nu N^\nu \tag{2.12}$$

but we have to deal properly with the terms including the cross section, as one time it is averaged with the number density and the other with the flux.

In our case we can state that these two are nearly equal and due to a given reference radiation $J_0 = J_0(\nu)$ from which the averaged cross section can be precomputed

$$\sigma_\gamma = \left(\int_{\nu_{H_I}}^{\infty} \mathrm{d}\nu \sigma^\nu 4\pi (h\nu)^{-1} J_0 \right) \left(\int_{\nu_{H_I}}^{\infty} \mathrm{d}\nu 4\pi (h\nu)^{-1} J_0 \right)^{-1} \tag{2.13}$$

and, additionally we can substitute the source term $\dot{N}_{rec}$ using the recombination coefficients α_A and α_B (e.g. [13]), which take into accont if the line of sight is respectively optically thin or thick to the radiation,

$$\dot{N}^\gamma_{rec} = \int_{\nu_{H_0}}^{\infty} \mathrm{d}\nu \dot{N}_{rec} = n_e n_{H_{II}} (\alpha_A - \alpha_B) \tag{2.14}$$

With these relations the system (2.10) can be written as

$$\partial_t N^\gamma + \nabla_i F^\gamma_i = -n_{H_I} \sigma_\gamma c N^\gamma + \dot{N}^\gamma_* + n_e n_{H_{II}} (\alpha_A - \alpha_B) \tag{2.15a}$$
$$\partial_t F^\gamma_j + \nabla_i K^\gamma_{ij} = -n_{H_I} \sigma_\gamma c F^\gamma_j \tag{2.15b}$$

Now it is evident that, in order to push further the analysis, we must know the hydrogen ionization fraction, which is given by the detailed balance of the process

$$\partial_t n_{H_I} = \alpha_A n_e n_{H_{II}} \beta n_e n_{H_I} - c\sigma^\gamma N^\gamma n_{H_I} \tag{2.16}$$

with the constraint due to the case taken into consideration

$$n_e = n_{H_{II}} \tag{2.17a}$$
$$n_{H_I} + n_{H_{II}} = \mathrm{cost} \tag{2.17b}$$

Obviously the energy equation of the gas must be taken into account, hence we can use equation (2.6c) written in term of the heating and the cooling rate

$$\rho \partial_t e_{int} = H - L \tag{2.18}$$

where e_{int} is the internal energy per unit density and, in this case, the heating is given by the photoionization

$$H = n_{H_I} hc \int_{\nu_{H_0}}^{\infty} \mathrm{d}\nu \, (\nu - \nu_{H_0}) \, \sigma N \tag{2.19}$$

while the cooling is given by the sum of the recombination, collisional ionization and bremsstrahlung (i.a. [17]).

System closure

We have yet to close the momentum system, and this can be done giving some assumption that allows to determines the Eddington tensor

$$\overleftrightarrow{D} = \frac{c^2}{N}\overleftrightarrow{K} \tag{2.20}$$

The relevant assumption in ATON is that the radiation angular distribution is axisymmetric around the flux, which we can write as

$$\overrightarrow{F} = (cNf)\,\hat{u} \tag{2.21}$$

so that the Eddinton tensor assumes the form

$$D_{ij} = \frac{1-\chi}{2}\delta_{ij} + \frac{3\chi-1}{2}u_i u_j \tag{2.22}$$

thus making the isotropic component, which gives rise to the diffuse radiation, separated from the free streaming one, which is aligned with flux direction $\hat{u}$: namely this approximation consist in describing the intermediate case with a linear combination of the extreme ones.
Note until this point the functional dependence of the Eddington factor $\chi = \chi(f)$ is constrained only by

$$\frac{1}{3} \leq \chi \leq 1 \tag{2.23}$$

and thus the M1 model (i.e. [1]) is further assumed, which rules that

$$\chi = \frac{3+4f^2}{5+2\sqrt{4-3f^2}} \tag{2.24}$$

which is the most simple and meaningful, since it corresponds to the angular distribution of a isotropic radiation Lorentz boosted along $\hat{u}$, which is similar to the case of the CMB dipole.

2.2.2 Computing scheme

The code implementation is achieved by succesive steps: first the number of ionizing photon is updated in time for every cell, the sourceless hyperbolic moment system (2.15) is solved and finally the thermochemical step is computed, namely the right hand side of equations (2.15a) and (2.15b), which must be solved accordingly to the heating and cooling evolution.
The actual discretization is simply given by the equation seen so far, solved with the operator splitting technique depicted above.

Here the relevant issue we want to discuss is the resolution time used for the evolution. Focusing on the in the second step hinted above and using a notation similar to the Ramses hydrodynamic implementation (see Section 2.1.2), we can write the coupled equations in (2.15) for time n and at the point i as

$$\frac{\mathcal{Q}\left(n+1,i\right)-\mathcal{Q}\left(n,i\right)}{\Delta t}+\frac{\mathcal{F}\left(m,i+\frac{1}{2}\right)-\mathcal{F}\left(m,i-\frac{1}{2}\right)}{\Delta x}=0 \tag{2.25}$$

where $\mathcal{Q}$ represents either N or $\overrightarrow{F}$ and $\mathcal{F}$ its associated flux which is respectively $\overrightarrow{F}$ or $\overleftrightarrow{K}$. The time m is selected accordingly to the solving scheme, which can be chosen to be explicit, fixing $m=n$, or implicit, namely $m=n+1$.
Fixing a scheme gives different constraint on the time step Δt and rules the solving method for the flux at time m.

Using the implicit scheme is computational costly and difficult to implement, while using an explicit scheme yields an heavy constraint on the time step. What is done in ATON is to rely on the latter scheme, using a relaxed condition for the time step: the evolved at time $n+1$ flux is given by (i.a. [10])

$$\mathcal{F}\left(n,1+\frac{1}{2}\right)=\frac{\mathcal{F}\left(n,1+1\right)+\mathcal{F}\left(n,1\right)}{2}-\frac{c}{2}\mathcal{Q}\left(n,1+1\right)-\mathcal{Q}\left(n,1\right) \tag{2.26}$$

where the c factor arise as the maximum wave propagation speed has been taken equal to the speed of light.
The Courant condition (see section 2.1.1) on the time step would imply

$$\Delta t<\frac{1}{3}\frac{\Delta x}{c}$$

which, in the cosmological environment, would rule a time interval much smaller than the actual evolution time scale, thus augmenting the computational time in quite a needless way.
The solution chosen is to replace the speed of light in all[2] of the equations considered so far with effective speed of light c_{eff}, typically in the range

$$10^{-3}<\frac{c}{c_{eff}}<1$$

Even if this is an approximation, it has been shown that this technique is allowed in the cosmological background we are to simulate, since it gives no relevant errors (e.g. [1]).
However this argument does not apply to the energy equation, which, as we have

[2]Namely only in Section 2.2.

seen, in this context is substituted by the system of coupled equations for the evolution of the temperature and of the ionization fraction; this happens because the cooling processes become more quick then the chosen Δt as the temperature approach $T \sim 10^4$ K.
To recover the correct evolution the calculation of the energy is performed within every radiative transfer main step as a subcycle, with a time step of the order of the cooling time scale.

2.3 GRAFIC

The initial conditions for the particles distributions of our simulation have been created using the group of utilities that goes under the name GRAFIC (i.e. [4]), which is an acronym for Gaussian RAndom Field Initial Conditions.

The underlying concept is that it is possible to generate a perturbation for the matter component on varius scale lengths with periodic boundary using the transfer function method (i.a. [6]), so that the perturbation itself is given by convolving the transfer function T with a Gaussian white noise ζ

$$\delta\left(\overrightarrow{x}\right) = \int \mathrm{d}\overrightarrow{y}\,\zeta\left(\overrightarrow{y}\right) T\left(|\overrightarrow{x} - \overrightarrow{y}|\right) \tag{2.27}$$

where the power spectrum of the noise is simply

$$\left\langle \zeta\left(\overrightarrow{x}\right)\zeta\left(\overrightarrow{y}\right)\right\rangle = (2\pi)^3 \delta_d\left(\overrightarrow{x} - \overrightarrow{y}\right) \tag{2.28}$$

and δ_d is the three-dimensional Dirac delta function. Note that, by definition, the transfer function T is linked to the matter power spectrum $P(k)$ via

$$\tilde{T}(k) = \sqrt{P(k)} \tag{2.29}$$

thus, implementation aside, this code relies on the method used to calculate $P(k)$, which can be done evolving the cold dark matter initial power spectrum (i.a. [21])

$$P_{_{CDM}}(k) \propto k^n \left(1 + C_1 k + C_2 k^{\frac{3}{2}} + C_3 k^2\right)^{-2} \tag{2.30}$$

by interpolating (e.g. [3]) it in the range of interest and up to the starting redshift; here C_i are fixed constants, the index n is related to the shape of the perturbation at the time it cross the horizon

$$\delta_{t_{enter}}(k) \propto k^{\frac{n}{2}-2} \tag{2.31}$$

and the normalization is usually given in term of the value of σ_8, which[3] is the standard deviation of the mass distribution over 8 comoving Mpc.

Note that, in principle, equation (2.30) could be derived performing a numerically integration of the advanced results of the perturbation theory hinted in Chapter 1: in this Thesis we are to expose the analytical view point in Section 4.2.1.

[3]See equation (4.5b).

Chapter 3

Scintillation theory

Anything that happens, happens. Anything that, in happening, cause something else to happen, causes something else to happen. Anything that, in happening, causes itself to happen again, happens again. It doesn't necessarily do it in chronological order though.

1992, Mostly harmless, Douglas Adams

3.1 Formal treatment

In this Section we are going to analyze the scintillation phenomenon from a mathematical view point and this task is both difficult and subtle: the fundamental issue is that the equations depend on random component that can't be measured directly; this fact rules that the problem can only be dealt with approximate methods, thus our discussion is focused on the implications and the limits of these techniques.

3.1.1 Basic wave equation

The first thing to do in order to understand how the scintillation works is to describe the electromagnetic field: the relevant equations we are interest in are the following:

$$\overrightarrow{\nabla} \times \overrightarrow{E} = -\frac{1}{c}\partial_t \overrightarrow{B} \tag{3.1a}$$

$$\overrightarrow{\nabla} \times \overrightarrow{H} = \frac{1}{c}\partial_t \overrightarrow{D} + \frac{4\pi}{c}\overrightarrow{J} \tag{3.1b}$$

$$\overrightarrow{\nabla}\overrightarrow{D} = 4\pi\rho \tag{3.1c}$$

$$\overrightarrow{\nabla}\overrightarrow{B} = 0 \tag{3.1d}$$

where

$$\overrightarrow{D} = \epsilon\overrightarrow{E} \tag{3.2}$$

Let's suppose for simplicity sake that the magnetic field is unaffected by matter, this assumption could be written as

$$\overrightarrow{H} = \overrightarrow{B} \tag{3.3}$$

Note that, since in our problem we have a localized source, equation (3.1c) can be splitten into two, one which rules the behavior field near the source and one which is valid in the transmission region: the former is a continuity equation, while in the latter case we can safely ignore the current and charge density

$$\overrightarrow{\nabla}\,\overrightarrow{J} + \partial_t \rho = 0 \tag{3.4a}$$

$$\overrightarrow{\nabla}\,\overrightarrow{D} = 0 \tag{3.4b}$$

hence in the transmission region we have

$$\overrightarrow{\nabla}\,\overrightarrow{E} = -\overrightarrow{E}\,\overrightarrow{\nabla}\log(\epsilon) \tag{3.5}$$

Now let's try to reduce the problem to a single fundamental equation; taking the curl of (3.1a) yields

$$\overrightarrow{\nabla} \times \overrightarrow{\nabla} \times \overrightarrow{E} = -\frac{1}{c^2}\partial_{t^2}\epsilon\overrightarrow{E} - \frac{4\pi}{c}\partial_t \overrightarrow{J} \tag{3.6}$$

where one can develope the double curl with the usual vector product rules to find

$$\nabla^2\overrightarrow{E} - \frac{1}{c^2}\partial_{t^2}\epsilon\overrightarrow{E} = \frac{4\pi}{c}\partial_t\overrightarrow{J} - \overrightarrow{\nabla}\left(\overrightarrow{E}\overrightarrow{\nabla}\log\epsilon\right) \tag{3.7}$$

The second term in the right end side of the equation describe polarization changes of the medium and this effect is usually negligible (e.g. [32]).
As one expects the time scale variability of the the dielectric is order of magnitude larger than the ones for the electric field and the current, hence equation (3.7) can be Fourier analyzed as if one has to deal with the void case

$$\begin{cases} \overrightarrow{E} = \overrightarrow{E}\,(\overrightarrow{r})\exp(-i\omega t) \\ \overrightarrow{J} = \overrightarrow{J}\,(\overrightarrow{r})\exp(-i\omega t) \end{cases} \Rightarrow \left(\nabla^2 - f(\epsilon)\right)\overrightarrow{E}\,(\overrightarrow{r}) = -4\pi i\frac{\omega}{c}\overrightarrow{J}\,(\overrightarrow{r})$$

where f is implicitly defined as the function

$$f(\epsilon) = \frac{e^{i\omega t}}{c^2}\partial_{t^2}e^{-i\omega t}\epsilon = \left(k^2 - \frac{2ik}{c}\partial_t + \frac{1}{c^2}\partial_{t^2}\right)\epsilon$$

It quite trivial to see that the first term is the dominant one (ibidem) so we can reduce equation (3.7) to

$$\left(\nabla^2 + k^2\epsilon\,(\overrightarrow{r},t)\right)\overrightarrow{E}\,(\overrightarrow{r}) = -4\pi ik\overrightarrow{J}\,(\overrightarrow{r}) \tag{3.8}$$

The problem with equation (3.8) is that in the context we are to work the functional dependence of ϵ is not given esplicitly, as it is due to the turbulent motion of the medium itself.

For now we are to postpone the analysis of turbulence, treating this chaotich behavior of the medium by splitting the dielectric constant into an average time independent part and a fluctuating term: the latter is responsible for the scintillation and, since it is directly due to the underlying turbulence, it must be regarded as a stochastic fluctuation to be described with its power spectrum, like in the hydrodynamical environment.
Relying on the hydrodynamic treatment we are implicitly making an important assumption: we are supposing that this process is ruled by the ergodic theorem, which, crudely, assures that one can confuse spatial average with temporal one.

3.1.2 Geometrical optics

In order to solve (3.8) we employ something similar to the WKB approximation, the one used, for instance, to deal with time dependent frequency harmonic oscillators; the discussion do not lose generality if considered in the scalar version so, for notation simplicity sake, in the following we are to examine only this case.

Let's take an electric field of form

$$E = A\left(\overrightarrow{r}\right) e^{ik\Psi\left(\overrightarrow{r}\right)} \tag{3.9}$$

where the function Ψ is called the iconal, and is central to this analysis. Expanding the amplidute in series of power of the wavelength

$$A\left(\overrightarrow{r}\right) = \sum_{j=0}^{\infty} (ik)^{-j} A_j\left(\overrightarrow{r}\right) \tag{3.10}$$

equation (3.8) can be rewritten gathering terms with equal power of k

$$0 = \left(\nabla^2 + k^2\epsilon\right) E = \sum_{j=0}^{\infty} (ik)^{2-j} f_i\left(A_{l_1}, \ldots, A_{l_m}, \Psi, \epsilon\right) \tag{3.11}$$

with f_i functions to be calculated case by case and where we have dropped the source term J since we are to work in the so called transmission regime.
As the equation has to hold for every wavelength we impose that every f_i vanishes individually; checking the first one, for $j = 0$, yields

$$\left(\overrightarrow{\nabla}\Psi\right)^2 = \epsilon \tag{3.12a}$$

This is the iconal equation: the knowledge of ϵ determines[1] the functional shape of Ψ and the next term, $j = 1$, gives a transport equation

$$2\overrightarrow{\nabla}\Psi\left(\overrightarrow{r}\right)A_1 + A_1\nabla^2\Psi = 0 \tag{3.12b}$$

Here comes the geometrical optics relevant assumption: if we restrict ourselves to the case in which we do not consider successive order equations we are obviously committing an error: calling A_1 simply A and inserting the first order truncated solution found for E back into (3.8), it is easy to see that this system of equations is equivalent to (3.12) only if the term

$$\frac{1}{k^2}\frac{\nabla^2 A}{A}$$

can be neglected. Now we do assume this, assuring that the consequences are to be examined later.

Wave trajectory

We want to calculate the ray path: almost by definition the wave front is given by the condition $\Psi =$ costant, being these planes perpendicular to the trajectory; parametrizing the latter with the variable s chosen to be proportional to the arc-length, the tangent vector

$$\hat{t} = \frac{\mathrm{d}}{\mathrm{d}s}\overrightarrow{r}$$

become a versor, and thus the iconal equation formally can be uniquely solved:

$$\Psi = \int \mathrm{d}s\sqrt{\epsilon(s)} \tag{3.13}$$

or, writing it locally,

$$\overrightarrow{\nabla}\Psi = \sqrt{\epsilon}\hat{t} \tag{3.14}$$

Deriving the equation just found along the curve which describes the path

$$\begin{aligned}\frac{\mathrm{d}}{\mathrm{d}s}\left(\sqrt{\epsilon}\frac{\mathrm{d}}{\mathrm{d}s}\overrightarrow{r}\right) &= \frac{\mathrm{d}}{\mathrm{d}s}\overrightarrow{\nabla}\Psi = \\ &= \left(\frac{\mathrm{d}}{\mathrm{d}s}\overrightarrow{r}\overrightarrow{\nabla}\right)\overrightarrow{\nabla}\Psi = \\ &= \frac{1}{\sqrt{\epsilon}}\left(\overrightarrow{\nabla}\Psi\overrightarrow{\nabla}\right)\overrightarrow{\nabla}\Psi = \\ &= \frac{1}{2\sqrt{\epsilon}}\overrightarrow{\nabla}\left(\overrightarrow{\nabla}\Psi\right)^2\end{aligned}$$

[1] Since the f_i with $i > 0$ are independent of ϵ.

and using again equation (3.12a) the trajectory is given by

$$\frac{\mathrm{d}}{\mathrm{d}s}\left(\sqrt{\epsilon}\frac{\mathrm{d}}{\mathrm{d}s}\overrightarrow{r}\right) = \overrightarrow{\nabla}\sqrt{\epsilon} \tag{3.15}$$

One-dimensional case

It is useful to apply what we have seen about the geometrical optics approximation to a particular case: suppose the dielectric constant depends only on one coordinate and let this coordinate be $\hat{z}$.
To further solve the problem we have to choose initial conditions: we can set α_0 and $\frac{\pi}{2}$ to be the initial inclination angles between $\hat{x}$ and $\hat{y}$; by inserting these conditions in equation (3.15) we have

$$\hat{x} \mapsto \sqrt{\epsilon}\frac{\mathrm{d}}{\mathrm{d}s}x = \sqrt{\epsilon\left(z=0\right)}\cos\left(\alpha_0\right) \tag{3.16a}$$

$$\hat{y} \mapsto \sqrt{\epsilon}\frac{\mathrm{d}}{\mathrm{d}s}y = 0 \tag{3.16b}$$

Calling $\alpha = \arccos\left(\frac{\mathrm{d}x}{\mathrm{d}s}\right)$ the angle of inclination along the trajectory we recover Snell's law, while the meaning of equation (3.16b) is that the the motion is on the plane ($\hat{x}$,$\hat{z}$) only.

Now we can turn our attention to the $\hat{z}$ component equation, which, combined with (3.16a) gives

$$\hat{z} \mapsto \frac{\mathrm{d}^2}{\mathrm{d}x^2}z = \frac{\sec^2\alpha_0}{2\epsilon(0)}\partial_z\epsilon \tag{3.16c}$$

This equation can be rapidly solved and yields x as a function of z

$$x = \cos\alpha_0\int_0^z \mathrm{d}u\left(\frac{\epsilon(u)}{\epsilon(0)} - \cos^2\alpha_0\right)^{-\frac{1}{2}} \tag{3.17}$$

Now we want to calculate the wave properties in this context and see the effects of a perturbation around this case.

Phase

By the definition of the iconal the phase of the wave is given by

$$S = k\Psi = k\int \mathrm{d}s\sqrt{\epsilon} \tag{3.18}$$

and, specializing the medium to be a slab of thickness d and using the equation for the trajectory, we can write

$$\begin{aligned} S =& k \int_0^d \mathrm{d}z \sqrt{\epsilon \left(1 + \frac{\mathrm{d}^2}{\mathrm{d}z^2} x\right)} = \\ =& k \int_0^d \mathrm{d}z \left(\epsilon(z) - \epsilon(0) \cos^2 \alpha_0\right)^{-\frac{1}{2}} \epsilon(z) \end{aligned}$$

where we can note that in the case of $\epsilon(z)$ being a simple constant this equation reduces to

$$S = \frac{kd}{\sin \alpha_0} \tag{3.19}$$

Now let's turn to something more interesting: suppose that ϵ can be splitten into a stationary part and a small fluctuating one

$$\epsilon = \epsilon(z) + \Delta\epsilon\left(\overrightarrow{r}, t\right) \quad \text{with} \quad \frac{\Delta\epsilon}{\epsilon} \ll 1 \tag{3.20}$$

so that the now time dependent phase can be written as

$$S(t) = k \int \mathrm{d}s \left(\sqrt{\epsilon} + \frac{\Delta\epsilon}{2\sqrt{\epsilon}}\right) \quad + \circ\left(\Delta\epsilon^2\right)$$

In this way the phase can be divided into a nominal value and a random component

$$S(t) = S_0 + \phi(t) \tag{3.21a}$$

where

$$\phi = \frac{1}{2} k \int \mathrm{d}s \frac{\Delta\epsilon}{\sqrt{\epsilon}} \tag{3.21b}$$

For instance, in the case of a star seen through the atmosphere $\epsilon(z)$ would be equal to 1 and the phase shift would be given as

$$\phi = \frac{1}{2} \frac{k}{\sin \alpha_0} \int_0^\infty \mathrm{d}z \Delta\epsilon$$

Angle of arrival

As we have seen for a given ϵ the trajectory is completly determined by equation (3.15). Again we add a small fluctuating component to the refraction index: now is quite obvious that the $\hat{y}$ component doesn't vanish

$$\hat{y} \mapsto \frac{\mathrm{d}}{\mathrm{d}s} \left(\frac{\mathrm{d}}{\mathrm{d}s} y \sqrt{\epsilon + \Delta\epsilon}\right) = \frac{1}{2} \left(\epsilon + \Delta\epsilon\right)^{-\frac{1}{2}} \partial_y \Delta\epsilon$$

With the usual limit we can define the angular shift as

$$\delta\theta_\perp = \frac{\mathrm{d}}{\mathrm{d}s}y = \frac{1}{2\sqrt{\epsilon(0)}}\int \frac{\mathrm{d}s}{\sqrt{\epsilon(s)}}\partial_y\Delta\epsilon \tag{3.22a}$$

where the subscript $\perp$ is to remind that the unperturbed trajectory layes on the $(\hat{x},\hat{z})$ plane; turning our attention to the perturbation on this plane we define

$$\delta\overrightarrow{n} = -\delta x\sin\alpha\hat{x} + \delta z\cos\alpha\hat{z}$$

as the vector which describe the variation; here we have implicitly assumed that the x and z component could be written as an unperturbed part plus a small component. With the introduction of $\delta\overrightarrow{n}$ and the normal derivate, defined as

$$\partial_n = \cos\alpha\partial_z - \sin\alpha\partial_x$$

we can simultaneously solve the remaining equations

$$\delta\theta_n = \frac{\mathrm{d}}{\mathrm{d}s}y = \frac{1}{2\sqrt{\epsilon(0)}}\int \frac{\mathrm{d}s}{\sqrt{\epsilon(s)}}\partial_n\Delta\epsilon \tag{3.22b}$$

By recalling the definition of the phase shift given in equation (3.21b) we can write (3.22a) and (3.22b) as

$$\delta\overrightarrow{\theta} = \frac{1}{k\sqrt{\epsilon}}\overrightarrow{\nabla}_\perp\phi \tag{3.23}$$

where $\delta\overrightarrow{\theta}$ is the angular vector error as defined by Chandrasekhar.

Amplitude

Having solved the iconal equation we can focus on the amplitude, which, as said, is described by the transport equation. Combining these informations

$$\begin{aligned} A(r) &= A(0)\exp\left(-\frac{1}{2}\int_0^r \frac{\mathrm{d}s}{\sqrt{\epsilon(s)}}\nabla^2\Psi\right) = \\ &= A(0)\exp\left(-\frac{1}{2}\int_0^s \frac{\mathrm{d}s}{\sqrt{\epsilon(s)}}\nabla^2\int_0^s \mathrm{d}s'\sqrt{\epsilon'}\right) \end{aligned}$$

The laplacian can be expressed in term of the coordinates normal and along the trajectory

$$\nabla^2 = \partial_{s^2} + \nabla_\perp^2$$

if one puts this in the equation for the amplitude it is easy to seen that the term rising form the normal gradient vanishes, as Ψ is tangent to the trajectory

$$A(r) = A(0)\exp\left(-\frac{1}{2}\int_0^r \frac{\mathrm{d}s}{\sqrt{\epsilon(s)}}\partial_{s^2}\Psi\right) = \\ = \exp\left(-\frac{1}{4}\frac{\log\epsilon(r)}{\log\epsilon(0)}\right)$$

In turn a dielectric perturbation could be affected by the gradient in the normal direction

$$A(r) + \delta A = A(r)\exp\left(-\frac{1}{4}\int_0^s \frac{\mathrm{d}s}{\sqrt{\epsilon(s)}}\nabla^2\int_0^s \mathrm{d}s'\frac{\Delta\epsilon'}{\sqrt{\epsilon'}}\right)$$

Note that the nominal amplitude has been absorbed into the prefactor, and thus is useful to describe this variation as the logarithmic amplitude fluctuation χ

$$\log\left(\frac{A(r)+\delta A}{A(r)}\right) = \log(1+\chi) \tag{3.24}$$

Exploiting the approximation

As promised we have to analyze the predictability constraints imposed by geometrical optics approximation; it can be shown that the term

$$\frac{1}{k^2}\frac{\nabla^2 A}{A}$$

is vanishing respect to the others coming from equation (3.8) if a set of conditions holds.
The first one, usually called the smooth medium condition, states that the dielectric is slow varying over one wavelength:

$$\lambda\frac{\left|\overrightarrow{\nabla}\epsilon\right|}{\epsilon} \ll 1 \tag{3.25}$$

We have been considering the dielectric composed by a slow varying part plus a fluctuation and here we can regard the average term as being constant

$$\lambda\left|\overrightarrow{\nabla}\Delta\epsilon\right| \ll 1 \tag{3.26}$$

Since $\Delta\epsilon$ has stocastic value we are insterest in its variance

$$\left\langle\left(\overrightarrow{\nabla}_\perp\Delta\epsilon\right)\left(\overrightarrow{\nabla}_\perp\Delta\epsilon\right)\right\rangle \ll 1 \tag{3.27}$$

and using the power spectrum representation yields

$$\lambda^2 \int \kappa^2 \mathrm{d}\overrightarrow{\kappa}\, \Phi_\epsilon \ll 1 \tag{3.28}$$

In the case where the power spectrum has a minimum admissible scale k_{in}^{-1} this states that the condition $\lambda \ll k_{in}^{-1}$ is a way to crude limit.

Another aspect of the approximation is that rays can not converge too rapidly. Let the pencil of radiation lay along $\hat{x}$, the angle of arrival must satisfy

$$\delta\theta_z (R - x) \ll z \tag{3.29}$$

and we have already solved the equation for $\delta\theta$ so

$$\frac{1}{2}(R - x) \int_0^x \mathrm{d}x_1 \partial_z \Delta\epsilon(x_1) \ll z$$

Now we can derive the above expression by z, evaluate it at $x = \frac{R}{2}$, do a similar calculation for the angle $\delta\theta_y$ and sum the results to obtain

$$\frac{R}{4} \int_0^{\frac{R}{2}} \mathrm{d}x \nabla_\perp \Delta\epsilon \ll 1$$

Again we need to average this out, but before doing this it is worth noting that

$$\frac{R}{4} \int_0^{\frac{R}{2}} \mathrm{d}x \nabla_\perp \Delta\epsilon = \frac{3}{2}\chi$$

so the caustic condition is equivalent to

$$\langle \chi^2 \rangle \ll 1 \tag{3.30}$$

Thus we are mainly interested in phase variation.

3.1.3 Moments in geometrical optics approximation

As the scintillation process is due to the underlying turbulent motion of the medium, to have testable predictions we have to resort to average the observable quantities, which are functions of the electric field; thus we must exploit their dependence on the fluctuations and reveal the nature of the distribution of fluctuations as well: the electric field is

$$E = E_0(1 + \chi)\exp(i\phi) \tag{3.31}$$

but, within the contest of geometrical optics, in relation (3.30) we have seen that the amplitude fluctuation must be negligibly small

$$\chi \ll 1 \quad \Rightarrow \quad E \simeq E_0 \exp(i\phi)$$

so, altougth we are able to determine the first moments of the field itself we are not allowed to say anything useful about the intensity of the radiation, hence we can reduce our analysis to the phase fluctuation and, to achieve this aim, it is fundamental to calculate the structure phase function.

Structure phase function

In equation (3.21b) we have defined the phase of the wave, now we want to infer the variation of this quantity due to the multiple ray paths mixed by the turbulent motion of the medium; in particular we need the phase structure function, which is a measure of the difference in phase perceived by adjacent observers and averaged over a finite sampling length:

$$D_\phi(\overrightarrow{\sigma}) = \left\langle \left(\phi(\overrightarrow{r}_1) - \phi(\overrightarrow{r}_2)\right)^2 \right\rangle \tag{3.32}$$

where $\overrightarrow{\sigma} = \overrightarrow{r}_1 - \overrightarrow{r}_2$. Since basic statistic assures

$$\langle(\phi_1 - \phi_2)^2\rangle = 2\left(\langle\phi^2\rangle - \langle\phi_1\phi_2\rangle\right)$$

we can examine this problem step by step.

Single phase variance

The first thing we need is the single phase variance; recalling the fact that now we can't suppress the vector notation as we have two distinct ray paths and that $\Delta\epsilon$ is supposed to be a zero mean stochastic variable by (3.21b) we have

$$\langle\phi^2\rangle = \frac{1}{4}k^2 \int \mathrm{d}\overrightarrow{s}\,\mathrm{d}\overrightarrow{s}'\,\langle\epsilon(\overrightarrow{s})\epsilon(\overrightarrow{s}')\rangle \tag{3.33}$$

The integrand can be handled by decomposing it in its Fourier components and, since almost by definition they are linked by the turbulence power spectrum, we get

$$\langle\epsilon(\overrightarrow{r})\,\epsilon(\overrightarrow{r}+\overrightarrow{\sigma})\rangle = \int \mathrm{d}\overrightarrow{\kappa}\,\Phi_\epsilon(\overrightarrow{\kappa},\overrightarrow{r})\exp(i\overrightarrow{\kappa}\,\overrightarrow{\sigma})$$

Defining κ_s as the wave vector component along the path difference our phase variance becomes

$$\langle\phi^2\rangle = \frac{1}{4}k^2 \int \mathrm{d}s\mathrm{d}s'\mathrm{d}\overrightarrow{\kappa}\,\Phi_\epsilon\left(\overrightarrow{\kappa},\frac{s+s'}{2}\right)\exp(i\kappa_s(s-s')) \tag{3.34}$$

A nice feature is that, postponing the kernel integration, there is no urge to force a specific turbulent power spectrum, but, in order to integrate along the ray path, we do have to choose something about the propagation.
Following our purpose we take a medium made of a slab of thickness R so that the power spectrum is slow varying with position: under this condition it is safe to take rays which are nearly parallel one to the other and let their paths to be along $\hat{x}$

$$\langle\phi^2\rangle = \frac{1}{4}k^2 \int \mathrm{d}\overrightarrow{\kappa}\,\Phi_\epsilon(\overrightarrow{\kappa})I \quad \text{where} \quad I(\kappa_x,R) = \int_0^R \mathrm{d}x \int_0^R \mathrm{d}x' \exp(i\kappa_x(s-s'))$$

Noting that the domain is a square and the integrand is even in the real part and odd in the imaginary one the propagation is given by

$$I = 2\left(\frac{1-\cos(k_s R)}{k_x^2}\right)$$

To proceed further we specialize to isotropic turbulence, $\Phi_\epsilon = \Phi_\epsilon(\kappa)$: in this case the integral can be calculated analytically

$$\langle\phi^2\rangle = 2\pi k^2 R \int_0^\infty \kappa \mathrm{d}\kappa \Phi_\epsilon(\kappa) F(\kappa R) \tag{3.35}$$

where $F(\kappa R)$ is the function due to integration on the angular κ components

$$F(x) = -\frac{1-\cos x}{x} + \int_0^x \frac{\mathrm{d}x'}{x'} \sin x' \tag{3.36}$$

If the turbulence has a maximum scale κ_{out}^{-1} and the ray path is greater than this length, the condition $R \gg \kappa_{out}^{-1}$ is satisfied and equation (3.35) reduces to

$$\langle\phi^2\rangle = \pi^2 k^2 R \int_0^\infty \kappa \mathrm{d}\kappa \Phi_\epsilon \tag{3.37}$$

Autocorrelation

For the next piece, as expected, setting us in the same environment in which the single phase variance has been calculated does not get completely rid of the path difference term, as a matter of fact integrating the angular part of the cross correlation yields

$$\langle\phi(\overrightarrow{r}_1)\phi(\overrightarrow{r}_2)\rangle = \pi k^2 \int_0^\infty \kappa \mathrm{d}\kappa \Phi_\epsilon(\kappa) \int \mathrm{d}s_1 \int \mathrm{d}s_2 \frac{\sin\left(\kappa\,|\overrightarrow{s}_1 - \overrightarrow{s}_2|\right)}{|\overrightarrow{s}_1 - \overrightarrow{s}_2|} \tag{3.38}$$

In order to keep simplifying this expression we have to distinguish the form of the wave near the source, as the difference in path lengths are unavoidably determined

by the boundary conditions; however is still possible to carry on the functional dependence of the turbulence spectrum: as done for the single phase variance we are to split equation (3.38) into a kernel and a propagation part I

$$\langle \phi(\overrightarrow{r}_1)\phi(\overrightarrow{r}_2)\rangle = \pi k^2 \int_0^\infty \kappa \mathrm{d}\kappa \Phi_\epsilon(\kappa) I\left(\kappa, \overrightarrow{s}_1, \overrightarrow{s}_2\right)$$

where obviously

$$I = \int \mathrm{d}s_1 \int \mathrm{d}s_2 \frac{\sin\left(\kappa\,|\,\overrightarrow{s}_1 - \overrightarrow{s}_2|\right)}{|\,\overrightarrow{s}_1 - \overrightarrow{s}_2|}$$

Now we can focus our attention to two commonly encountered cases.

Spherical wave If the source is emitting spherical wave the difference between two successive wavefronts is given by

$$|\,\overrightarrow{s}_1 - \overrightarrow{s}_2| = s_{1-2} = \sqrt{s_1^2 + s_2^2 - 2s_1 s_2 \cos\theta} \tag{3.39}$$

where we have called θ the angle formed by $\overrightarrow{s}_1$ and $\overrightarrow{s}_2$; by definition the propagation part is symmetrical in s_1 and s_2, so it can be computed on the triangular domain of integration

$$I = 2\int_0^R \mathrm{d}s_1 \int_0^{s_1} \mathrm{d}s_2 \frac{\sin\left(\kappa s_{1-2}(s_1,s_2,\theta)\right)}{s_{1-2}(s_1,s_2,\theta)} \tag{3.40}$$

To handle this rather coumbersome expression we have to resor to a triky change of variables

$$\begin{cases} s = s_1 \\ \zeta = \dfrac{1}{\sin\theta}\sqrt{1 + \left(\dfrac{s_2}{s_1}\right)^2 - 2\dfrac{s_2}{s_1}\cos\theta} \end{cases}$$

and, by direct substitution, one finds

$$I = 2\int_0^R \mathrm{d}s \int_{(\cos\frac{1}{2}\theta)^{-1}}^{(\sin\theta)^{-1}} \mathrm{d}\zeta \frac{\sin(\zeta s\kappa\sin\theta)}{\sqrt{\zeta^2 - 1}} \tag{3.41}$$

If the path deviation is small, and thus the angle deviation is small, $I(\kappa,\theta)$ turn out to be related to the zero order Bessel function

$$\theta \ll 1 \quad \Rightarrow \quad I = 2\int_0^R \mathrm{d}s J_0(\kappa s\theta)$$

and finally, exploiting the path length dependence, equation (3.38) becomes

$$\langle \phi(\overrightarrow{r}_1)\phi(\overrightarrow{r}_2)\rangle = \pi^2 k^2 R \int_0^\infty \kappa \mathrm{d}\kappa \Phi_\epsilon(\kappa) \int_0^1 \mathrm{d}w J_0(\kappa R\theta w) \tag{3.42}$$

In the limit of small angle the separation[2] σ is given by $R\theta$ and thus for the spherical wave case equation (3.32) reduces to

$$D_{\phi,s}(\sigma) = 2\pi^2 k^2 \int_0^\infty \kappa \mathrm{d}\kappa \Phi_\epsilon(\kappa) \int_0^1 \mathrm{d}w \left(1 - J_0(\kappa\sigma w)\right) \tag{3.43}$$

Plane wave Oddly enough, this calculation is not easier than the previous case. Let the rays lay along $\hat{x}$, then the path difference is given by

$$|\overrightarrow{s}_1 - \overrightarrow{s}_2| = s_{1,2} = \sqrt{(x_1 - x_2)^2 + \sigma^2} \tag{3.44}$$

By a peaceful switch of variables

$$\begin{cases} x_1 = x \\ w = x_1 - x_2 \end{cases}$$

the propagation can be easily integrated one time

$$I = 2\int_0^R \mathrm{d}x (R - x) \frac{\sin\left(\kappa\sqrt{x^2 + \sigma^2}\right)}{\sqrt{x^2 + \sigma^2}} \tag{3.45}$$

The term multiplied by x, when integrated again, gives

$$\frac{2}{\kappa}\left(\cos\kappa\sigma - \cos\kappa\sqrt{R^2 + \sigma^2}\right)$$

and, since is proportional to the turbulence scale, which in this context is negligible compared to the total path length R, it is to be ignored.
The surviving term can be evaluated making use of the variable $\zeta = \sigma^{-1}\sqrt{x^2 + \sigma^2}$

$$I = 2R\int_1^{\zeta_R} \mathrm{d}\zeta \frac{\sin\zeta\kappa\sigma}{\sqrt{\zeta^2 - 1}} + \circ\left(\frac{k_{out}}{R}\right) \tag{3.46}$$

where the integration upper limit is

$$\zeta_R = \sqrt{1 + \left(\frac{R}{\sigma}\right)^2}$$

As in the previous case $R \gg \sigma$ thus

$$I = \pi R J_0(\kappa\sigma) \tag{3.47}$$

[2]By the conditions chosen only the magnitude of $\overrightarrow{\sigma}$ is important.

and the phase structure function is

$$D_{\phi,p}(\sigma) = 2\pi R k^2 \int_0^\infty \kappa \mathrm{d}\kappa \Phi_\epsilon \left(1 - J_0(\kappa\sigma)\right) \tag{3.48}$$

Comparing last equation to (3.43), we find out that the structure functions of the cases we analyzed are linked by the relation

$$D_{\phi,s}(\rho) = \int_0^1 \mathrm{d}w \; D_{\phi,p}(w\rho) \tag{3.49}$$

Phase distribution

We have introduced $\Delta\epsilon$ as a stochastic variable and, under the assumption that we are dealing with a stationary process, we can logically impone that the dielectric fluctuation follows a Gaussian distribution.
As ϕ is linearly dependent on $\Delta\epsilon$ one concludes that even the phase shift is distributed as a Gaussian variable

$$\mathrm{d}P(\phi) = \frac{\mathrm{d}\phi}{\sqrt{\langle\phi^2\rangle}} \exp\left(\frac{\phi^2}{2\langle\phi^2\rangle}\right) \tag{3.50}$$

For the phase difference the situation is a bit more complex: having seen that $\langle\phi_1\phi_2\rangle$ is no-vanishing leads to a bivariate distribution for $\Delta\phi = \phi_1 - \phi_2$

$$\mathrm{d}P(\phi_1,\phi_2) = \frac{\mathrm{d}\phi_1\mathrm{d}\phi_2}{2\pi\langle\phi^2\rangle\sqrt{1-\mu}} \exp\left(-\frac{\phi_1^2 + \phi_2^2 - 2\mu\phi_1\phi_2}{2\langle\phi^2\rangle(1-\mu)}\right)$$

where we have introduced for convenience $\mu = \langle\phi_1\phi_2\rangle\langle\phi^2\rangle^{-1}$. To work out this expression one has to switch variables to the sum and the difference of phase and integrate over the former

$$\mathrm{d}P(\Delta\phi) = \frac{\mathrm{d}\Delta\phi}{2\sqrt{\langle\phi^2\rangle}\sqrt{1-\mu}} \exp\left(-\frac{(\Delta\phi)^2}{4\langle\phi^2\rangle(1-\mu)}\right)$$

Using the definition of D_ϕ given in (3.32) one has

$$\mathrm{d}P(\Delta\phi) = \frac{\mathrm{d}\Delta\phi}{\sqrt{2\pi D_\phi}} \exp\left(-\frac{\Delta\phi^2}{2D_\phi}\right) \tag{3.51}$$

Electric field moments

As said the field strength is primary determined by the phase

$$E = E_0 \exp(i\phi) \tag{3.52}$$

thus the average of this quantity is obtained with an integration by taking the phase probability as the measure

$$\langle E \rangle = \int P(\phi) \mathrm{d}\phi E_0 \exp(i\phi)$$

Using equation (3.50) the integral become straightforward

$$\langle E \rangle = E_0 \exp\left(-\frac{\langle \phi^2 \rangle}{2}\right) \tag{3.53}$$

The method is the same for the mutual coherence function, but now the measure must be due to the phase difference

$$\langle E^\dagger(\phi_1) E(\phi_2) \rangle = \int P(\Delta\phi) \mathrm{d}E_0^2 \exp(i\Delta\phi)$$

Equation (3.51) easily solves the situation and we get

$$\langle E^\dagger E \rangle = E_0^2 \exp\left(-\frac{D_\phi}{2}\right) \tag{3.54}$$

An immediate result is that light received at points separated by ρ is mutually coherent only if $D_\phi(\rho) < 1$; thus it is natural to define the field coherence length s_d as

$$D_\phi(s_d) = 1 \tag{3.55}$$

Note that this is directly related to the atmospheric seeing.

$$\theta_d = \frac{\lambda}{s_d} \tag{3.56}$$

3.1.4 Rytov approximation

Regardless the mathematical tools developed until now, we are not ready to treat properly diffraction, as, almost by definition, this effect do not belong to the geometrical optics regime: to mend this defect one needs to carry on the approximation to higher order and there are several ways this result can be achieved.

For instance, in the Born method the field is divided into successive higher power of the dielectric constant

$$\overrightarrow{E} = \sum_{i=0}^{\infty} \overrightarrow{E}_i^{\mathbf{B}} \tag{3.57}$$

This approach has a intuitive physical meaning: every $\overrightarrow{E}_i^{\mathbf{B}}$ corresponds to a scattering order: $\overrightarrow{E}_0^{\mathbf{B}} = \overrightarrow{E}_0$ is the unperturbed wave, $\overrightarrow{E}_1^{\mathbf{B}}$ is linked to the single scattering term, $\overrightarrow{E}_2^{\mathbf{B}}$ represent the double scattering and so on.
The downside of the Born approximation is that even if the condition $\Delta\epsilon \ll 1$ is fulfilled there is no guarantee that the serie is rapidly convergent, quite the opposite, it can be shown (i.a. [33]) that the condition for a fast convergence is too restrictive, so it's fruitful to seek a different approach.

Rytov devised a method that not only solves this problem, but also is an extension of geometrical optics; what we want to do now is to present briefly the main result we are interested in without, entering in the full details and restricting to the scalar case.
In equation (3.8), expressing the dielectric constant as $\epsilon = 1 + \Delta\epsilon$, Rytov found a transformation of the electric field that makes the the stochastic term $\Delta\epsilon$ to be seen as an additional source; the first step is to write E as

$$E(\overrightarrow{r}) = E_0(\overrightarrow{r}) \exp \Psi (\overrightarrow{r}) \tag{3.58}$$

Here E_0 is the unperturbed field and Ψ is called the surrogate function; even if at first glance it can be mistaken with the iconal, now

$$\Psi : \mathbb{R}^3 \mapsto \mathbb{C}$$

and this, combined with the fact we are not to neglect the Laplacian, makes the function Ψ able to describe both phase and amplitude fluctuations.

Inserting definition (3.58) into the wave equation (3.8) yields a system of equations that can be separated into one for the free field

$$\left(\nabla^2 + k^2\right) E_0 = -4\pi i k J \tag{3.59a}$$

and one for the surrogate function

$$\nabla^2 e^{\Psi} + 2(\overrightarrow{\nabla} \log E_0)\overrightarrow{\nabla} e^{\Psi} + k^2 e^{\Psi} \Delta\epsilon = -4\pi i k \left(\frac{e^{-\Psi} - 1}{E_0}\right) J \tag{3.59b}$$

Focusing our attention to the second equation we can drop the source[3] and rearrange the terms to get

$$\nabla^2 \Psi + (\nabla\Psi)^2 + 2\left(\overrightarrow{\nabla}\Psi_0\right)\overrightarrow{\nabla}\Psi = -k^2 \Delta\Psi \tag{3.60}$$

[3] Again we are interest to solve the equation only into the transmission region.

where we conveniently set $E_0 = \exp\Psi_0$. In order to solve this equation one can expand the surrogate function in power of the dielectric variation

$$\Psi\left(\overrightarrow{r}\right) = \sum_{i=1}^{\infty} \Psi_i\left(\overrightarrow{r}\right)$$

thus equation (3.60) is substituted by the set

$$\begin{cases} \nabla^2\Psi_i + 2\left(\overrightarrow{\nabla}\Psi_0\right)\overrightarrow{\nabla}\Psi_i + \sum_{p=1}^{i-1}\left(\overrightarrow{\nabla}\Psi_p\right)\overrightarrow{\nabla}\Psi_{i-p} = 0 & \forall\ i > 1 \\ \nabla^2\Psi_1 + 2\left(\overrightarrow{\nabla}\Psi_0\right)\overrightarrow{\nabla}\Psi_1 + k^2\Delta\epsilon = 0 & i = 1 \end{cases} \tag{3.61}$$

Basic Rytov solution corresponds to the first order, and, making use of $\Psi_1 = Q\exp(-\Psi_0)$, can be written as

$$\left(\nabla^2 + k^2\right)Q = -k^2\Delta\epsilon\exp\Psi_0 \tag{3.62}$$

which is normal Helmholtz equation that can be solved with the Green method

$$\Psi_1(\overrightarrow{r}) = -k^2\int \mathrm{d}\overrightarrow{x}\,G\left(\overrightarrow{r},\overrightarrow{x}\right)\Delta\epsilon\left(\overrightarrow{x},t\right)\frac{E_0\left(\overrightarrow{x}\right)}{E_0\left(\overrightarrow{r}\right)} \tag{3.63}$$

where the kernel is

$$G\left(\overrightarrow{x},\overrightarrow{y}\right) = \frac{\exp\left(ik\left|\overrightarrow{x}-\overrightarrow{y}\right|\right)}{4\pi\left|\overrightarrow{x}-\overrightarrow{y}\right|} \tag{3.64}$$

To have a clear physical insight of this we can relate the Rytov term to the first Born correction

$$E_1^{\mathbf{B}} = E_0(\overrightarrow{r})\exp\Psi_1(\overrightarrow{r}) \tag{3.65}$$

Here start to become evident that this expression is much more richfully than the geometrical optics description: the phase and the logarithmic amplitude fluctuations are directly linked as they are the imaginary and the real part of the same expression: in fact let A and B be two real valued functions such that

$$G\left(\overrightarrow{y},\overrightarrow{x}\right)\frac{E_0\left(\overrightarrow{x}\right)}{E_0\left(\overrightarrow{y}\right)} = A\left(\overrightarrow{y},\overrightarrow{x}\right) + iB\left(\overrightarrow{y},\overrightarrow{x}\right) \tag{3.66}$$

hence the fluctuations are defined by

$$\psi = -k^2\int \mathrm{d}\overrightarrow{x}\,B\left(\overrightarrow{r},\overrightarrow{x}\right)\Delta\epsilon\left(\overrightarrow{x},t\right) \tag{3.67a}$$

$$\chi = -k^2\int \mathrm{d}\overrightarrow{x}\,A\left(\overrightarrow{r},\overrightarrow{x}\right)\Delta\epsilon\left(\overrightarrow{x},t\right) \tag{3.67b}$$

Taking the due limits these expressions do reduce themselves to the geometrical optics ones, moreover it can be showed that the field moments calculated within the geometrical optics environment remain valid.
The difference is that their range of appicability is far more wider than their optical counterparts: either atmospheric experiments or analitic proofs (e.g. [33]) assure that the limit of validity for the logarithmic amplitude fluctuation is

$$\langle \chi \rangle < 1 \tag{3.68}$$

while the phase shift remains unbounded.

Given this one can hope to have an expression for intensity fluctuation as well; to show that one needs to analyze successive order approximations, and thanks to the recursive structure of the system (3.61) this can be easily achieved: the relevant equation is

$$\nabla^2 \Psi_2 + 2 \left(\overrightarrow{\nabla} \Psi_0 \right) \left(\overrightarrow{\nabla} \Psi_2 \right) = - \left(\overrightarrow{\nabla} \Psi_1 \right)^2 \tag{3.69}$$

Since Ψ_1 is given by equation (3.63), another exponential substitution yields

$$\Psi_2(\overrightarrow{r}) = -k^2 \int \mathrm{d}\overrightarrow{x} G(\overrightarrow{r}, \overrightarrow{x}) \left(\overrightarrow{\nabla} \Psi_1(\overrightarrow{x}) \right)^2 \frac{E_0(\overrightarrow{x})}{E_0(\overrightarrow{r})} \tag{3.70}$$

After the proper calculation are made (ibidem) one has as an additional result a direct link between the two approximation methods in the small exponent limit:

$$\begin{cases} \Psi_1 = B_1 \\ \Psi_2 = B_2 - \dfrac{1}{2} B_1^2 \\ \Psi_3 = B_3 + \dfrac{1}{3} B_1^3 - B_1 B_2 \\ \dots \end{cases} \quad \text{with} \quad B_i = \frac{E_i^{\mathbf{B}}}{E_0^{\mathbf{B}}}$$

Intensity fluctuation

With the first two order of the Rytov approximation one is ready to calculate intensity fluctuations, and it is easier to do this task expressing the logharitmic irradiance in function of the normalized Born terms

$$\zeta = \log \left(\frac{I(\overrightarrow{r})}{I_0} \right) = \Re(B_1) + 2\Re(B_2) - (\Re(B_1))^2 + (\Im(B_1))^2 \tag{3.71}$$

The mean intensity for plane or spherical wave, as expected, is directly related to the amplitude fluctuation, even if the calculation is not trivial

$$\langle \zeta \rangle = -2 \left\langle (\Re(B_1))^2 \right\rangle = -2 \left\langle \chi^2 \right\rangle \tag{3.72}$$

Usually the relevant quantity is the scintillation index m_r; calling $\delta I = I - \langle I \rangle$ one defines the intensity covariance as

$$C_I\left(\overrightarrow{s}\right) = \left\langle \frac{\delta I\left(\overrightarrow{x}\right)\delta I\left(\overrightarrow{x}+\overrightarrow{s}\right) - \left\langle I\left(\overrightarrow{x}\right)\right\rangle^2}{\left\langle I\left(\overrightarrow{x}\right)\right\rangle^2} \right\rangle \tag{3.73}$$

and the scintillation index is defined as

$$m_r = \sqrt{(C_I(0)} \tag{3.74}$$

But this is simply the root mean square of the variance of the intensity evaluated at $\overrightarrow{s} = 0$, which, for a plane wave, can be calculated using equation (3.72)

$$\left\langle \left(\frac{\delta I}{\langle I \rangle}\right)^2 \right\rangle = \langle \exp 2(\zeta) \rangle - 1$$

thus m_r is given by

$$m_r = \sqrt{\exp(4\left\langle \chi^2 \right\rangle) - 1} \tag{3.75}$$

Note that even if we used the same notation, now χ is due to the first order Rytov approximation:

$$\left\langle \chi^2 \right\rangle = \pi^2 R k^2 \int_0^\infty \kappa \mathrm{d}\kappa \Phi_\epsilon(\kappa) F_\chi(\kappa) \tag{3.76}$$

where the function F_χ for a plane wave is

$$F_\chi(\kappa) = \frac{1}{2}\left(1 - \frac{\sin\left(R\kappa^2 k^{-1}\right)}{R\kappa^2 k^{-1}}\right) \tag{3.77}$$

This is more general that the one from geometrical optic approximation, and in the limit of small scattering parameter

$$R\kappa^2 k^{-1} \ll 1 \quad \Rightarrow \quad F_\chi(\kappa) \propto \kappa^4$$

the two descriptions coincide

$$\left\langle \chi^2 \right\rangle = \frac{4}{3}\pi^2 R^3 \int_0^\infty \kappa^5 \mathrm{d}\kappa \Phi_\epsilon \tag{3.78}$$

3.2 ISM scintillation

Having settled the necessary mathematical tools to deal with the scintillation, it is time to get closer to the real issue: in this Section we try to summarize the last twenty years of literature on the subject, which focus their attention on the problem of a source in our galaxy neighborhood, such as a pulsar, viewed by the observer througth a single screen of scintillating matter.
But, before this, we have to understand how turbulence can be treated.

3.2.1 Turbulence spectrum of the interstellar medium

Until now there is no satisfactory turbulence theory of the magnetized plasma in the cosmological environment: the wide range of state of the ISM clouds, where the temperature can go from 10^2 K to 10^6 K, is an hint that the underlying physical cooling processes are different and thus there are different dissipation scales.
Even about the power input there is not unique answer yet: either it is caused by a combination of clouds motion, echoes of shock and large scale winds, or there are arguments about shock instability, which may be directly responsible for the creation of the chaotic structure.
Further, from the hydrodynamical analysis of turbulence, the density is only a passive tracer of such irregularity, and this could lead to difficulty in observable determinations; moreover, when coming to the inertial range, the difficulty is to find a nonlinear method of transfer allowing a nearly self similar cascade of vortices, and till now there has been no certain agreement, as Alfen wave and magneto-acustic one have yet a little theory about their nonlinear interactions.

With that in mind we can begin our analysis on turbulence spectrum of the ISM, which, not having a better model, will be adopted for the IGM as well.
Since we are dealing with a plasma the index of refraction is to be written as

$$n^2 = \epsilon = \left(1 - \left(\frac{\omega_p}{\omega}\right)^2\right) \tag{3.79}$$

where the plasma frequency ω_p is given by

$$\omega_p = \sqrt{\frac{n_e e^2}{m_e \epsilon_0}}$$

Thus the dielectric fluctuation is proportional to the electron density variation

$$\Delta\epsilon = r_e \lambda^2 \Delta n_e \tag{3.80}$$

where r_e is the classic electron radius; considering that the power spectrum is quadratic in the variable we have

$$\Phi_\epsilon = r_e^2 \lambda^4 \Phi_N \tag{3.81}$$

As the turbulence inertial range is much smaller than the thickness of the scintillating medium that will be considered, we can regard the problem to be a multi-scale one, splitting the power spectrum into a part due to proper turbulence and a multiplicative term that describes the large scale structure of the vortices[4]

$$\Phi_N\left(\overrightarrow{r}, \overrightarrow{k}\right) = C_N^2\left(\overrightarrow{r}\right) P\left(\overrightarrow{k}\right) \tag{3.82}$$

[4]We are allowed to speparate the spectrum this way thanks to the Rytov theory.

where C_N is a slow varying function in space; assuming isotropy

$$P\left(\overrightarrow{k}\right) = P(k)$$

the form for the power spectrum we adopt is the one usually used (e.g. [24])

$$P(k) = \left(k^2 + k_{out}^2\right)^{-\frac{\beta}{2}} \exp\left(-\frac{k}{k_{in}}\right) \tag{3.83}$$

where β is a free parameter, k_{in}^{-1} and k_{out}^{-1} are respectively the inner and the outer scale, which, for the ISM are about 10^{12} cm and 10^{18} cm (e.g. [14]).
In the inertial region equation (3.83) reduces to

$$P(k) = k^{-\beta} \quad \text{per} \quad k_{out} \ll k \ll k_{in} \tag{3.84}$$

and if, as it is usually done, one assumes $\beta = \frac{11}{3}$ a Kolmogorov like power spectrum can be recovered.

3.2.2 Thin screen approximation

Let's analyze the InterStellar Scintillation model: we have a source located at z_s with a angular width θ_s and an observer at $z = 0$, supposing that, along their line of sight, there is a medium that has a spatial extent l which is small relative either to its distance from the observer r_{s-o} and either to r_{s-s}, the one from the source to the screen.
Note that, for now, we don't need to bother with redshift dependence as we can safely recover it later. It is useful to define the scattering measure

$$\mathrm{SM} = \int_0^l C_N^2\left(\overrightarrow{x}\right) \mathrm{d}z \tag{3.85}$$

which is a quantity that give a order of magnitude strength of the scintillation; for our future purpose we can safetely restrict the analysis considering a constant density screen which, since $C_N = C_N(n_e)$, yields

$$\mathrm{SM} = C_{N,0}^2 l \tag{3.86}$$

where the subscript is to emphasize it is a constant; introducing the nominal galactic value for the scattering measure $C_{N,gal}^2 = 10^{-3.5}\ \mathrm{m}^{-\frac{20}{3}}$ (e.g. [8]) we can write SM as

$$C_{N,0}^2 = C_{N,\mathrm{gal}}^2 \left(\frac{n_e}{0.02\ \mathrm{cm}^{-3}}\right)^2 \tag{3.87}$$

In what follows it is sometime useful to use the galactic value as a reference level for the scattering measure, so we can define

$$\mathrm{SM}_{-3.5} = \mathrm{SM}\ C_{N,gal}^{-2}\ \mathrm{Kpc}^{-1}$$

Now, recalling the phase structure function definition (3.32) and using a β power law spectrum (3.84), we can analytically solve D_ϕ for the plane wave case

$$D_\phi(s) = \mathrm{SM}\ \pi^2 r_e^2 f(\beta) s^{\beta-2} \tag{3.88}$$

where the dimensionless factor $f(\beta)$ is

$$f(\beta) = \begin{cases} 8\Gamma\left(\frac{\beta}{2}\right)\Gamma\left(2-\frac{\beta}{2}\right)\left((\beta-2)2^{\beta-2}\right)^{-1} & \text{for} \quad s > k_{in}^{-1} \\ \Gamma\left(2-\frac{\beta}{2}\right)k_{in}^{-\beta} & \text{for} \quad s < k_{in}^{-1} \end{cases}$$

using the following Γ function properties

$$\begin{cases} \Gamma(z)\Gamma(z-1) = \dfrac{\pi}{\sin(\pi z)} & \text{for} \quad z \notin \mathbb{N} \\ \Gamma(z+1) = z\Gamma(z) \end{cases}$$

yields in the intertial range

$$D_\phi(s) = \mathrm{SM}\ 8\pi^3 r_e^2 s^{\beta-2} \frac{1-\frac{\beta}{2}}{\beta-2} \frac{2^{2-\beta}}{\sin\left(\pi\frac{\beta}{2}\right)} \tag{3.89}$$

In particular, for $\beta = \frac{11}{3}$, we can write the characteristic scattering angle $\frac{\lambda}{s_d}$ as (cfr [8])

$$\theta_d = 2.93 \nu_{10}^{-\frac{11}{5}} l_{Kpc} \left(\frac{n_e}{0.02\ \mathrm{cm}^{-3}}\right)^2 \mu\mathrm{as} \tag{3.90}$$

where the subscripts indicate these scalings

$$\begin{cases} \nu_{10} = \dfrac{\nu}{10\ \mathrm{GHz}} \\ l_{Kpc} = \dfrac{l}{10^3\ \mathrm{pc}} \end{cases}$$

The scattering medium is compressed onto a plane perpendicular to the line of sight and thus we can use Fresnel theory but, since we are needing it for later, we do not want to assume that the distance between the source and the screen is large compared the screen-observer one. The Fresnel radius is defined as

$$r_F = \sqrt{\lambda D_F} \tag{3.91}$$

where D_F is given by (i.a. [15])

$$D_F = \frac{r_{s-s} r_{s-o}}{r_{s-s} + r_{s-o}} \tag{3.92a}$$

thus, using a modified distance $\tilde{d}$

$$\tilde{d} = \frac{(r_{s-o})^2}{D_F} = (r_{s-s} + r_{s-o}) \frac{r_{s-o}}{r_{s-s}} \tag{3.92b}$$

we can write the Fresnel angle as

$$\theta_F \simeq 2.57 \nu_{10}^{-\frac{1}{2}} \tilde{d}_{Kpc}^{-\frac{1}{2}} \ \mu\text{as} \tag{3.93}$$

3.2.3 Effects and interpretations

To have a picture of the physics behind the above formulae it is meaningful to have a qualitative pause, and think scintillation as to be treated into two conceptually different ways.

Diffraction

Diffractive scintillation is based on physical optics and is due to interference among multiple ray paths from the source to the receiver; the principle is similar to interferometry, as each ray form a different sub-image to be viewed as a slit on an imaginary plane perpendicular to the unperturbed line of sight crossing the screen; thus to have the fringes coherently summed one has to require that

$$\theta_s < \frac{s_d}{r_{s-o}} = (k \theta_d \tilde{d})^{-1} \tag{3.94}$$

This condition alone is not sufficent to assure the creation of multiple images; to have that the flux scintillation must be strong, in the sense that the modulation index m_r must be greater than one, or, equivalently

$$\theta_d > \theta_F \tag{3.95}$$

If this latter condition is not satisfied the the net result is similar to the refractive case; here, quite obviously, the length for fluctuations is given by s_d.

Refraction

Refraction is a geometrical optics effect due to focus and defocus of light, which leads to a random magnification of sub-images of the source; it is possible when the

flux from the source at the screen has a section smaller than the coherence length, or, written in term of angles,

$$\theta_s < \theta_d \tag{3.96}$$

For a point source $\theta_s \ll 1$, and the effect is a displacement of the image, while for an extended one is a distortion.
As hinted above, both θ_d and θ_F lead to a refraction effect, and the effective size of the image, or its displacement, is found convolving the source surface brightness with the point spread function of the medium, and this calculation yields (e.g. [11])

$$\theta_{eff} = \sqrt{\left(\theta_s^2 + (0.71\theta_d)^2 + (0.85\theta_F)^2\right)} \tag{3.97}$$

Moreover the index of modulation must be given by this combined effect, thus can be written as (e.g. [11])

$$m_r = 0.114\nu_{10}^{-2}\mathrm{SM}_{-3.5}^{\frac{1}{2}}\tilde{d}_{Kpc}^{-\frac{1}{6}}\left(\frac{\theta_{eff}}{10\ \mu\text{a.s.}}\right)^{-\frac{7}{6}} \tag{3.98}$$

Since the refractive effect is inchoerent the fluctuations that matter are the ones with a scale lenght larger than the projection on the scattering sceen so, due to the form of the Fresnel radius, a lower bound for their size s is given by s_r, which is defined as

$$s_r = \theta_{eff} D_F \tag{3.99}$$

with the obvious constraint

$$s \gtrsim s_r$$

Time scales

Having pinpointed the fluctuation sizes the relative flux modulation time scales can be easily estimated: they are given by

$$t_{ref} = \frac{s_r}{v_\perp} = \frac{D_F}{v_\perp}\theta_{eff} \tag{3.100a}$$

for refractive scintillation and

$$t_{dif} = \frac{s_d}{v_\perp} = (k\theta_d v_\perp)^{-1} \tag{3.100b}$$

for the diffractive case. Here $v_\perp$ is the velocity of the inregularity, and we are to use the medium sound speed as a lower bound (e.g. [8]).

3.3 IGM scintillation

Having formalized the scintilation and having seen in particular how it behaves in the thin screen case, it is finally time to look more closely at what we are really interest in.
In the scenario we deal with a source which is located at $z \sim 2$ and an observer placed at $z = 0$; between these there is a continuum of matter, namely the InterGalactic Medium, which, in principle, could act as a scintillation source.
Obiviously this medium can not be treated like a thin screen, since its physical properties are not slow-varying along line of sight and, perhaps more important, there is no guarantee that further order of the electric field are vanishingly small: as said every term in the approximation[5] takes into account increasing scattering events, and one can easily see that the longer the path length the more important these multiple scattering have to be.

We need a slightly different approach: our medium is to be slit up into multiple thin screens. Moreover, as the effect of the average ISM distribution of matter produce a only a slight perturbation on the wave and since the relative estimate on the IGM scattering measure, calculated in two clouds of typical sizes, is (i.e. [11])

$$\frac{SM_{IGM}}{SM_{ISM}} \sim 10^{-4}$$

it is safe to assume that the scintillation due to said thin screens can be resolved with a forward scattering approximation; moreover, as the flux modulation is usually weak even with the ISM, we can restrict our analysis to the refractive scintillation only.

Looking to the simulation it is natural to adopt as a candidate for this discretization the smallest cell resolved along the choosen line of sight, but, in order to have at least a refraction event, a cell must give a characteristic scattering angle high enough to satisfy condition (3.96), as if it has a low scattering measure it does not scintillate. Thus the screen is given by the ensamble of contiguous cells up to obtain a significant correlation length: the patch ranging from m_1 to m_2 is considered a unique screen, where, given equation (3.90), m_2 is defined as the smallest integer greter equal m_1 such that

$$\theta_s < 2.93\nu_{10}^{-\frac{11}{5}} \left(\sum_{i=m_1}^{m_2} \left(\frac{a(i)}{a_s} \right)^{\frac{11}{3}} \mathrm{SM}_{-3.5,i} \right)^{\frac{3}{5}} \mu\mathrm{as} \tag{3.101}$$

Where SM_i is the scattering measure due to cell i, $a(i)$ its expansion factor and a_s the one of the source.

[5] This is strictly valid only for the Born approach, but, as hinted in Section 3.1.4, the Rytov terms can be seen as combinations of the former ones.

Moreover note that to assure coherence, which is needed by the scintillation, the source angle θ_s for all but the first screen has to be given by the effective diffractive angle produced by the previous screens.
Having established this sort of scintillation mean free path, for now we can assume to have such screens and turn our attention back to the problem and estabilish how these screens interact.

3.3.1 Extension of the thin screen model

Considering we are dealing with objects located at different redshift let's fix our notation. The source is located at $R = a_s x_0$ and has a intrinsic spatial dimension $d_s = a_s h_0$ and thus the subtended angle viewed by a distance r is given by[6] $\theta_s(r) \simeq d_s r^{-1}$.
As said, this is true only for the first screen: after that scattering event we identify the source angle with the previous diffraction angle, thus the model is morally unaffected by a variation of the parameter d_s of the source.

The unperturbed line of sight is straight, and taking a specific one the radiation encounters $i = 1, \ldots, N$ thin screens on his path, being the N-th the farthest form the source; the i-th screen has characteristic angle $\Delta\theta_{i,d}$, distance from the observer $r_i = (z_i + 1)^{-1} x_i$ and of length $l_i = (z_i + 1)^{-1} h_i$.
When needed, namely to avoid subscript prolification, said subscripts will be removed and replaced by a fictional functional dependence, e.g. $r_i \mapsto r(i)$.

Remembering that we are using the same power spectrum of the ISM and using the settled notation, the scattering measure of the i-th screen is given by

$$SM_{-3.5}(i) = \left(\frac{n_e^2(i)}{0.02 \text{ cm}^{-3}} \right)^2 l_{Kpc}(i) \tag{3.102}$$

and using equation (3.90) one can write the characteristic angle as

$$\Delta\theta_{i,d} = 2.93 \nu_{10}^{-\frac{11}{5}} \left(\frac{a(i)}{a_s} \right)^{\frac{11}{3}} SM_{-3.5}^{\frac{3}{5}}(i) \tag{3.103}$$

The j-th interaction is between an "observer" located at r_{j+1} and a "source" placed in r_{j-1}: the Fresnel radius must be calculated accordingly to such prescription

$$r_F(j) = \sqrt{\lambda \frac{a(i)}{a_s} D_F(j)} \tag{3.104a}$$

[6] Here the usual redshift factor for the angle is not indicated, the motivation are given below.

where, since the screen are chosen to be one beside the other, $D_F(j)$ can be calculated using the screen width l

$$D_F(j) = \frac{1}{2}\frac{(l_j + l_{j+1})(l_j + l_{j-1})}{(l_{j-1} + 2l_j + l_{j+1})} \tag{3.104b}$$

and thus the j-th effective distance we are to use is

$$\tilde{d}(j) = \frac{1}{2}(l_{j-1} + 2l_j + l_{j+1})\frac{(l_j + l_{j+1})}{(l_j + l_{j-1})} \tag{3.105}$$

Indicating the associated Fresnel angle as $\Delta\theta_{i,F}$ the resulting refraction angle due to the screen is given by adapting equation (3.97)

$$\Delta\theta_{eff,i} = \sqrt{\theta_s^2(i) + (0.71\Delta\theta_{d,i})^2 + (0.85\Delta\theta_{F,i})^2} \tag{3.106}$$

Scintillation angle

The angles $\Delta\theta_{eff,i}$ are to be treated as the norm of a bidimensional vector laying on the plane perpendicular to the line of sight, which direction is given by a random unit vector $\hat{n}_i$; this can be done as the natural choise for this vector is to be built with the transverse velocity

$$\hat{n}_i = \frac{1}{\sqrt{v_{x_i} v_{y_i}}}(v_{x_i}, v_{y_i})$$

and this definition yields an angle variable α_i

$$\hat{n}_i = (\cos\alpha_i, \sin\alpha_i)$$

which is nearly uniformly distibuited. Since the refraction is a cumulative effect of the screens, the resulting angle at the i screen must be given by the vector sum of the variation given by every screen between the first and the i-th

$$\overrightarrow{\theta}_i = \sum_{j=0}^{i} \Delta\theta_{eff,j}\hat{n}_j \tag{3.107}$$

and obviously a similar result holds for the diffraction angle, even if in the latter case we expect that the effect is quenched by the smallness of the $\frac{\Delta\theta_{d,i}}{\Delta\theta_{F,i}}$ ratio.

Intensity variation

To deal with this issue, one can calculate the modulation index of the line of sight starting from the indices of each screen; $m_r(i)$ is defined as a variance, and, assuming that there is no cross correlation between the screens[7] appears natural that the total index M_r is given by the quadratic sum of the individual ones

$$M_r = \sqrt{\sum_i m_r^2(i)} \tag{3.108}$$

where the modulation index of the i-th screen can be calculated using equation (3.98), yielding

$$M_r = 0.114\nu_{10}^{-2}\sqrt{\sum_i \mathrm{SM}_{-3.5}(i)\tilde{d}_{Kpc}^{-\frac{1}{3}}(i)\left(\frac{\Delta\theta_{eff}(i)}{10\ \mu\text{a.s.}}\right)^{-\frac{7}{3}}\left(\frac{a(i)}{a_s}\right)^4} \tag{3.109}$$

Equivalent scattering measure

In comparing the results it is useful to define the equivalent scattering measure, where the word equivalent stands for regarding the full line of sight as a thin screen

$$\mathrm{SM}_{eq} = \sum_{i=1}^{N} \mathrm{SM}(i) \tag{3.110}$$

Note that this is to be regarded as being a identifier of a line of sight used mostly for taxonomy purpose, since, even if one expects an increase of this quantity as scintillation strengthens, by no mean SM_{eqi} can be mistaken for the scattering measure required to have a resulting effective angle θ_N.
Using the scattering measure definition is possible to make an analytical estimate of this quantity in the case of a smooth universe:

$$\overline{\mathrm{SM}}_{-3.5,eq} = \overline{\mathrm{SM}}_0 \int_{a_s}^{1} \frac{\mathrm{d}a}{a^7 E(a)} \tag{3.111}$$

where $E(a)$ is implicitly defined in equation (1.14)

$$\begin{cases} E(a) = \sqrt{\Omega_\lambda + \Omega_r a^{-4} + \Omega_m a^{-3}} \\ \overline{\mathrm{SM}}_0 = \left(\dfrac{\rho_c \Omega_b}{m_p 0.02\ \mathrm{cm}^{-3}}\right)^2 \dfrac{c_{Kpc}}{H_0} \end{cases}$$

[7] If this assumption does not hold what follows is to be regarded as an upper estimate.

where μ is the mean molecular weight. In a tipical ΛCDM universe with a primordial composition, in the full ionization limit and with a chosen value for the Hubble constant

$$\begin{vmatrix} h = 0.75 \\ \mu = 0.6 \\ \Omega_b = 0.04 \end{vmatrix} \quad \begin{vmatrix} \Omega_\lambda \simeq 0.6 \\ \Omega_m \simeq 0.4 \\ \Omega_r \simeq 0.01 \end{vmatrix}$$

we get a mean value of

$$\overline{\mathrm{SM}}_{-3.5,eq} \simeq 8.20\ 10^{-2} \tag{3.112}$$

which has to be checked against the simulation results.

Error in performing the thin screen limit

From formulae (3.105) it is clear that in taking into account the finite size of the screen we are making a relative error of the order of

$$\delta_i = \frac{\Delta r_F(i)}{r_F(i)} = \frac{l_i}{l_{i-1} + l_{i+1}}$$

calculated by recovering the usual expression of the Fresnel radius.
As the scintillation is expected to be refractive the downside is obivious: since the relation are all polynomials the error δ_i propagates down to every quantity q_i we have calculated with only a prefactor, and for every Q such that

$$Q = \sum_i q_i \quad \text{with} \quad q_i = q_i\left((r_F)^m\right)$$

we have a relative error

$$\Delta_Q = \frac{\Delta Q}{Q} = \frac{m}{Q}\sum_i \delta_i q_i$$

and one can note that the uncertanty could be quite large. The bright side of this is that the theory is still predictive enough to have an estimate of the process.

3.3.2 Temporal behaviour

There are two relevant times to consider: one is given by the composition of each refractive or diffractive time scales owned by the screens, the other is due to the displacement interpretation of the effective scattering angle; the former is the proper time scale responsible for the variation in the physical quantities due to scintillation, while the latter could arise as a feature in the spectra.

Time scales

There are yet some theoretical modification to be done to the model just exposed, which are due to the difference in time scale between the screens: note that in the above formulae for the scintillation angle and modulation index we have not specified the bound of the index i because actually this depends on the measuring time, let's call it T_{obs}.
Thus the $i-th$ screen effect has to be included only if its scintillative time scale t_i is less than T_{obs}, such that the final refraction angle $\Theta = \theta_N$ in equation (3.107) is given by

$$\Theta = \Theta\left(T_{obs}\right) = \left| \sum_{i=0}^{N} \Delta\theta_{eff,i} \hat{n}_i \chi\left(T_{obs} - t_i\right) \right| \tag{3.113a}$$

and equation (3.108) reads

$$M_r\left(T_{obs}\right) = \sqrt{\sum_{i=0}^{n} m_r^2(i) \chi\left(T_{obs} - T_i\right)} \tag{3.113b}$$

where we indicated with χ the step function; this is a crude approximation but embodies the spirit of the physical situation: as the mean effect calculated on a period is not zero we must sum over every i-th screen if t_i is less then the observed time T_{obs}, and we must neglect the contributes from those screens whose time scale is larger than T_{obs} as they are to be considered almost stationary.

To complicate things further, as we have seen, the time scale t_i in the last equation could be either the refractive or difractive, as can be obtained simply adding the redshift factor to the equations (3.100a) and (3.100b)

$$t_{ref}(i) = \frac{a_0}{a_i} \frac{l_i}{v_i} \Delta\theta_{eff,i} \tag{3.114}$$

$$t_{dif}(i) = \frac{a_0}{a_i} \left(k \Delta\theta_{i,d} v_i\right)^{-1} \tag{3.115}$$

where we have taken v_i to be the thermal velocity of the i-th screen. Thus, from this point of view, the scintillative regime the i-th screen belongs to is also dependent on T_{obs}: we eventually see the direct implication of this in Chapter 5 when analyzing the results.

Time delay

Interstellar scintillation has been invoked more than once (i.a. [5]) as possible explanation for the shape of the signal from a pulsar.

In this environment we can translate it as a broadening of the line from a quasar.

We are to follow a line of thought due to a simple geometrical argument: successive rays going througth the i-th screen experience a path deviation

$$l_i \left(1 - \cos^2 \left| \overrightarrow{\theta}_i \right| \right)$$

thus, in the small angle limit, the time delay due to the single screen is given by

$$\Delta\tau_i \simeq \frac{l_i}{2c} \left| \overrightarrow{\theta}_i \right|^2 \tag{3.116}$$

and the total effect at the i-th screen is the sum of the individual time delay of all the preceding ones:

$$\begin{aligned} \tau_i =& \sum_{s=0}^{i} \Delta\tau_i = \frac{1}{2c} \sum_{s=0}^{i} l_s \left| \overrightarrow{\theta}_s \right|^2 = \\ =& \frac{1}{2c} \sum_{s=0}^{i} l_s \left(\sum_{m=0}^{s} \theta_{eff,s} \hat{n}_s \right)^2 \end{aligned}$$

so that the effect of the line of sight is given by τ_N, which should act as a broadening feature for the quasar spectrum.
Before moving on note that the speed of light in the medium is taken to be c, as in a plasma the first approximation of the dispersion relation

$$\omega^2 = k^2 c^2 + \omega_p \tag{3.117}$$

would yield a wave group velocity

$$v_g = c\sqrt{1 - \left(\frac{\omega_p}{\omega}\right)^2} \tag{3.118}$$

which could be safely be approximated to c due to the context we are working within.

Chapter 4

Simulation results

I like the stars. It's the illusion of permanence, I think. I mean, they're always flaring up and caving in and going out. But from here, I can pretend . . . I can pretend that things last. I can pretend that lives last longer than moments. Gods come, and gods go. Mortals flicker and flash and fade. Worlds don't last; and stars and galaxies are transient, fleeting things that twinkle like fireflies and vanish into cold and dust. But I can pretend.

Destruction to Dream

1993, Brief lives, Neil Gaiman

4.1 Physical and computational settings

4.1.1 Resolution

Since the final aim of our Thesis is to investigate scintillation due to the baryonic component along a line of sight stretching from an high redshift object up to $z = 0$, we have to pick a box size which is long enough to ensure that spurious effect from the numerical evolution are beyond the range of interest of the phenomena we want to inquire: every simulation size translates into a cutoff beyond which the perturbations overgrown and thus the simulation itself cannot be considered realistic.
Hence we choose our box length in comoving units to be 100 h^{-1} Mpc, which also assures that we can evolve the initial conditions starting from the linear regime, being the size large enough to grant the initial symmetries.

Next we have to decide the number of dark matter particles of the simulation: this is an important iussue since, even if the spatial resolution is agumented by the fact we are using a AMR code, therefore is formally due to the maximum level of refinement selected, the mass resolution is fixed, and it does determine gravitational evolution of the system, and it is to remember, as we explained in Chapter 2, that

the enhanced resolution is available only for the baryon component.
We set the total particle number to be 128^3, and choose 5 additional level of refinement: this rules that the unit mass is $1.65\ 10^{10}\ \Omega_{dm} h^{-1}\ M_\odot$ and the spatial resolution $0.39\ h^{-1}$ Mpc for the cartesian grid, with a maximum available resolution of $12.2\ h^{-1}$ Kpc.

It is usually pointed that, in order to have a realistic simulation, one must have a mass resolution of $10^8\ h^{-1}\ M_\odot$, but as we are mainly interested in the diffuse matter, our results are to be considered reliable even with the order of magnitude of difference.
Qualitatively speaking, we can not expect to have a proper treatment of effect such as the star formation process and its feedback on the medium, which can affect the scintillation, even if not as the dominant contributors.

4.1.2 Cosmological parameters

As anticipated we want to work with a ΛCDM universe, and thus we have chosen the various components to be in the ratios

$$\Omega_m = 0.350 \qquad \Omega_b = 0.045$$
$$\Omega_\Lambda = 0.649 \qquad \Omega_k = 0.$$

and in our run the value selected for the Hubble constant is

$$h = 0.750$$

These are reasonably near enough the accepted parameters in accordance to the so called concordance model (e.g. [2]).

We have generated the initial perturbation from a "flat" power spectrum, namely the one obtained by setting $n = 1$ in equation (2.30), normalized via $\sigma_8 = 0.9$[1], further, as an additional initial condition, we set a $Y = 0.24$ helium mass fraction and zero metallicity, which yield a primordial mean molecular weight of $\mu = 0.59$.

4.2 Analysis

Since in this Section we present and discuss the simulation performed, when confronting different redshifts it is useful to define the normalized density Δ as

$$\Delta = \frac{\rho}{\overline{\rho}} \tag{4.1a}$$

[1] Which is formally defined in equation (4.5b).

where $\overline{\rho} = \overline{\rho}(z)$ is the mean density at redshift z, analytically

$$\overline{\rho}(z) = \Omega_x \rho_c (1+z)^3 \tag{4.1b}$$

and we reserve the right to chose x accordingly whether talking about dark matter or baryons.

As the dark matter dominates the evolution of the universe from $z \gtrsim 10^3$ and at later times the structure formation, we start analyzing this component and, after that, we focus our effort on the baryons, as their ionized fraction is responsable for the scintillation and this is the final goal of the Thesis.

4.2.1 Dark matter component

As depicted in Section 1.3, we expect the structure formation to be due to the dark matter potential wells, risen from the inhomogeneity of the initial perturbations and grown into clusters thanks to the gravitational instability, which, upon exiting the linear stage, is likely to mold the dark matter into filamentar shapes, as predicted by the Zeldovich approximation we have qualitatively analyzed in Section 1.3.3, and as we can see in figure (4.1), which shows cuts of the volume density field with blending techniques.

To begin talking quantitatively we have to analyze the dark matter power spectrum $P(k)$, as it yields almost all the information relevant to the formation history, since, for instance, the number of structures and its size at a given redshift can be inferred from $P(k)$, as we eventually see.

The power spectrum

Preliminary, it is convenient to define the dimensionless power spectrum P_Δ as

$$P_\Delta^2(k) = \frac{1}{2\pi^2} k^3 P(k) \tag{4.2a}$$

and to recall that $P(k)$ is given by

$$P(k) = \left|\delta^2(k)\right| \tag{4.2b}$$

where $\delta(k)$ is the Fourier transform of the dark matter overdensity.

In Section 1.2 we prompted the analysis of the density perturbation, and we stopped by showing the equations responsable for the evolution of the matter density perturbation; resuming from there, it is easy to see that qualitatively equations (1.30) and (1.31) state that there are two kind of perturbations: the ones on scales greater

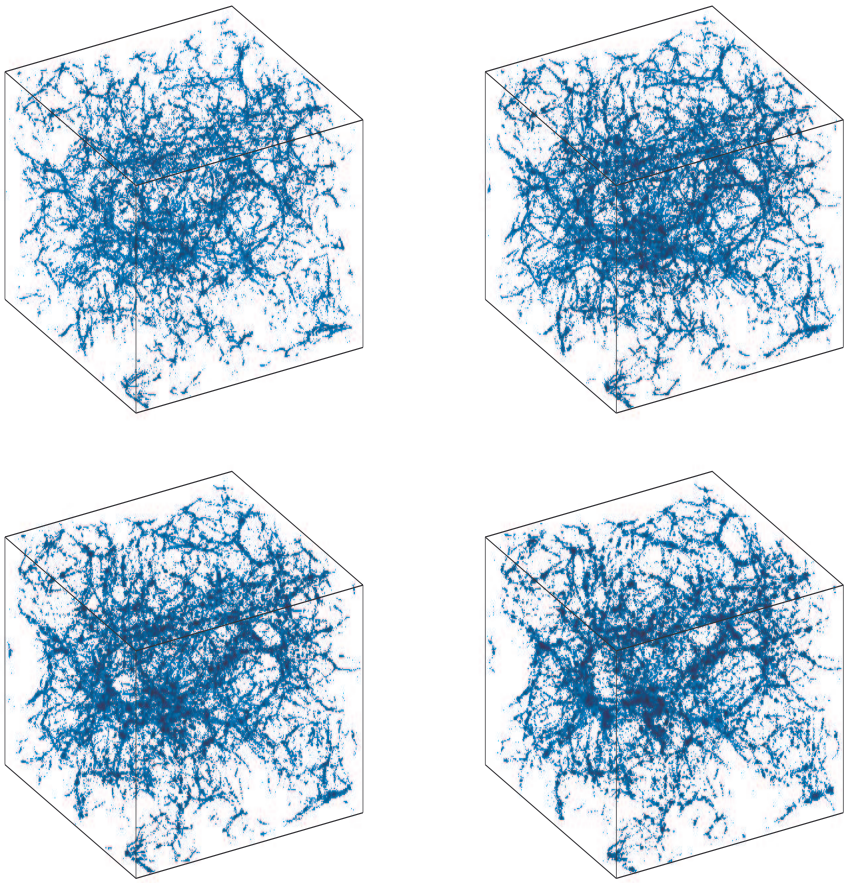

Figure 4.1: Volume rendering of dark matter structures of the entire simulation box respectively for, from the top left corner, $z = 2$, 1, 1.5 and 0; note that the image poor resolution is the reflection of the mass resolution, as the mesh refinement acts only on the baryon component.

then the wavelength associated with the Hubble horizon, and the ones with wavelengths smaller than this critical value k_H; thus the growth of the perturbations depend either on this ratio and either on the dominant universe component that is determining the metric evolution.
Hence the scale free power spectrum we are employing is naturally defined as

$$P_\Delta\left(k_H\right) = \text{const} \tag{4.3}$$

and, using equation (4.2a), we can approximate the power spectrum as

$$P(k) \propto k \quad k \lesssim k_H \tag{4.4a}$$
$$P(k) \propto k^3 \quad k \gtrsim k_H \tag{4.4b}$$

where the correct match between the two trends is given by analyzing the growth of the perturbations upon the passage from the radiation dominated era to the matter dominated epochs.

In figure (4.2) we can see the calculated power spectrum for various redshifts: to

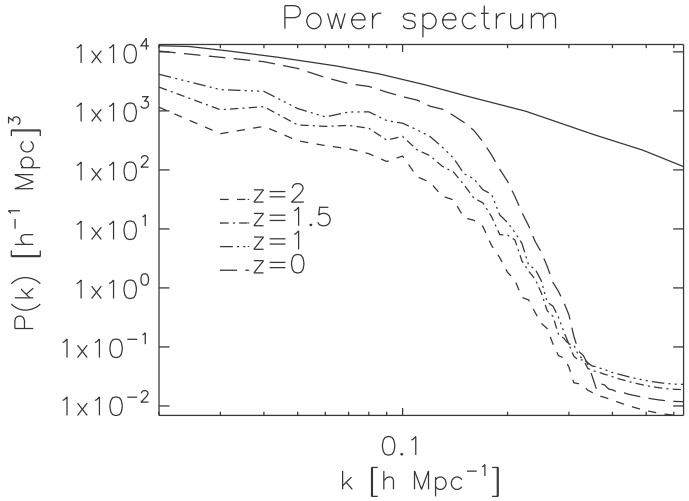

Figure 4.2: Evolution of the power spectrum for various redshifts, as indicated in the graph; the solid line is the best fit of the $z = 0$ data in accordance to the ΛCMD model as calculated in [29].

deny spurious effect from the finite size of the computational box, the lower k bound has been chosen to be greater than the reciprocal of the box length, while, since the density has been inferred using a gaussian kernel [2], the sampling length must be limited by the smoothing length, which hence acts as an upper bound on the k axis. What we can note is that, near the smoothing length, the power spectrum trend change due to the kernel, and thus we should have deconvolved its contribution, but, from the confrontation with the best fit to the current epoch $P(k)$ (i.a. [29]), we seen that we would have wasted our efforts, as our power spectrum diverge from the cited one for smaller k.

Thus, low spatial dark matter resolution fault, we expect no small scale structures, where for small scale we mean less then $\sim 3h^{-1}$ Mpc, but, obviously, this bias does not interfere with the larger scale of the simulation, hence we can and should check if the number of virialized objects at a given redshift inferred from the power spectrum matches the simulated one.

[2] See Section 5.1.1 for details on the smoothing process.

Halo mass function: Press-Schechter analysis

The estimate of the number of virialized structure is given by an analytical approximation called Press-Schechter theory (i.e. [22]). The argument consist in smoothing the density field on the length scale corresponding to the non linear mass.
To find the typical virial mass for any epoch one can naively argue that that mass is naturally associated to the mean density sphere with radius given by k_{nl}, which is the particular wavelength that distinguishes if a perturbation is in the linear or nonlinear stage of the evolution, namely

$$P_\Delta\left(k_{nl}\right) = 1 \tag{4.5a}$$

Even if the resulting mass, $M \sim \overline{\rho} k_{nl}^3$, surely gives the correct order of magnitude, formally the non-linear mass is expressed starting from the definition of square mass fluctuation enclosed in a sphere of radius R

$$\sigma^2 = \int \mathrm{d}^3 k \widehat{W}^2(kR) P(k) \tag{4.5b}$$

where $\widehat{W}$ is the Fourier transform of the top hat function; note that, again, every M corresponds to an R through

$$M = \frac{4}{3}\pi\overline{\rho}R^3 \tag{4.5c}$$

Approximating locally the power spectrum with a power law and recovering its time dependence with the transfer function T

$$P = T^2(z) k^m \tag{4.5d}$$

the non-linear mass is to be defined as

$$\sigma\left(M_{nl}\right) = 1 \tag{4.5e}$$

and hence scale as

$$M_{nl} \propto \left(T(z)\right)^{\frac{6}{3+m}} \tag{4.5f}$$

Now, as the density field is gaussian the probability to have a mean overdensity higher than δ_c in the R sphere is

$$p = \sqrt{\frac{2}{\pi}} \frac{1}{\sigma} \int_{\delta_c}^{\infty} \mathrm{d}\delta \exp\left(\frac{\delta^2}{2\sigma^2}\right) \tag{4.6}$$

and the number of collapsed object is thus

$$\mathrm{d}n = \frac{\overline{\rho}}{M} \frac{\mathrm{d}p}{\mathrm{d}M} \mathrm{d}M \tag{4.7}$$

Now, inserting the non-linear mass, defined as

$$\sigma\left(M_{nl}\right) = \delta_c \tag{4.8}$$

with a fixed δ_c, we get

$$\frac{\mathrm{d}n}{\mathrm{d}M} = \left(1 + \frac{m}{3}\right)\sqrt{\frac{2}{\pi}}\frac{\overline{\rho}}{M^2}\left(\frac{M}{M_{nl}}\right)^{\frac{m-3}{6}} \exp\left(-\frac{1}{2}\left(\frac{M}{M_{nl}}\right)^{\frac{m+3}{3}}\right) \tag{4.9}$$

which is the halo mass function expressed in term M_{nl}. The last point is to assume

$$\delta_c = 1.686 \tag{4.10}$$

which have been tested in many cosmological simulation (i.a. [19]).

Confronting with the Press-Schechter theory

It is best to test our simulation using the halo multiplicity function defined in [31]

$$f_{mult} = A_1(\sigma^{-A_2} + A_3)e^{-\frac{A_4}{\sigma^2}} \tag{4.11}$$

related to the mass function n via

$$f_{mult} = \frac{M}{\overline{\rho}}\frac{\mathrm{d}}{\mathrm{d}\log\sigma^{-1}}n \tag{4.12}$$

To find the virialized objects in our simulation we have used a Friend Of Friend algorithm (i.a. [9]), which defines a group of particles to be a cluster if these are within a given length, let's call it $h^\star$, which must be carefully pinpointed as it is crucial in determining the correct groups: since this scale must be related to the non-linear mass M_{nl}, our choice must be related to the value of δ_c fixed in equation (4.10), and hence, given the spatial resolution and the simulation box size, the linking length must be of order $\sim 0.657h^{-1}$ Mpc.
We have set $h^\star = 0.5h^{-1}$ Mpc, and the application of the group finder, along with the result given by the Press-Schechter theory (cfr. [19]) can be found in figure (4.3).

What we can say is that the Press-Schechter tend to overpredict objects in the high mass region, and underpredict the ones in the low mass zone (i.a. ibidem), thus overall the comparison could be treated as successful.
Note that it is natural that our result becomes less smooth as the mass increase, behaving like a step function near $m \geq 0.2\ 10^5\mathrm{M}_\odot$, since having a finite box size give us a bias on the statistical significance at highest mass scale.

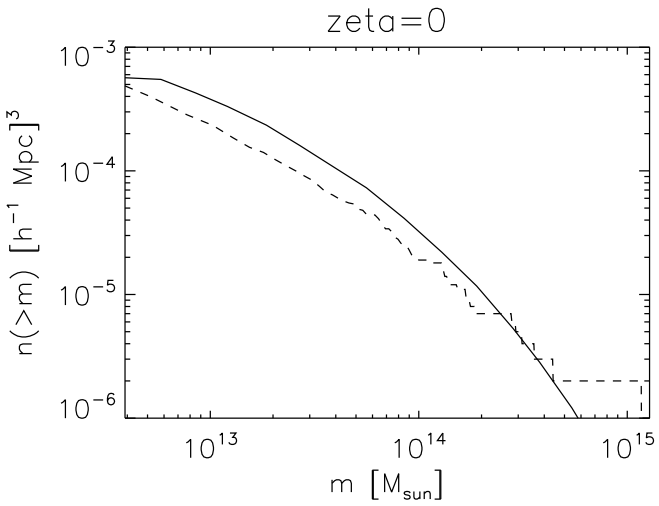

Figure 4.3: Comparison at $z = 0$ of the cumulative number n of virialized object with mass greater than m: the confront is between the prediction of the Press-Schechter theory (solid line) and the cluster resulting from the simulation (dashed line), which have been inferred with the FOF method with a linking length $h^\star = 0.5h^{-1}$ Mpc.

4.2.2 Baryonic component

After $z \sim 10^3$ the evolution of baryons is coupled to the other components of the universe in a peculiar way: dark matter rules the baryons through the gravitational action, which in turn cause perturbations on the photon component, namely the Cosmic Microwave Background and, furthermore, the baryons sub-components self interact among themselves in multiple ways.
What we want to check here is that the clustering process occurs accordingly to what we have seen in Section 4.2.1 and that the thermal history resemble the correct one.

Mean evolution

Before rushing in a deeper analysis, it is meaningful to observe the evolution of the baryonic quantities averaged over the whole simulation box.

In figure (4.4) we can see that the mean inferred density overlaps the analytical trend, as expected from the high degree of homogeneity of our universe, and, in figure (4.5), that the electron ionization fraction is within the limit given by the classical Gunn Peterson test (i.a. [20]) and is nearly constant in the range shown.

On the other hand, as we can see in figure (4.6), the temperature behavior is twofolded: while the mean evolution roughly resemble and follow the ionizzation

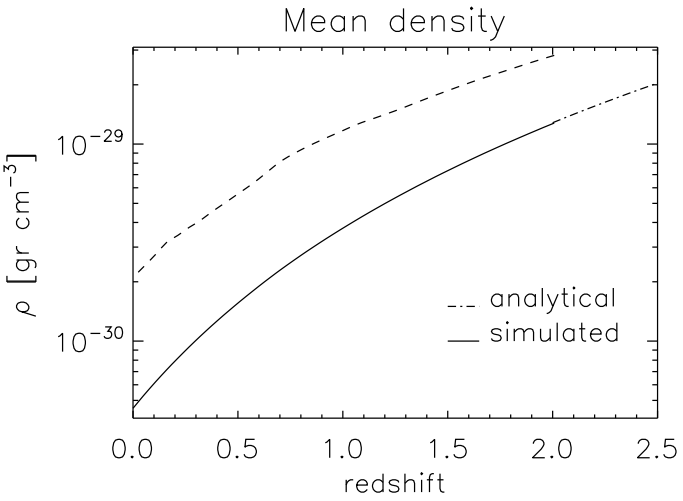

Figure 4.4: Evolution of the density: the solid line is the mean density, the dashed one is the root mean square variance component about the mean and the dashed dotted line is the analytical dependence given in equation (4.1b). As noted in the text, the computed and the analytical means overlap.

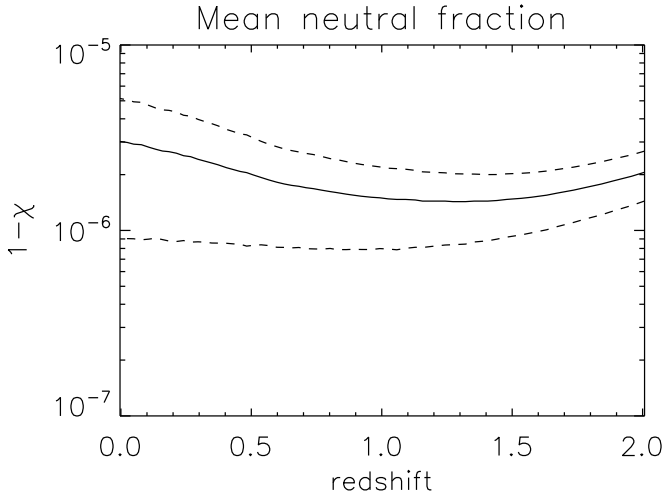

Figure 4.5: Evolution of the ionization fraction with redshift: the solid line is the average neutral electron fraction, the dashed ones represent the $\pm 1\sigma$ r.m.s. about the mean.

fraction evolution, the 1-σ component goes beyond the order of magnitude bound given by this process, hinting that the heating mechanism must be principally due

to the shock caused by the gravitational instability.

The pressure history, in figure (4.7) is inverse to the temperature one: while the

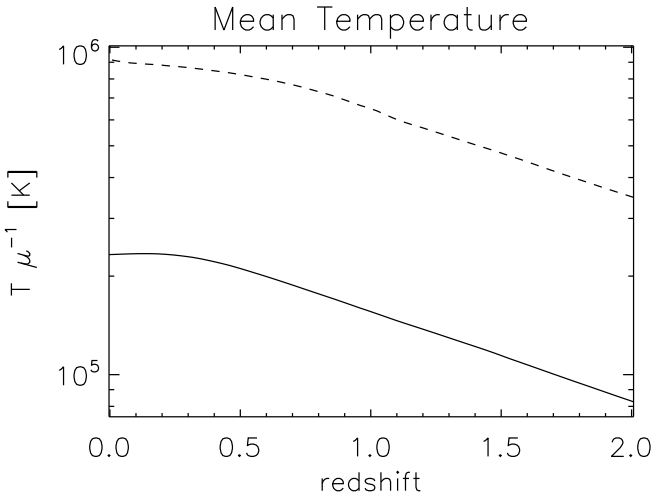

Figure 4.6: Temperature evolution with redshift: the solid line represents the mean and the dashed one is the $+1\sigma$ r.m.s. about the mean.

latter is increasing, the former is decreasing, meaning that the baryons are trying to achieve equilibrium as the shocks are less frequent and intense; note that its sigma has a oscillating trend superposed to the decline of which follows the one of the average: this indicates that the time scale of this process is different depending on the regions.

Structure maps

Figure (4.8) is a visual proof of the shock driven high temperature: we can see that, for the same kinetic energy, the highest peak of the temperature map correspond to three dimensional episodes, while progressively milder events arise when the clashing velocities appears only in two out of the three axes: in these cases, and with the right coordinate, it could be shown that the shocks are approximately bidimensional and thus their energy input is to be less influent.
We have chosen to show this particular redshift, $z = 4$, as the web structure of the matter is more evident and recognizable, since in later epochs there are progressively fewer shock events.

Next we present some the evolution of a simulation slice with its density maps

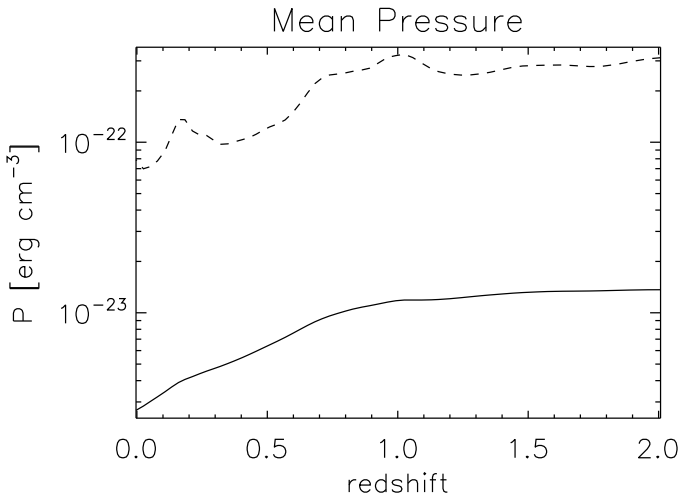

Figure 4.7: Evolution of the pressure with redshift: again the solid line is the mean and the dashed one represents again the $+1\sigma$ r.m.s. about the mean.

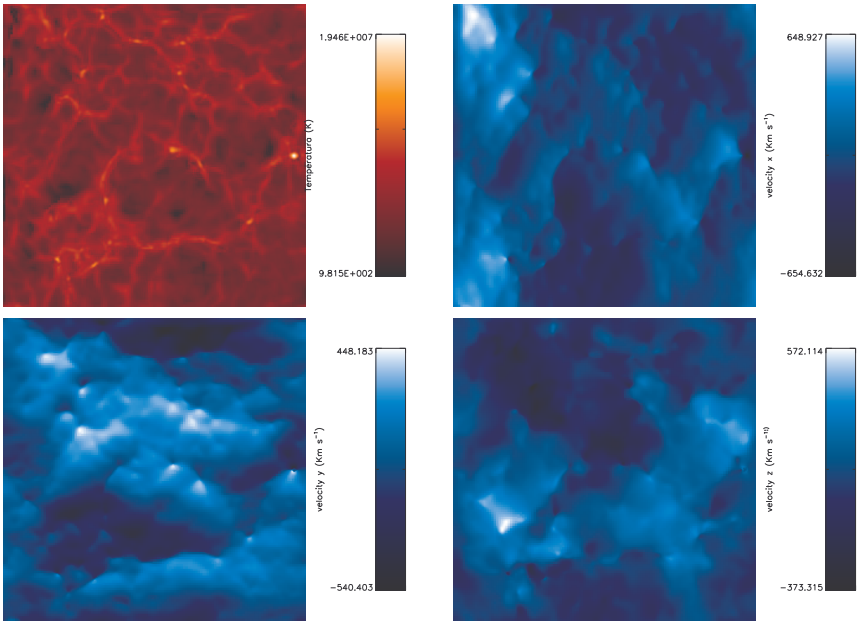

Figure 4.8: Temperature map for $z = 4$ and the cartensian components of the velocity of the corresponding slice; note that while the color is logarithmic for the temperature, the velocity scale is linear.

at various redshift, shown in figure (4.9), and their corresponding temperature and pressure maps, in figure (4.10) and (4.11) respectively.

We can see that the correlation between the temperature and the pressure is

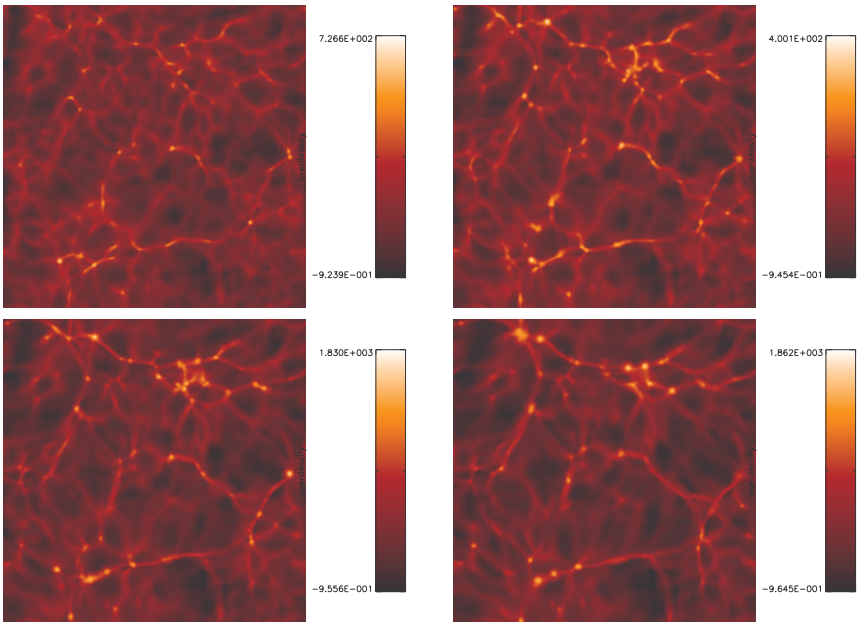

Figure 4.9: Evolution of a density map: from the top right corner $z = 2, 1.5, 1, 0$; the colors corresponds to the overdensity and are in logarithmic scale.

stronger than the existing one between the density and the temperature: it is like to have a family of equation of state, as we eventually see.

Note that in these maps the resolution is intrinsically higher than in (4.1) because of the AMR method employed to solve the baryons: the five additional levels of refinement allows to solve structure one order of magnitude smaller than the dark matter component, and this is exactly what we need since the scintillation magnitude roughly goes as the density squared times the length of the screen[3], and thus a proper treatment critically depend on the degree of resolution achieved, as the smoothing process tend to bias the scattering measure.

Thermodynamics of the InterGalactic Medium

To analyze the gas density distribution, shown in figure (4.12), we want to follow the same line of thought indicated in [7]: for low density we can assume that the

[3]See equation (3.102).

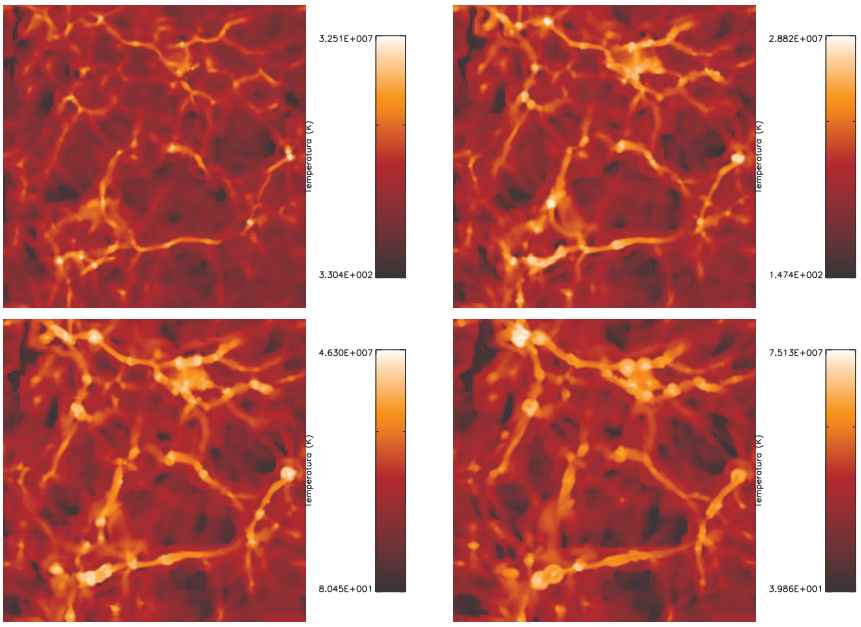

Figure 4.10: Temperature maps at various redshift: from the top right corner $z = 2,\ 1.5,\ 1,\ 0$; the colors corresponds to the temperature in unit of Kelvin over mean molecular weight and are in logarithmic scale.

gas is expanding at constant velocity and thus, for the normalized density, we have

$$\Delta \propto a^{-\frac{3}{2}} \tag{4.13}$$

Let's say that Δ start this decrease when the overdensity δ reach a fixed value; since $\delta \propto a$ and its initial conditions are gaussian we would expect

$$\mathrm{d}P \propto \exp\left(\text{const } \Delta^{-\frac{4}{3}}\right) \Delta^{-\frac{8}{3}} \mathrm{d}\Delta \tag{4.14}$$

As the assumption are strictly true in the linear regime we have to employ a slightly different formula to fit our distribution

$$\frac{\mathrm{d}P}{\mathrm{d}\Delta} = A_1 \exp\left(-\frac{\left(\Delta^{-\frac{2}{3}} - A_2\right)^2}{A_3}\right) \Delta^{-A_4} \tag{4.15}$$

which assures that this treatment can be used near the linear regime, namely $\delta \ll 1$, and which reduces to equation (4.14) in the $\Delta \ll 1$ limit, when $A_3 \gg 1$, and to a gaussian when $A_3 \ll 1$; since in the former case we have a peak for $\Delta \propto A_3^{-\frac{3}{4}}$ and the density for the void goes as $\Delta \propto a^{-\frac{3}{2}}$, the sigma parameter inside the gaussian

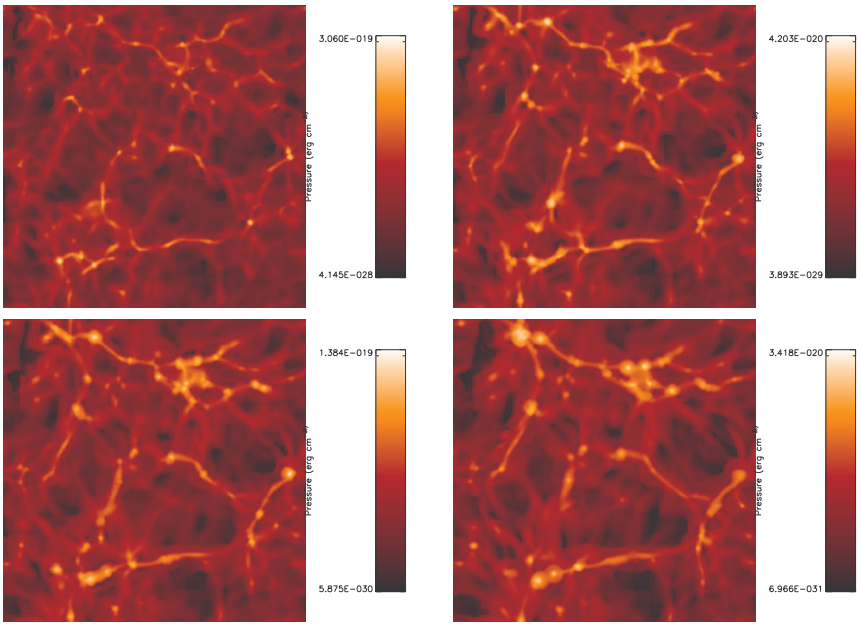

Figure 4.11: Pressure maps at various redshift: from the top right corner $z = 2,\ 1.5,\ 1,\ 0$; the colors corresponds to the pressure in cgs unit and are in logarithmic scale.

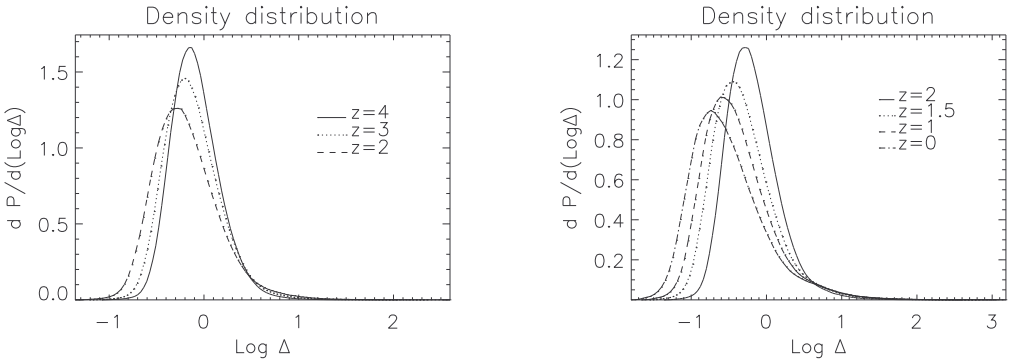

Figure 4.12: Differential distribution of the baryon normalized density for redshifts in the interval $z \in [0,4]$; for details on how the distribution is calculated see Section 5.1.1, for the normalization of the density see equation (4.1b).

is expected to evolve linearly with the expansion parameter or, being more precise using the result illustrated in [7], we expect that

$$\delta_0 = 7.61a \tag{4.16a}$$

where

$$A_3 = 2\left(\frac{2}{3}\delta_0\right)^2 \tag{4.16b}$$

In figure (4.13) it is possible to see the fit in the $z = 2$ case, with parameters

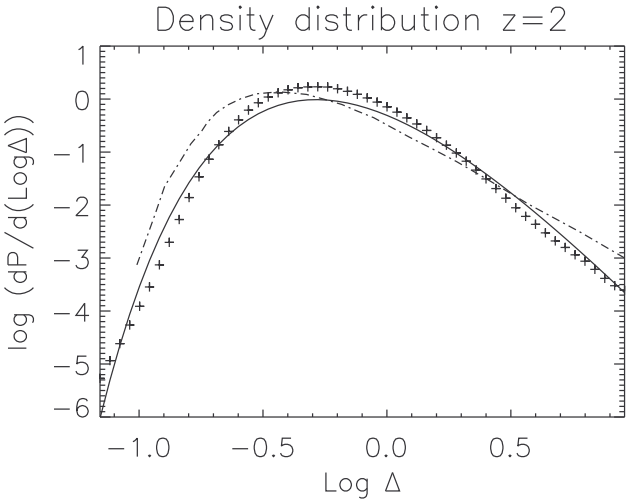

Figure 4.13: Logarithmic differential density distribution of the baryon normalized density for redshift $z = 2$; the distribution is indicated with the crosses while the solid line is its fit; with the slash dot line we have reported the analytical fit to the data obtained in [7].

$$A_1 = 17.3 \quad A_2 = 2.9$$
$$A_3 = 4.1 \quad A_4 = 2.3$$

the variance of which is of order 10%. We can note that, confronting with the result obtained in [7], that we have less baryons in the low density zone, and, obviously by mass conservation, less in the high density part of the plot: the crucial point is that, again, our power spectrum is less efficient in forming deep potential wells and hence the baryon collapse is damped.
Nonetheless we can note that the crucial parameter, the slope of the power law and the width of the gaussian, are within a 10% range of the ones in [7] for the same redshift.

Next we want to check the equation of state of the baryons for the current epoch, which can be seen in figure (4.14).

As a general definition baryons in the IGM can be splitten into three category: the

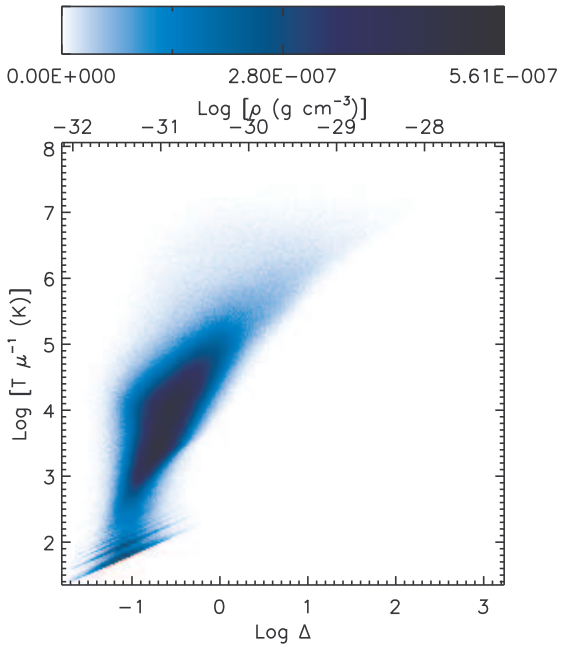

Figure 4.14: Equation of state for the baryons at $z = 0$: the colorbar is linear and represents the probability function; while the ratio temperature to mean molecular weight is expressed in unit of Kelvin, the density is represented in cgs units and its corresponding value normalized to the mean analytical average, given in equation (4.1b).

cold and the hot matter, which are both high density and are distinguished by their temperature, and the diffuse matter, which is cold and rarefied; the critical value for the temperature is fixed at (i.a. [23])

$$\frac{T_c}{\mu} = 10^5 \text{ K}$$

As we see in (4.14) we have no cold IGM in our simulation this is due to the fact that we lack the mass resolution to form galaxies or luminous object in general, as the power spectrum is inefficient beyond $\sim 3h^{-1}$ Mpc, and thus the cooling process is not fast enough to allow us to see the gas changing equilibrium from pressure to centrifugal supported.

The evolution of the two remaining phase can be seen in figure (4.15). It is to note that the lack of the cold IGM should in principle enhance the scintillation process, but it is to remember that having no cold phase means that we have no material from which one can form stars, which through the creation of H_{II} regions and feedback

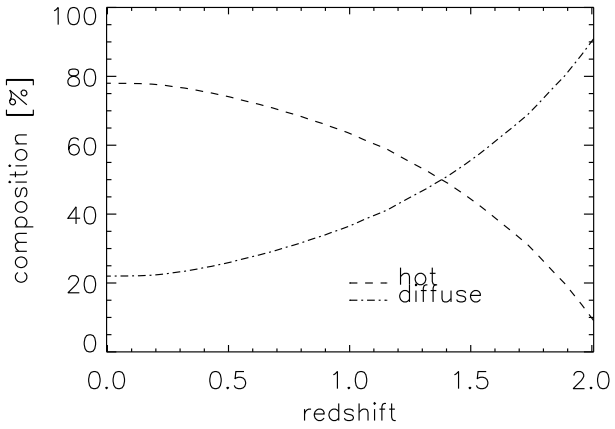

Figure 4.15: Evolution of the baryon phase state with redshift: the slashed line represents the hot component and the slash dotted line the diffuse one, the distinction between the two components is based on a critical point for the temperature of $\frac{T_c}{\mu} = 10^5$ K, as explained in the text. Obviously, as we do not have cold IGM, the graph is symmetric.

process, like metal enrichment, could counterbalance or overcome the effects on the scintillation given by the cold medium.
As these processes are rather complicated to be taken into account analytically and we do not have the necessary mass resolution to see that in the simulation performed, what we can say here is that since the cold gas fraction is to be below a $\sim 10\%$ level (e.g. [23]), the variation can be regarded as being marginal and we can safetly use this simulation to test our model, which, as explained in Chapter 3, has an intrinsically higher uncertainties.

Chapter 5

Simulating the scintillation of high-redshift sources

On Roundworld, things happen because the things want to happen[†].

[†]*In a manner of speaking. They happen because things obey the rules of the universe. A rock has no detectable opinion about gravity.*

1999, The science of Discworld, Terry Pratchett

5.1 Preparing the analysis

5.1.1 Methods employed

Building the lines of sight

Now that we have a healthy universe at our disposal we want to apply our scintillation model and, to achieve this, we have chosen some line of sight across the entire simulation: this is done taking snapshots of the simulation at different redshifts in a way such that every box is contiguously attached to the previous one, namely if i and $i+1$ identify the quantity of two snapshot then the link between a_i and a_{i+1} is implicitly given by

$$L = \frac{c}{H_0}\int_{a_i}^{a_{i+1}} \frac{a}{E(a)}\mathrm{d}a \tag{5.1}$$

where L is the comoving box length and $E(a)$ is implicitly defined in equation (1.14). Obviously choosing the position of the quasar, which in our case[1] is $z = 2$, and using recursively the last equation the boxes are fixed and concatenated with one another.

[1]Actually, as equation (5.1 is used backward from the observer, our source is located at $z = 2.0247...$)

After this set up, to both have uncorrelation from one snapshot to the other and to be computationally efficient, a chosen number of cuts are made in the $\hat{z}$ direction in every boxes, and then these are randomly gathered together to assemble a line of sight; as in our case the entire line is composed of nearly sixty simulation snapshot, selecting something like twenty lines in every snapshot assures that our sample is not biased if it number elements are large enough to ensures statistical significance for our analysis, which we have mainly based on the probability distribution of the scintillation relevant quantities.

Probability distribution function

The distributions we seek are calculated in a way similar to the Smoothed Particle Hydrodynamic method (i.a. [18]): in general for a function f and an ensemble $\{x_i\}$ where its value is known its density estimator is given by

$$f(x) = \sum_i f(x_i) K(x_i,x) \tag{5.2a}$$

where K is the smoothing kernel, which we have elected to be gaussian

$$K(x_i,x_j) = \frac{1}{(2\pi h)^{\frac{3}{2}}} e^{-\left(\frac{x_i - x_j}{h}\right)^2} \tag{5.2b}$$

with a constant bandwidth h that we have chosen using the rule of thumb given in [28]

$$h = 1.06 \sqrt{\langle x_i^2 \rangle} N^{-\frac{1}{5}} \tag{5.2c}$$

where here N is the number of points of the sample.

In this Chapter we use an f given by

$$f(x) = \begin{cases} 1 & x \in \{x_i\} \\ 0 & \text{otherwise} \end{cases}$$

thus enabling us to interpret this as a point probability distribution: in this case equation (5.2a) becomes

$$\frac{\mathrm{d}P}{\mathrm{d}x}(x) = \text{cost} \sum_i K(x_i,x) \tag{5.2d}$$

where the constant is chosen such that the probability is normalized to unity. Aside, we can note that now h can be viewed as the natural extension of the bin length of an histogram.

In this context, when needed, the error of the distribution will be calculated using a montecarlo method: let $\{\delta_i\}$ be the error associated with the sample $\{x_i\}$, from these ones it is possible to construct a certain number, call it k, of $\{y_i\}_k$ sets of points modified by the error, which is treated as uniformly distributed; now from every set is possible to extract its probability distribution function $\overline{\frac{\mathrm{d}P_k}{\mathrm{d}x}}$, and thus the upper bound of the distribution function $\frac{\mathrm{d}P}{\mathrm{d}x}$ in the point $\widetilde{x}$ is given by

$$\max_k \overline{\frac{\mathrm{d}P_k}{\mathrm{d}x}}(x)\bigg|_{x=\widetilde{x}} \tag{5.2e}$$

and clearly the lower bound is calculated in a similar way; the number k is chosen such that the variations due to its augmentation are less than 10^{-4}.

Remark on the frequency dependence

The last reminder is that, since formally the frequency seems to factorize from the formulae, one is inclined to think that the results can be simply generalised to other frequencies using a reference one and exploiting the analytical dependence, but, it is to remember that the various scintillation observables depend on the screens encountered, which in turn depend implicitly on the frequency via condition (3.101).

Thus, even if the leading term is correctly recovered by the analytical argument, this correction is crucial in obtaining the right results, as we eventually see in Section 5.2.3.

5.1.2 Analyzing a single line of sight

Before rushing in the complete analysis we have to focus on a single frequency and on a single line to get the insight necessary to achieve a overall view of the problem. Thus we elect a particular line of sight, with $SM_{-3.5,eq} = 1.627$, to be our typical one; we will see in the next Section that this is around the calculated mean equivalent scattering measure and that the results exposed are near enougth to the their means to really trust this line as a representative one.

Let's pick a monochromatic source emitting with $\nu = 100$ Ghz: the first thing to check is if we are indeed in the refractive regime, and this can be shown plotting the $\frac{\theta_d}{\theta_f}$ ratio for every screen, which is shown in figure (5.1).

As this value is strongly peaked at 2.152 10^{-5} the assumption of being in the weak scintillaton regime made in Chapter 3 can be regarded as correct, and thus we can carry on the analysis with the tool developed so far, being error related to the inaccuracy of the thin screen approximation only.

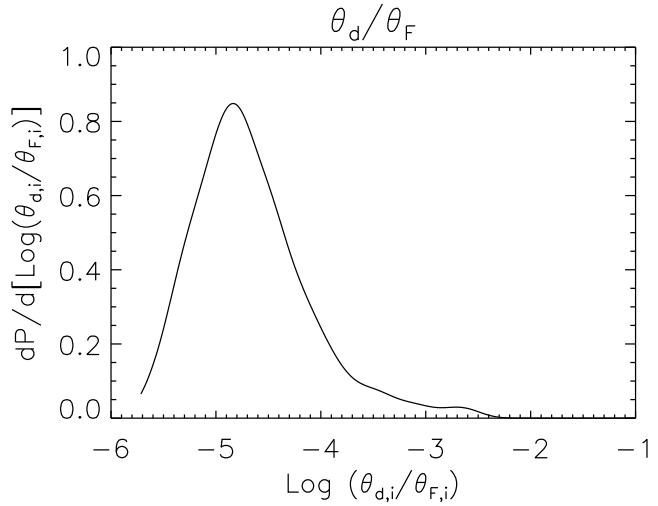

Figure 5.1: Probability distribution function for $\log_{10} \frac{\theta_d}{\theta_f}$ in a $SM_{-3.5} = 1.627$ line of sight obtained with a 100 Ghz monochromatic source.

After checking this assumption it is imperative to look at the time scales of the process, and thus we have calculated the distributions for the refractive and the diffractive times for every screen, which can be seen in figure (5.2), which states that the first two moments are are given by

$$\begin{vmatrix} \text{mean } (t_{rif}) = 0.381 \text{ days} \\ \text{sigma } (t_{rif}) = 1.665 \text{ days} \end{vmatrix} \quad \begin{vmatrix} \text{mean } (t_{dif}) = 2.646 \text{ years} \\ \text{sigma } (t_{dif}) = 3.957 \text{ years} \end{vmatrix} \tag{5.3}$$

and this tells us that the refraction is responsible for the daily variation while the annual one is due to diffraction.

From this point of view the refractive angle Θ is to be identified with the angle measured in one day, namely $\Theta{=}\Theta\,(1d)$, and is to be interpreted as a displacement of the source, as it main contributions are due to the Fresnel angles, and its evolution in this case can be seen in in figure (5.3).

When analyzing the intensity fluctuation, we will be interested in this two reference time, and so the relevant modulation indices will be $M_r(1d)$ and $M_r(365d)$.
Further more, as every screen indices depends on the scintillation angle, this will be the effective angle when the modulation is refractive and θ_d when the observational time match the diffractive time, even if the scintillation formally is in the refractive regime, since, as said, this distinction does not take into account the dominant time

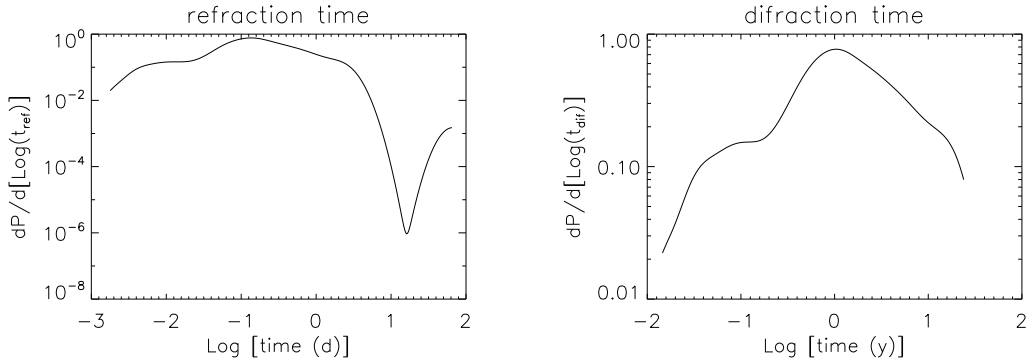

Figure 5.2: Distribution of the $\log_{10}$ time scales for diffraction and refraction process in a $SM_{-3.5} = 1.627$ line obtained with a 100 Ghz monochromatic source.

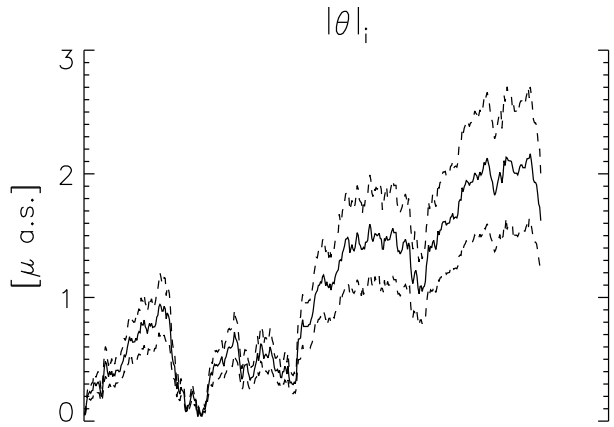

Figure 5.3: Evolution of the refraction angle θ_i throught the $SM_{-3.5} = 1.627$ line of sight obtained with a 100 Ghz monochromatic source: the error bars (dashed lines) are given by the uncertainty coming from the extended thin screen model. There is no horizontal axis as it would simply enumerate the index i of the encountered screen.

scale of the process:

$$M_r(1d) = \sum_i m_r\left(i, \Delta\theta_{eff}(i)\right) \tag{5.4}$$

$$M_r(365d) = \sum_i m_r\left(i, \Delta\theta_d(i)\right) \tag{5.5}$$

This distinction is important as, knowing the nature of diffraction, we should expect a larger modulation index due to diffractive effect even if the diffraction angle is negligibly small compared with the Fresnel one.

En passant we can underline that, regrettably, the delay due to the variation of the path travelled by the radiation, which as said is important for the pulsar scintillation through the ISM, in this context is too small to be of any use.

5.2 Statistical properties of scintillation

5.2.1 Order of magnitude

The first task is to evaluate the strength of the scintillation, and thus we have calculated the probability density for the equivalent scattering measure, which could be seen in figure (5.4): it comes immediately to the mind that the mean $SM_{-3.5,eq}$ differs form the analytical mean calculated in (3.112) by an order of magnitude; this can be explained by looking at the functional dependence of the scattering measure, which is linear in the distance and quadratic in the density, hence making this a sensible quantity that cannot be evaluated correctly by averaging the density over cosmological distances, as SM is not a scale invariant.

Thus the clustering process, even if[2] does not affect the mean density and even if it is not efficient enougth to produce galaxies in every line of sight, could augment drastically the scattering measure:

$$\text{mean}\,(SM_{-3.5,eq}) = 1.835 \tag{5.6a}$$

$$\text{sigma}\,(SM_{-3.5,eq}) = 1.292 \tag{5.6b}$$

Obviously the scintillation itself is enhanced by the increase of $SM_{-3.5,eq}$, but it is to remember that this is strictly true only in the single thin screen limit, or within the restriction of this model only with a infinite observational time, and thus one can not suddenly jump to conclusions, although it is certainly a point to be underlined that the effect of the IGM scintillation is comparable with the ISM one, and, as a side effect, it is beginning to become clear that the line used in the last section is indeed a typical one.
Note that, quite obviously, the fractional difference between the equivalent scattering measure calculated with the mean density and the one inferred average over the line of sight is not dependent on the power spectrum used to describe the IGM.

Having the distribution it is possible to calculate the probability for a line of sight

[2] And obviously it does not.

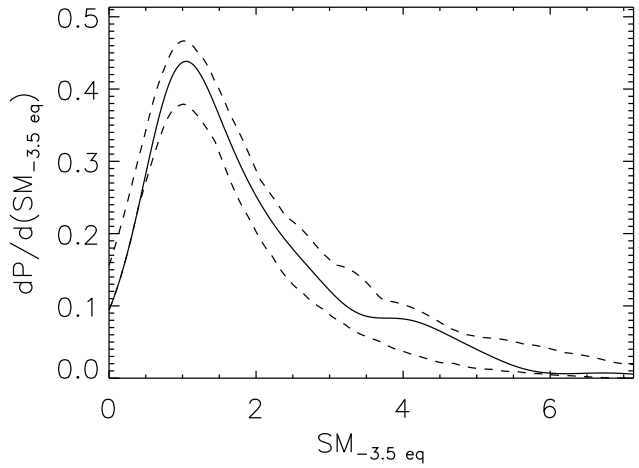

Figure 5.4: Probability distribution of the scattering measure in the selected lines of sight; the dashed lines represent the uncertanty resulting from the propagation on probability function of the approximation employed, as indicated in equation (5.2e).

to have a equivalent scattering measure laying in a certain range, for instance in the interval [mean − sigma,mean + sigma], in which case one would have[3]

$$SM_{-3.5,eq} = 1.835 \pm 1.292 \quad \Rightarrow \quad P = (71.82 \pm 10.95)\,\% \tag{5.6c}$$

It is worth stressing that this result is frequency independent, as the equivalent scattering measure is a summable quantity and thus does not depend on the number of screens.

5.2.2 Monochromatic source

Let's again concentrate our effort on a single frequency, again $\nu = 100$ Ghz, to begin a statistical analysis of the scintillation: the following results are presented using $3.5\ 10^2$ lines of sight from the source, the curves in the graphs are realized with 10^3 points and the errors of the probability distribution functions are calculated with a montecarlo with $2\ 10^4$ iterations.

[3]In the rest of this Section, sometimes it may seem that we forget that we are dealing with positive definite quantity and that the probability is capped at 100%. Obviously this is not the case, and it is done only to present the resuls without an unpleasant, and in this case not really necessary, notation.

Time scales

We present in figure (5.5) the time scales associated with the lines of sights, which are calculated as simple mean either for the refractive and the diffractive case, and are indicated with $\overline{t_{rif}}$ and $\overline{t_{dif}}$; thus, in this case, the uncertainty, from which the error of the distributions are calculated, are given by the variance of time scale itself on each line; calculating the mean value and the variance of this distributions yields

$$\begin{array}{l|l} \text{mean}\left(\overline{t_{rif}}\right) = 0.384 \text{ days} & \text{mean}\left(\overline{t_{dif}}\right) = 2.205 \text{ years} \\ \text{sigma}\left(\overline{t_{rif}}\right) = 0.458 \text{ days} & \text{sigma}\left(\overline{t_{dif}}\right) = 0.659 \text{ years} \end{array} \tag{5.7a}$$

with a probability to be between $\pm 1\sigma$ around the mean given by

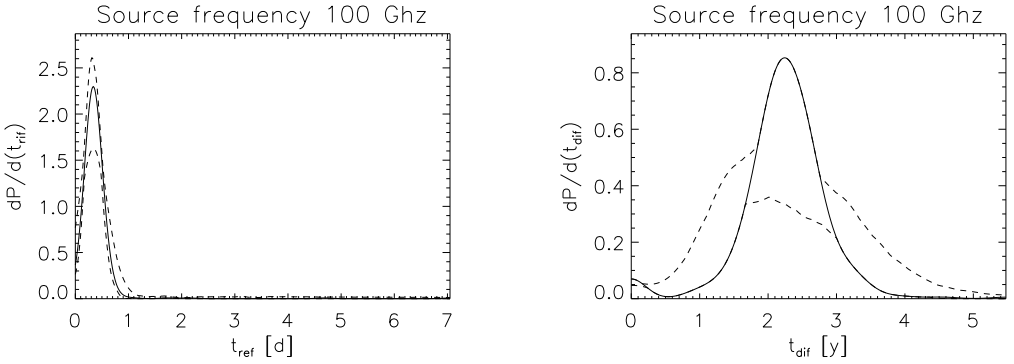

Figure 5.5: Probability distribution functions of the line of sight mean refractive and diffractive time scales; the dashed lines indicate the error bars of the distributions and are calulated accordingly to equation (5.2e), taking the r.m.s. variance of the time scale on a line of sight as the error of the corresponding mean value.

$$\overline{t_{dif}} = (0.384 \pm 0.458) \text{ years} \quad \Rightarrow \quad P = (98.19 \pm 23.46)\,\% \tag{5.7b}$$

$$\overline{t_{rif}} = (2.205 \pm 0.659) \text{ days} \quad \Rightarrow \quad P = (63.66 \pm 22.72)\,\% \tag{5.7c}$$

which again states that the dayly variation is due to refraction and the yearly to diffraction.

Refraction angle

The total angle of refraction $\theta_N = \Theta$ must be interpreted as a displacemente of the position of the source, and, being such, it has been calculated like having an

observable time of the order of a day, yielding

$$\text{mean}\,(\Theta) = 1.439\ \mu\text{a.s.} \tag{5.8a}$$
$$\text{sigma}\,(\Theta) = 1.009\ \mu\text{a.s.} \tag{5.8b}$$

as one can see in figure (5.6).

Following the same pattern used in the previous Section, let's calculate the proba-

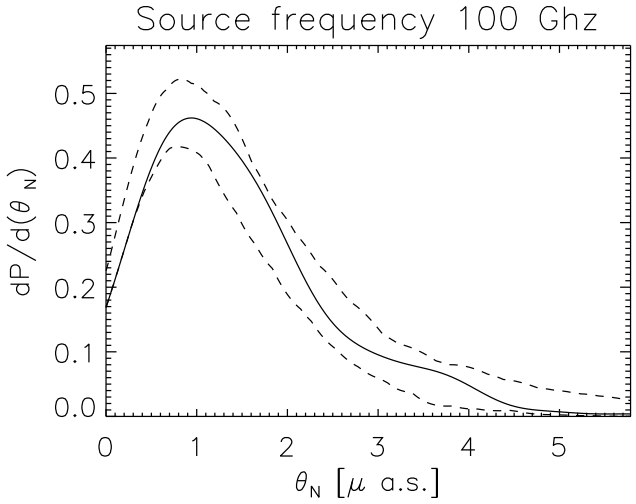

Figure 5.6: Probability distribution function of the refraction angle; again the error bars (dashed line) are calculated using equation (5.2e) propagating the error due to the approximation used, as for figure (5.4).

bility for the angle to be within one sigma from the mean

$$\Theta = (1.439 \pm 1.009)\ \mu\text{a.s.} \quad \Rightarrow \quad P = (70.87 \pm 11.34)\,\% \tag{5.8c}$$

Intensity fluctuations

As said in section 3.3.2 the modulation index $M_r = M_r\,(T_{obs})$ must be calculateed with the (5.4) prescription, thus actually here we are dealing with a refractive modulation index with for $T_{obs} \sim 1$ day, as depicted in figure (5.7) and diffractive one with $T_{obs} \sim 1$ year, which is shown in figure (5.8).

By looking at the graphics, or by calculating their first moments, we have

$$\begin{vmatrix} \text{mean}\,(M_r\,(1d)) = 5.53\ 10^{-4} \\ \text{sigma}\,(M_r\,(1d)) = 2.39\ 10^{-4} \end{vmatrix} \quad \begin{vmatrix} \text{mean}\,(M_r\,(365d)) = 0.0897 \\ \text{sigma}\,(M_r\,(365d)) = 0.0339 \end{vmatrix} \tag{5.9a}$$

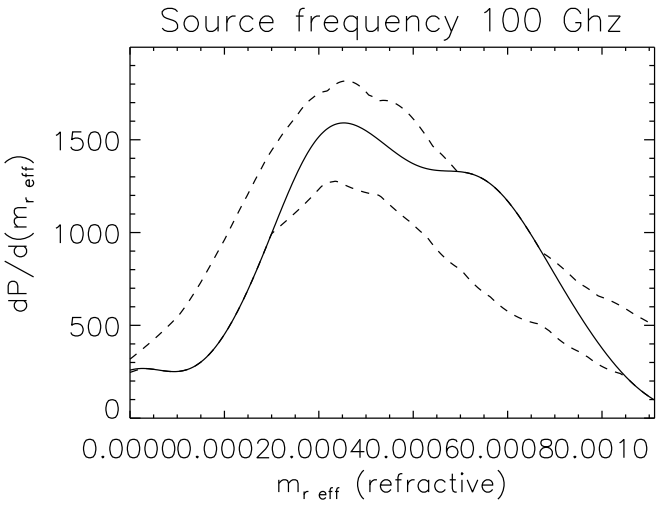

Figure 5.7: Distribution function of the refractive modulation index computed for a time of observation of one day (solid line); for details on the error bars of the distribution (dashed lines) see figure (5.4).

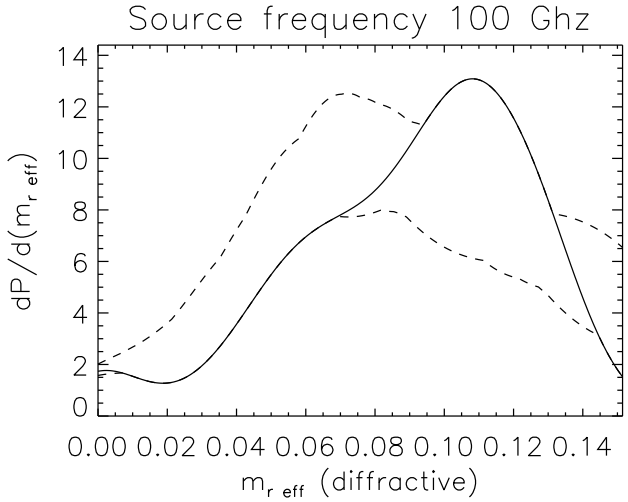

Figure 5.8: Probability distribution function of the diffractive modulation index (solid line), calculated on a period of one year; for details on the error bars of the distribution (dashed lines) see figure (5.4).

It is easy to see that their behavior is very different: while the probability of the refraction modulation is spread over a large area and always yields a negligibly small

effect, less then 0.01%, the point distribution of the diffraction is narrow peacked around a sound value of $\sim 10\%$ with a probability of

$$M_r\,(365d) = (8.968 \pm 3.391)\,\% \quad \Rightarrow \quad P = (64.76 \pm 17.15)\,\% \tag{5.9b}$$

5.2.3 Confronting the model with the observations

Until now we have treated our source as being monochromatic and the aim of this Section is to recover the correct effect in the multiwavelength case, in order to make our predictions testable.
Before beginning to expose the frequency dependence we start discussing the source, bearing in mind that, as the topic is far from completely understood and since it is not the main issue of our Thesis, here we merely want to use a simple model to describe the source and thus being able to deal with its main effects.

Source modelization

It is acknowledged (i.a. [27]) that the radio emission in a quasar is due to jets, which are made of plasma flowing out of the central region; since these jets are highly magnetized the emission mechanism involved is the synchrotron, and if the constituents of the flow are, as we assume, distributed with a power law, their intensity distribution I_ν is also a power law, either in the optically thin regime either in the self-absorption one; moreover, cosmological effects do not change its form, as

$$\frac{I_\nu}{\nu^3}$$

is a relativistic invariant. Thus, if one observe a radio active quasar with a radio band b_ν the quantity $\mathrm{d}m$ defined as

$$\mathrm{d}m = I_\nu b_\nu \mathrm{d}\nu \tag{5.10}$$

is to be regarded as the measure weighting the relative contribution of each frequency, so the general expression for a scintillation related quantity Q observed in the band b_ν from a source with intensity I_ν is to be given by

$$Q = \frac{\int_0^\infty Q_\nu \mathrm{d}m}{\int_0^\infty \mathrm{d}m} \tag{5.11}$$

where $Q_\nu = Q(\nu)$ is a frequency dependent quantity such as the ones calculated in the previous Section.
If we take b_ν to be a constant selection function and if its bandwidth interval $[\nu_1,\nu_2]$

is laying inside a region where the intensity is strictly a power law equation (5.11) reads

$$Q = \frac{\int_{\nu_1}^{\nu_2} b_\nu Q_\nu \nu^p \mathrm{d}\nu}{\int_{\nu_1}^{\nu_2} b_\nu \nu^p \mathrm{d}\nu} \tag{5.12}$$

where $I_\nu \propto \nu^p$. Obiously, if the bandwidth could be made arbitrarily small around a central value ν_0, then we can take

$$b_\nu \propto \delta(\nu - \nu_0)$$

and thus averaged Q coincides with the Q_ν evaluated in the center of the band, regardless of I_ν.

Frequency dependence

As mentioned before, it is not enougth to rescale a Q_ν with its frequency analytical dependence to obtain the correct value for $Q_{\nu'}$, since the screen themselves depend upon the frequency, thus the only available option is to recalculate all the results; in order to make the discussion feasible, here we are to expose only the trend those Q_ν which are quantities averaged on the lines of sight in the range

$$\nu \in [5 \text{ Ghz}, 100 \text{ Ghz}]$$

Figure (5.9) show that the diffraction time is increasing with frequency, while the

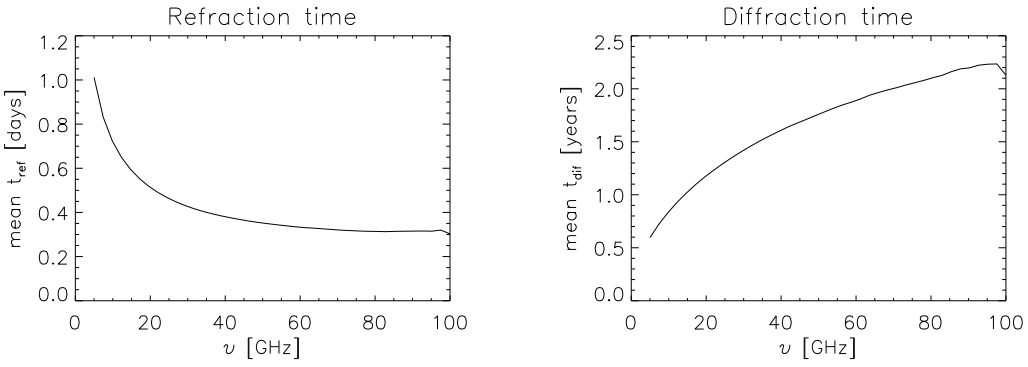

Figure 5.9: Frequency dependence of the mean refractive and diffractive time scales averaged on the lines of sight.

refraction one is decreasing, and that both the averaged screen characteristic times are only slightly dependent on frequency, thus we can continue to use the day and the year as the reference time scales for refractive and diffractive process respectively.

Instead, what may appear to be a surprise is that for frequency near 5 Ghz the overall dominant process switch from refraction to diffraction, as can be seen in figure (5.10) , which shows the frequency trend of $\frac{\theta_d}{\theta_f}$ averaged over the lines of sight. As a matter of fact, the existence of this, let's say, critical point can be foreseen from the analytical analysis, in fact for the i-th screen we have

$$\theta_{d,i} \propto \nu_{10}^{-\frac{11}{5}} \tag{5.13a}$$

$$\theta_{f,i} \propto \nu_{10}^{-\frac{1}{2}} \tag{5.13b}$$

thus, trivially,

$$\frac{\theta_{d,i}}{\theta_{f,i}} \propto \left(\frac{10 \text{ Ghz}}{\nu}\right)^{\frac{17}{10}} \tag{5.13c}$$

and the averaging operation is not supposed to cancel this dependence; however it is to remind that the right result can be obtained only computationally, since the ratio is dependent even on the screen own scattering measure and the screen length.

We can note that the awkward dependence of the last equation is due to the (5.13a), which is directly linked to the turbulence power spectrum we have used to describe the IGM internal structure, which we have assumed to be identical to the ISM one. Hence one can argue that it a consequence, not a result, that we have the critical point at 5 Ghz, since it is the same frequency for which the passage from the weak to the strong ISS is supposed to happen (e.g. [25]), but it is to remember that the screens responsable for the IGM scintillation are fixed only by imposing a condition on the diffraction angles (equation (3.101)), thus making the refraction angles indipendent of the former ones from this point of view.

To compare our results on the scintillation features we have decided to use the Micro-Arcsecond Scintillation-Induced Variability (i.e. [25]), which is a survey where the scintillation of a large number of high redshift quasar is observed at 5 Ghz with 2 days of observational time; note that, as the scintillation is not a zero mean value process, we can confront the data, which have an observational time of two days, with our model, calculated for $t = 1\text{d}$, considering it as a lower limit.

There the data, which can be seen in figure (5.11), are measured using the so called structure function[4], which quantifies the flux density variation of the source at the time lag t

$$D(t) = \frac{1}{N_t} \sum_{i,j} (S_i - S_j)^2$$

[4]As a matter of fact this is a skilful to infer so small refraction angles, considering that the resolution limit of VLBI is 10^2 μas at 86 Ghz.

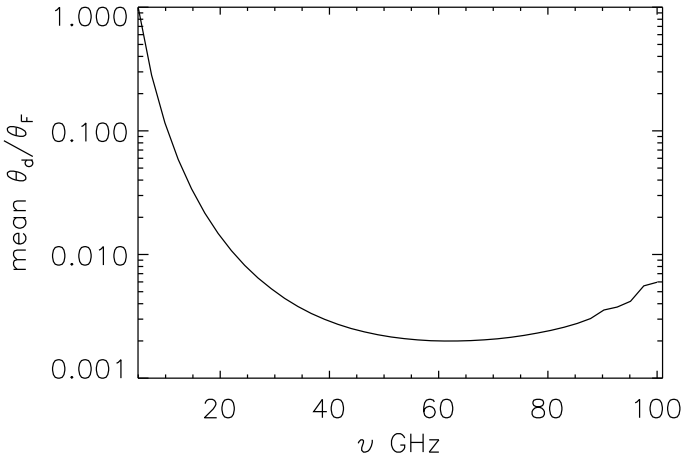

Figure 5.10: Frequency distribution of the ratio $\frac{\theta_d}{\theta_f}$ averaged on the lines of sight.

where S_i is a normalized flux density, the index range from 0 to 4 and counts the epochs of observation, N_t in a normalization to taken into account the pair of fluxes.

To infer the angle of refraction, a model must be imposed and the one used in [25] rules that the source emitting diameter, which is located at z is linked to the refraction angle as

$$\theta_{emit} = \Theta\sqrt{1+z}$$

To model the source the free parameter x is taken: it is the ratio of the flux of the source which is compact enought to be boosted and thus able to scintillate; the model dependence from the observable $D(2d)$ and the inferred θ_{emit} is shown in figure (5.12).

At $z = 2$ the mean observed structure function is $D(2d) = 1.2\ 10^{-3}$, as one can see in figure (5.11), and this would yield, in the range of the accepted parameter, a refraction angle

$$\text{MASIV at } z = 2 \quad \Theta \in [9.28,\, 62.35]\ \mu\text{as for } x \in [0.01,\, 1]$$

Ibidem it is it is underlined a discrepancy between the observed scintillation angles and the model for the ISS, and the possibility of the IGM scintillation, as an explanation, is ruled out as their model for the IGM, which is based on the H_I column densities and has a frequency dependence

$$\Theta \propto \nu^{-2.2}$$

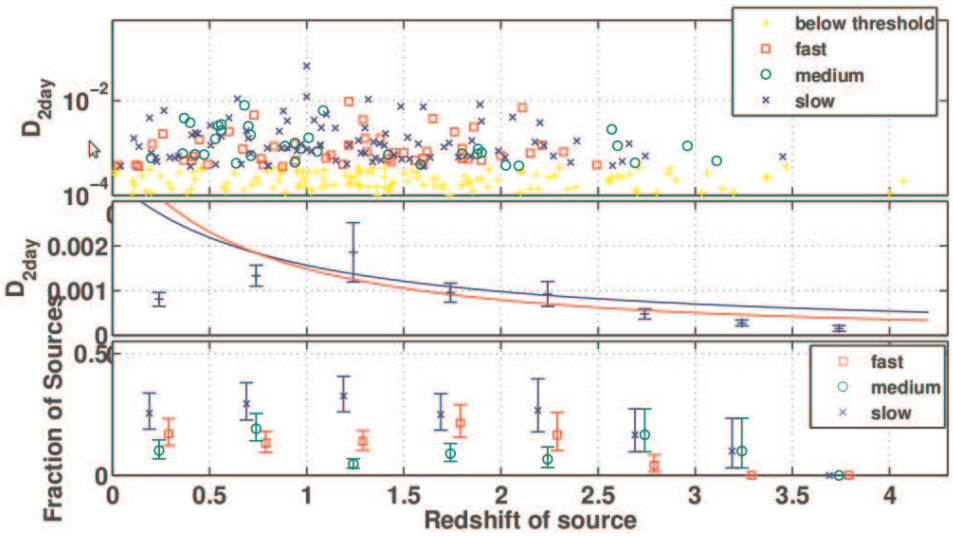

Figure 5.11: MASIV data in function of redshift taken from [25]: the plot shows in the upper pannel the scatter plot of $D(2d)$ with symbol depending on the classification of the ISS time scale (i.e. ibidem), the middle pannel the mean of the same quantity averaged in redshift bins and the lower pannel the fraction of source in the same bins distinguished by their time scale. The threshold is given by selecting the variable object if their modulation index is greater than the measure errors.

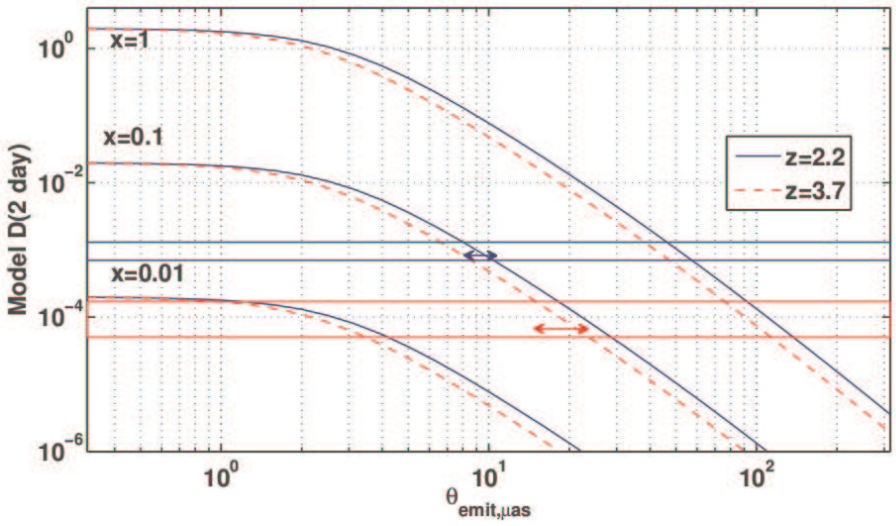

Figure 5.12: Theoretical relation model between the observed $D(2d)$ and inferred θ_{emit} in function of the compact fraction x for redshifts $z = 2.2$ and $z = 3.7$, taken from [25].

would produce an angle which is one order of magnitude lower than the lower limit angle inferred from the data, namely ~ 10 μas.
Instead this gap is comparable with our mean refraction angle at 5 Ghz $\Theta = 15.06$ μas, taken into account with the 1σ component ± 7.43 μas, as one can see in figure (5.13), which shows the comparison of the angle of refraction in a function of frequency between our model and the extrapolated one used in the MASIV to take into account the IGM scintillation contribution.

Thus, summing up, our result for the scintillation refraction angle given by the

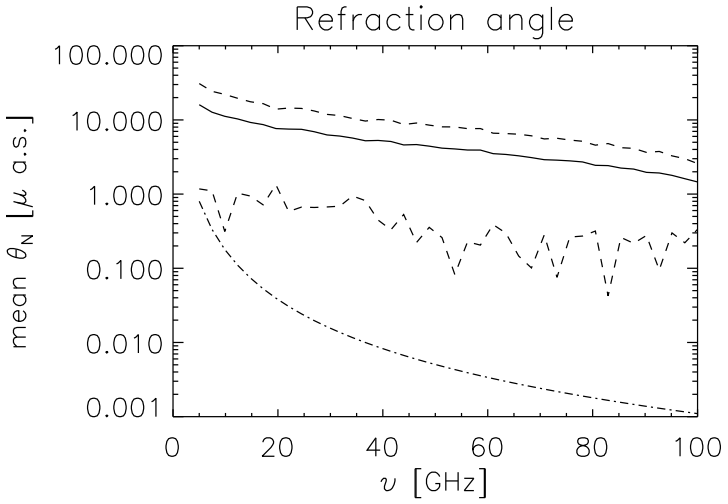

Figure 5.13: Frequency distribution of the scintillation refraction angle on a time scale of 1 day: the solid line is the angle inferred from our model averaged over the line of sight, the dashed lines represent the $\pm 1\sigma$ r.m.s component about the mean and the dashed dottted line is angle of refraction of the IGM model used in [25].

IGM has an order of magnitude comparable to the one required to explain the decrease in the theoretical ISS when compared to the MASIV observations, even if for now it is not possible to give a precise analysis, as our result has been obtained for a $z = 2$ source, while the survey has a much wider redshift range.

For what regards the modulation index we can say that the analytical frequency dependence is completely misleading, contrary to what happens in the refraction angle case just seen, for which the resulting trend is only slightly higher than expected one from a coherent sum of the interacting Fresnel angles, from equation (3.113a) $\Theta \propto \nu^{-\frac{1}{2}}$, with a breakdown at the passage between weak and strong scintillation, as explained above.

Hence in this case we must relay entirely on the model results, shown in figures (5.14) and (5.15), which shown the mean and the 1σ r.m.s. component about the average.
What one can immediately notice is that we have as the frequency decrease the ratio $\frac{\overline{m_r}}{\sigma(m_r)}$ increase and become higher than one[5], which is a symptom that for low frequency our model can not give satisfactory constraint on the modulation index. This is mainly due to the underlying assumption, which, as described in Chapter 3, rules a first order scheme to sum the modulation indices, by taking each scintillating screen uncorrelated one from the other.

Leaving aside the diffraction annual modulation, for which there is nearly no lit-

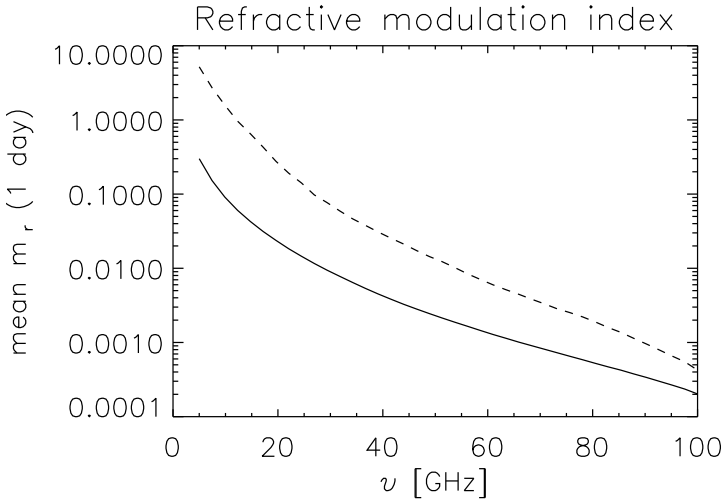

Figure 5.14: Frequency distribution of the modulation index on a time scale of 1 day: the solid line represents the line of sight mean value, while the dashed line gives the $+1\sigma$ r.m.s. component around the average.

erature to confront with, let's focus our attention to the dayly refractive intensity variation again using the MASIV survey as a comparison; moreover, in this case, the data are not model dependent, since measured structure function is directly coupled to the modulation index via (i.e. [16])

$$m_r(t) = \sqrt{\frac{1}{2}D(t)}$$

[5]Which is why we have not plotted the -1σ component about the mean.

and, as one can see in figure (5.11), the mean $D(2d)$ would yield at $z = 2$ a modulation index

$$\text{MASIV at } z = 2 \quad \text{mean } (m_r) = 0.0204 \quad \sigma\,(m_r) = 0.0087$$

which is within the limit of our mean m_r at 5 Ghz, as shown in figure (5.14)

$$\text{mean } (m_r) = 0.2143 \quad \sigma\,(m_r) = 3.728$$

but, as said early, the lack of a cross correlation term between the screens in our model yields a too large range for our scintillation index: as a matter of fact our

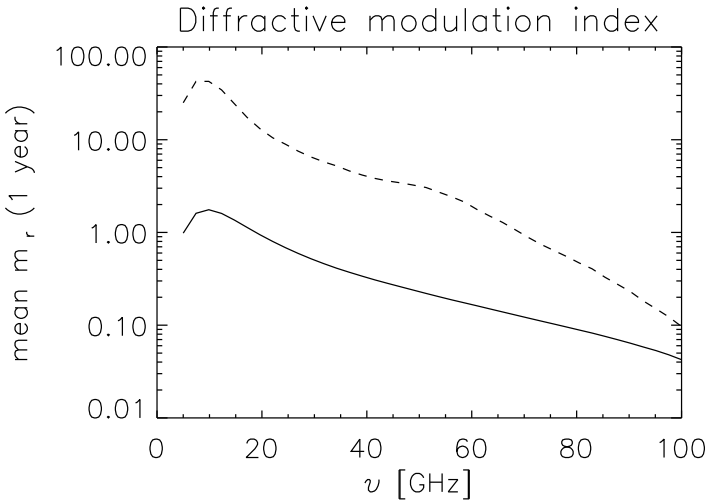

Figure 5.15: Frequency distribution of the mean modulation index on a time scale of 1 year: again, the solid line represents the averaged value, while the dashed line is the $+1\sigma$ r.m.s component.

inferred m_r makes, in principle, our model capable of being among the contributors of the flux modulation of the well studied 0917+624 quasar, which has a $\sim 20\%$ variability over the ISS (i.a. [26]), which is attributed to intrinsic dayly variation of the source, since the mean modulation index resulting from our model at that frequency is within $\sim 5\%$ of the observed value.

However, as we expect the IGM scintillation to be a background while the 0917+624 is among the most variable observed objects, we can not consider this as a proof of our analysis, but rather as an hint that our underlying model used to calculate the flux modulation must be refined, as considering only the first order interaction to infer the total modulation index of a line of sight gives result in accordance to the data, but heavily limits the constraint it can yield at low frequency.

Chapter 6

Conclusions

Man is a frivolous, a specious creature, and like a Chess player, cares more for the process of attaining his goal than for the goal itself.

Fyodor Dostoyevsky

6.1 Summary

In this Thesis we have studied the scintillation of a distant[1] quasar induced by the IGM: as its light travels from the source to the observer, it experiences random phase changes because of the variation of the refractive index, which is linked to the random irregularity of the density distribution of the ionized medium traversed, which forces an alteration of the characteristics of the light wave, with time scales dependent on the medium itself.

To achieve this goal, we started by analyzing the structure formation in the universe, both from the analytical and the computational point of view, as we have decided to use numerical techniques to simulate the cosmological background where we wanted to inquire the scintillation effects, and we focused our attention on the physical characteristics of the IGM and its turbulent behavior.

Then we reviewed the physical basis of the scintillation phenomenon, with particular attention to the model employed in the case where the scintillating medium is given by a thin screen, which is the one used to solve ISS: analyzing it we naturally extended this model to the IGM case by splitting the continuous medium between the source and the observer in a set of thin screens the contributions of which are properly summed to yield the effect of the entire line of sight.

[1] $z = 2$

As we specialized to the refractive case, it has been possible to uniquely select the screens in a way that is physically meaningful and preserve the coherence needed to have a simple model for the single screen contributions summation, which behave differently when considering different quantity, such as the refractive angle and the modulation index.

Finally we tested our model in the cosmological simulation performed, with a fixed source emitting a monochromatic wave in the radio band[2]: formerly, fixing the frequency, we analyzed the process either on a particular line of sight and either on a statistically meaningful sample, subsequently we discussed the behaviour as a function of frequency of the scintillation average quantities calculated on the line of sights and, finally, we used the statistical analysis of our model to compare it to the available observations.
The main results can be summarized as:

- Using a simple analytical treatment to deal with the cosmological part is insufficient to describe properly the phenomenon in the IGM case: when using analytical mean for the density the net strenght of the scintillation appears to be an order of magnitude less than what yields applying the model to a numerical cosmological simulation and taking the scattering measure averaged over 7.5 10^3 line of sights

  $$\text{with analytical density } \mathrm{SM}_{-3.5,eq} = 8.24\ 10^{-2}$$
  $$\text{with simulated density } \mathrm{SM}_{-3.5,eq} = 1.835$$

  This happens because the scattering measure, which gives the magnitude of the scintillation, is crucially dependent on the correct evaluation of the densities involved.
  Note that this result is independent of the frequency and a similar outcome can be achieved using a different power spectrum for the IGM.

- We have found that, in the IGM case, the time scales responsable for the refractive and diffractive scintillation are only slightly dependent on the frequency and can be estimated as

  $$t_{ref} = 1\mathrm{d} \quad t_{dif} = 1\mathrm{y}$$

  Moreover the passage from the weak scintillation to the strong regime, which happens when the ratio between the diffractive angle and the refractive angle[3]

[2]We have indicated the proper way to handle the more realistic case of a synchrotron spectrum, but we restricted ourself to the narrow observational band case.

[3]In this context given by the Fresnel angle.

approaches unity, in our case is given by

$$\frac{\theta_d}{\theta_f} \geq 1 \quad \text{when} \quad \nu \leq 5 \text{ Ghz}$$

Similar results hold in the ISS case.

- We have found that there are hints that our model could be used to solve the tension between scintillation observations and ISS models: in the MASIV survey (i.e. [25]) it was found that there is a discrepancy, with a lower bound of

  $$\Theta_{low} \gtrsim 10 \ \mu\text{as}$$

  between the inferred refraction angle and the ISM scintillation model, and their model for the IGM can not compensate the gap, as it yields a angle that is one order of magnitude lower than the minimum required.
  Instead, at the observational frequency, our model gives a mean refraction angle of

  $$\overline{\Theta} = 15.06 \ \mu\text{as} \quad \sigma(\Theta) = 7.43 \ \mu\text{as}$$

  or begin, more precise, a probability of $68.85 \pm 23.79\%$ of being within $\pm 1\sigma$ r.m.s. from the mean refraction angle indicated above, hence it is of the right order of magnitude to explain the phenomena.

- We have found that the results for the flux modulation are in agreement with the available data (e.g. [16] and [26]), but even that our model, which is based on a first order interaction scheme, which thus takes the different screen composing a line of sight as uncorrelated from one onother, does not gives, at low frequency, satisfactory constraints on the predictions.
  We think that considering a cross correlation term between the scintillating screen would improve the predictive power and thus, in the future, we want to develop this kind of approach.

6.2 Future developments & applications

Before talking about real improvements a consideration: the simulation have been performed with low resolution due to the limited computational resource available; the fact is not only a precision lacking issue, but a qualitative one, as we have been unable to observe a zoology of phenomena, such as galaxy and stellar formation and the resulting metal enrichment, which could play an important role in analyzing the scintillation; obviously this could be easily solved working with a computer cluster, but, for now, the results could be regarded to be in a rather crude state.

Furthermore several kind of developments are to be made:

- The model itself need a refinement, namely to add higher order perturbations of the solution of the Rytov equation, to introduce a more sophisticated power spectrum for the scintillating matter, obtained either from a model or a galactic scale simulation, and, more important, to handle properly the different time scales and the mutual interactions of the screens: with these changes we can agument the reliability of the theory employed and, in particular, the predictive power of the model in the case of the modulation index, which, as said, for now is poorly constrained, even if the results are in agreement with the observational data.

- Since the IGM and the ISM scintillations are in principle the same phenomenon, we can simulate, with the due different technique as a low resolution simulation for the former and a zoom simulation for the latter, both of the environments, and, by a statistical approach similar to the one employed in this Thesis, try to reproduce the actual data as a convolution of the ISS and the IGM scintillation.

- Using a real quasar spectra as the source would enhance the predictability of our model and allow to confront properly with the available data, and, moreover, we could try to correlate the scintillation study to the other matter probes, such as the Lyman-α forest analysis: while the former is sensible to ionized matter the latter rely mostly on neutral matter, hence, as they are indipendent from one onother, these can be used as complementary tools to investigate the baryonic fraction of the universe.

Bibliography

[1] *Aubert D., Teyssier R.*, 2008, MNRAS, 387, 295

[2] *Bahcall N. A., Ostriker J. P., Perlmutter S., Steinhardt P. J.*,1999 , Science, 284 (1481)

[3] *Bertschinger E.* 1995, arXiv:astro-ph/9506070v1

[4] *Bertschinger E.*, 2001, A.J. Suppl. 137:1

[5] *Boldyrev S., Königl A.*, 2006, Ap.J., 640:344-352

[6] *Dodelson S.*, 2003, Modern cosmology, Academic press

[7] *Escude J. M., Haehnelt M., Rees M.J.*,2000, Ap.J. 530 1-16

[8] *Ferrara A., Perna R.*, 2001, Mon.Not.Roy.Astron.Soc. 325 1643

[9] *Goetz M., Huchra J. P., Brandenberger R. H.*, 1998, arXiv:astro-ph/9811393v1

[10] *Gonzalez M., Audit E., Huynh P.*, 2007, A&A , 464, 429

[11] *Goodman, J.*, 1997, NewA, 2, 449

[12] *Haehnelt M.G., Madau P., Kudritzki R.P., Haardt F.*, 2000, arXiv:astro-ph0010631v1

[13] *Hui L., Gnedin N. Y.*, 1997, MNRAS , 292, 27

[14] *Lambert H.C., Rickett B.J.*, 2000, Apj 531:883-901

[15] *Lee L.C.*, 1977, APJ, 218:468-476

[16] *Lovell J.E.J., Rickett B.J., Macquart J.-P. et al.*, 2008, ApJ 689 108

[17] *Maselli A., Ferrara A., Ciardi B.*, 2003, MNRAS , 345, 379

[18] *Monaghan J.J.*, 1992, Annu. Rev. A&A 30:534-74

[19] *Norman M. L.*, 2010, arXiv:astro-ph.CO1005.1100v1

[20] *Peebles P.J.E.*, 1993, Principles of physical cosmology, Princeton series in physics

[21] *Peebles P.J.E.*, 1983 Ap.J. 263, L1

[22] *Press W.H., Schechter P.*, 1974, Ap.J., 187, 425-438

[23] *Rasera Y., Teyssier R.* 2006, A&A 445, 1-27

[24] *Rickett B.J.*, 1990, A&A, 28, 561

[25] *Rickett B.J., Lovell J.*, 2007, POS MRU, 46

[26] *Rickett B.J., Witzel A., Kraus A. et al*, 2001, Ap.J. 550:L11-L14

[27] *Rosswog S., Brüggen M.*, 2007, Introduction to high-energy astrophysics, Cambridge university press

[28] *Silverman B.W.*, 1986, Density estimation for statistics and data analysis, Chapman & Hall

[29] *Tegmark M. et al.*, 2004, PhRvD, 69 (10) 103501

[30] *Teyssier R.*, 2002, A&A 385, 337-364

[31] *Warren M. et al.*, 2006, ApJ, 646 (881)

[32] *Wheelon A.D.*, 2001, Electromagnetic scintillation, vol. 1, Cambridge university press

[33] *Wheelon A.D.*, 2001, Electromagnetic scintillation, vol. 2, Cambridge university press